36. PALEOMAGNETISM OF SEDIMENTS COLLECTED DURING LEG 90, SOUTHWEST PACIFIC[1]

C. E. Barton, University of Rhode Island and Bureau of Mineral Resources, Canberra, Australia
and
J. Bloemendal, University of Rhode Island[2]

ABSTRACT

Sediments recovered during Leg 90 (Sites 587–594, plus Site 586 cored during Leg 89) are, in general, extremely weakly magnetized carbonate oozes and chalks with NRM intensities seldom greater than 0.05 μG. The quality of the paleomagnetic records deteriorates with increasing depth caused by the combined effects of removal of primary magnetic oxides by sulfate reduction processes and the dispersal of magnetic grains during compaction.

Magnetic reversal sequences are generally recognizable back to the Gilbert, 3.4 to 5.35 m.y., except at equatorial Site 586 where only the Brunhes/Matuyama boundary could be identified. Longer reversal records were obtained at Site 588 (to Chron 13, about 13 m.y.) and Site 594 (base of Chron 5, about 5.9 m.y.).

Sediments are characterized by extremely high calcium carbonate contents (90–100%) with almost no biosiliceous components. Blebs and streaks of pyrite are common, and the presence of iron sulfides with poor magnetic stabilities is suspected, although not yet positively identified. Viscous components of magnetization are common, sometimes to the extent of dominating the primary remanence, and there is evidence to suggest that a magnetic remanence is imparted during core recovery. Siliceous carbonate oozes provide better paleomagnetic records than pure carbonate oozes.

INTRODUCTION

During Leg 90, long sequences of Neogene and late Paleogene shallow-water (1000–2000 m) carbonate sediments were recovered from Sites 587 to 593 along a north–northwest to south–southeast traverse of the Lord Howe Rise, and from Site 594 on the southern margin of the Chatham Rise, southeast of New Zealand. Site 586 on the northeastern edge of the Ontong-Java Plateau, cored during Leg 89, was included in the study. The principal objective of the paleomagnetic work was to provide a stratigraphic and chronological framework for biostratigraphic and paleoceanographic studies. Because of the relatively unconsolidated nature of the sediments, much of the coring was accomplished with the variable-length hydraulic piston corer (HPC) and the extended core barrel (XCB) rotary drilling technique. Most of the paleomagnetic results discussed here pertain to the HPC cores. Collection of duplicate HPC cores proved to be valuable.

The magnetic polarity time scale used is that of Berggren et al. (1983). Depths are given in meters below the top of the hole, which is nominally coincident with the seafloor. Intensities of magnetization are in microgauss: $1\ \mu G = 10^{-6} emu \cdot cm^{-3} = 10^{-3} Am^{-1}$. Low-field magnetic susceptibilities are quoted per unit volume in units of microgauss per oersted: $1\ \mu G\ Oe^{-1} = 10^{-6} emu \cdot cm^{-3} = 4\pi \times 10^{-6}$ SI units.

[1] Kennett, J. P., von der Borch, C. C., et al., *Init. Repts. DSDP*, Washington (U.S. Govt. Printing Office).

[2] Addresses: (Barton) Bureau of Mineral Resources, P.O. Box 378, Canberra, Australia; (Bloemendal) Graduate School of Oceanography, University of Rhode Island, Narragansett, RI 02882.

Note on Magnetic Chron Nomenclature[3]

The old system for naming magnetic chrons, as it appears in Berggren et al. (1983), is used throughout this chapter—namely, a succession of numbered chrons: C1 to C4 assigned to the Brunhes, Matuyama, Gauss, and Gilbert intervals, and C5 to C30 thereafter. It provides a convenient and widely adopted method of labelling the magnetic polarity timescale, but is somewhat arbitrary (Kent, personal communication, 1985).

The new nomenclature (LaBrecque et al., 1983; Berggren et al., in press) directly links magnetic chrons to the numbered and lettered marine magnetic anomaly sequence, using a "C" prefix. Each chron spans an upper, predominantly normal interval which corresponds to the magnetic anomaly, together with the preceding, lower, predominantly reversed interval, e.g., C5AN and C5AR for anomaly 5A. Comparisons between the two systems are illustrated in Figures 23 and 27.

GENERAL PROPERTIES OF THE SEDIMENTS

Sequences are largely composed of one lithological unit: a foraminifer–nannofossil ooze generally grading to chalk at depths of less than 300 meters. Carbonate contents are very high, typically 95 to 100%, and biosiliceous components are very low or absent, with only trace amounts of terrigenous material.

With the exception of the alternating pelagic and hemipelagic sediments of the upper 170 m at Site 594 (Unit I), all sequences display similar magnetic properties. This is true even for Site 586 on the Ontong-Java Plateau, de-

[3] Added after preparation of the manuscript.

spite its remoteness from the Lord Howe Rise. There is a surficial layer of a few tens of centimeters of oxidized sediment, pale brown-orange-yellow in color, which retains a strong magnetic remanence (1–10 μG). Reducing conditions prevail below this and iron sulfides (pyrite) are dispersed throughout as blebs, gray streaks, and gray coloration. Sediments are generally very pale gray to pale olive green to white in color. Green laminae and bands of altered volcanic ash are common. Neither these nor the iron sulfide concentrations carry a magnetic remanence noticeably higher than the surrounding sediments. Thus, it is unlikely that pyrrhotite and the less stable magnetic iron monosulfides play a significant role. Localized intensity and susceptibility spikes occur (see site chapters, this volume), but are uncorrelated with any obvious visible characteristics of the sediments.

Maximum intensities of magnetization occur in the surface oxidized layer and thereafter taper off with depth to extremely low values at typically 100 m, which are often below the noise threshold of the cryogenic magnetometer used ($\sim$0.005 μG). Reduced porosity at greater depths leads to slightly higher intensities, and in a few sequences there is a region of enhanced intensity within the Miocene.

Geometric mean intensities (Table 1) are in the range 0.03 to 0.08 μG, except for Site 588 (0.115 μG), which gave the best paleomagnetic record. These very low levels of magnetization result from dilution of the ferromagnetic content by very high carbonate contents and from diagenetic removal of primary magnetic oxides by sulfate-reducing reactions, with the accompanying production of iron sulfides (Berner, 1964; Karlin and Levi, 1983).

Deterioration, that is, increased scatter, of the paleomagnetic record with depth generally precludes polarity interpretation prior to the Gilbert (Chron 4), except at Sites 588 and 594. Median destructive field (MDF) values show considerable variation, but tend to follow the overall pattern of intensity and susceptibility variation—higher at the tops of sequences and in the deeper, more indurated sediments (a few 100 Oe), with lesser values ($\sim$50–150 Oe) in the most weakly magnetized sediments. The latter is consistent with preferential removal of the finer-grained, more stable magnetic oxides during diagenesis (Karlin and Levi, 1983).

Table 1. Some paleomagnetic statistics for Leg 90 sites.

Hole	Treatment	Axial dipole inclination (°)	Arithmetic mean inclination (°)	Geometric mean intensity (μG)	Depth range (m)
586	NRM	−1.0	5.0 ± 19.0	0.084 ± 0.72	0.00–044.4
586A	NRM		1.5 ± 32.7	0.031 ± 0.94	44.4–305.3
586B	NRM		−3.2 ± 35.2	0.044 ± 1.34	1.4–240.3
587	NRM	−37.8	−10.3 ± 42.2[a]	0.054 ± 1.51	14.4–096.2
588	NRM	−44.4	−5.0 ± 39.7[a]	0.115 ± 1.79	0.2–235.1
588A	NRM		−6.7 ± 51.6[a]	1.54 ± 1.08	236.2–336.5
588B	NRM		−10.5 ± 41.6	0.168 ± 1.76	1.0–271.8
589	NRM	−49.9	5.7 ± 48.6[a]	0.159 ± 1.14	0.2–035.0
590	NRM	−50.4	−26.5 ± 39.0[a]	0.335 ± 1.66	0.2–025.9
590A	NRM		−12.9 ± 37.6[a]	0.043 ± 1.05	27.2–280.5
590B	NRM		−5.2 ± 39.0	0.044 ± 1.14	0.1–334.3
591	NRM	−50.9	−9.1 ± 43.7[a]	0.066 ± 1.22	0.2–282.5
	AF				0.8–282.5
591A	NRM		−7.2 ± 44.0[a]	0.059 ± 1.33	0.4–253.3
592	NRM	−55.9	−5.8 ± 41.9	0.056 ± 1.14	0.2–387.1
	AF		−2.9 ± 39.8	0.021 ± 1.04	0.7–184.0
593	NRM	−59.7	−3.9 ± 41.7[a]	0.110 ± 1.63	0.1–569.6
	AF		9.8 ± 43.9	0.038 ± 1.72	0.1–569.6
593A	NRM		−2.3 ± 43.0	0.054 ± 1.10	0.2–256.4
	AF		−1.2 ± 42.1	0.025 ± 1.12	0.2–256.4
594	NRM	−20.7	−20.7 ± 38.4[a]	0.086 ± 1.21	0.2–488.1
	AF		−15.9 ± 42.3	0.050 ± 1.18	0.2–488.1
594A	NRM		−30.4 ± 33.7	0.133 ± 0.80	47.0–252.6

[a] After filtering.

The surface high-intensity zone extends up to a few tens of meters below the oxidized surficial layer, indicating that the bulk of the primary iron oxides survive the early stage of diagenesis. By far the best polarity record comes from this zone.

Bioturbation is common and intense in some sequences (e.g., Hole 586B). Because of high sedimentation rates, the length of the bioturbated zone (up to a few tens of centimeters) is very short compared with a typical polarity interval. The paleomagnetic record does not appear to be adversely affected by bioturbation.

INFLUENCE OF BIOGENIC SILICA

Previous studies of Cenozoic marine calcareous sequences have usually provided good paleomagnetic records (e.g., eastern equatorial Pacific—Kent and Spariosu, 1982b; northwest Pacific—Weinreich and Theyer, in press; Bleil, in press; South Atlantic—Tauxe et al., 1983, 1984), although seldom have NRM intensities been as low as encountered in this study. A characteristic of carbonate sequences that provide good paleomagnetic data is the presence of biogenic siliceous material (Kent and Spariosu's, 1982a, work on Caribbean cores is an exception, but these contained relatively large terrigenous components). Siliceous material is noticeably absent from or only present in trace amounts in most Leg 90 sediments. This is despite normal abundances in the present-day water column. Bleil (in press) comments "biosiliceous sediments carry a predominantly strong remanent magnetism, whereas increasing amounts of calcareous components result in drastic reduction of the NRM intensities." A contributing factor to this contrast may be differences in the sediment matrix created by calcareous fossils, which tend to be rounded, and siliceous fossils, which are generally "skeletal." This must affect the physical stability of very fine-grained interstitial magnetic particles during compaction.

CARBONATE DILUTION

On the Lord Howe Rise, which is well above the calcium carbonate compensation depth and has high carbonate productivity, dilution of the ferromagnetic input results in very low levels of magnetization. The scale of the effect is illustrated in Figure 1, which is based on a starting composition of 99% nonmagnetic matrix ($CaCO_3$ in this case), and 1% magnetic component. At these dilutions the NRM intensity is very sensitive to small fluctuations in carbonate content. The sensitivity drops off fairly rapidly for lower initial carbonate contents. Since carbonate contents close to 100% are not uncommon, a substantial part of the observed intensity variation could thus be caused by small fluctuations in carbonate content. However, this explanation is not sufficient to explain the intensity variations completely since a positive correlation exists between NRM intensity and modified Koenigsberger-ratio variations. Based on a sim-

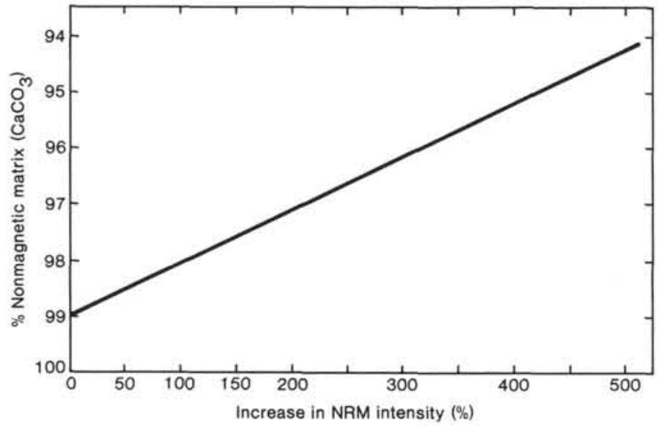

Figure 1. Variation of NRM intensity with calcium carbonate content, assuming a constant rate of input of magnetic material. The curve is based on an initial composition of 99% nonmagnetic matrix and 1% magnetic component.

ple dilution model, these two parameters would be constant.

METHODS

Sampling densities were typically three specimens per core section for HPC cores from the first hole, two specimens per section for HPC and XCB cores from the second hole, and one specimen per section for conventional, rotary-drilled cores. Results demonstrate that this sampling density is barely adequate (see, e.g., Site 588 results) despite the very large collection of specimens produced—more than 5900.

Shipboard measurements of the horizontal NRM component (D and H) of whole-core sections was abandoned after Site 588. It became apparent that there was little prospect of improving on the amount of information available from normal subsampling, because the very low remanence intensities were not sufficiently above instrumental noise and rust contamination levels. The shipboard Digico magnetometer was used for NRM measurements of some of the more strongly magnetized material, generally the surficial zone only. All subsequent remanence measurements were made on the three-axis SCT cryogenic magnetometer at the University of Rhode Island. Software modifications were made to permit user-selected integration times to improve the signal-to-noise ratio. To allow longer integration times a two-position (instead of three) measuring sequence was adopted to give full cancellation of vertical holder and induced moments, but incomplete cancellation of the horizontal component of the holder. Thus inclination (Z, to be precise) is better determined than declination. In interpretation, data were discarded if (1) intensities were less than 0.008 μG; (2) the angle between the magnetic vector for each of the two specimen positions exceeded 45°; or (3) an internal measurement variance threshold was exceeded. Despite these very loose criteria, typically 10–15% of the data were discarded. This process is referred to as "filtering."

VRM Tests

To evaluate the importance of viscous remanence (VRM), selected specimens from Sites 590, 593, and 594 were (1) AF demagnetized at 600 Oe; (2) left in a field of 10 Oe for 1000 hr. and measured periodically; (3) placed in the shielded sense region of the cryogenic magnetometer and measured periodically for an interval of 1000 s; (4) returned to the 10-Oe field to restore the VRM; (5) progressively AF demagnetized. Results are summarized in Table 2. An ambient field of 10 Oe was used to produce a more easily measurable remanence. By assuming a linear field dependence of VRM for the time scale concerned (Shimizu, 1960), then VRMs acquired in 0.5-Oe ambient field (i.e., a realistic site value) can be estimated by dividing by 20. As a measure of the relative importance of VRM, the ratio $R = 0.05\ J_V/J_N$ is used, where J_V is the viscous remanence acquired in 10 Oe after 1000 hr. and J_N is the natural remanence. Values greater than 10% are considered to be high. Since sediments are more susceptible to VRM prior to AF demagnetization (e.g., Lowrie and Kent, 1978), our estimates of R should be treated as lower bounds.

Table 2. Summary of NRM and VRM test data.

		NRM		VRM		
Sample (level in cm)	Depth (m)	J_N (μG)	MDF_N (Oe)	J_V* (μG)	MDF_V (Oe)	$J_V/20 \times J_N \times 100$
590-1-4, 130	5.80	0.196	344	1.10	59	28
590A-8-2, 20	95.10	0.046	244	0.52	51	57
590A-12-1, 125	133.05	0.138	130	0.20	69	7
593-1-1, 10	0.10	2.374	300	11.97	43	25
593-1-1, 45	0.45	1.361	>600	1.07	117	4
593-6-2, 125	46.25	0.198	244	0.37	62	9
593-7-6, 25	60.85	0.100	231	0.18	89	9
593-9-6, 25	80.05	0.154	207	0.15	86	5
593-13-5, 75	117.45	0.160	116	0.06	~80	2
593-16-4, 125	145.25	0.103	98	0.08	~70	4
593-22-1, 25	197.35	0.264	217	0.05	119	1
593-28-5, 25	260.95	0.065	185	0.11	100	8
593-31-5, 25	289.75	0.217	175	0.06	146	1
593-36-2, 125	334.25	0.125	469	0.30	96	12
593-40-4, 75	375.15	1.120	95	10.67	62	48
593-44-3, 75	412.05	2.345	276	19.61	153	42
593-45-6, 75	426.15	3.809	~190	21.57	67	28
593-48-3, 75	450.45	0.297	364	3.73	92	63
593-54-3, 25	507.55	0.059	145	0.07	78	6
593-60-3, 125	566.15	0.050	190	0.08	172	8
594-1-1, 25	0.25	0.535	331	3.82	83	36
594-1-1, 75	0.75	0.509		2.09	69	21
594-1-4, 75	5.25	3.686	127	6.31	91	9
594-3-3, 75	19.25	0.509		1.42	64	14
594-3-5, 75	22.25	0.374	300	1.09	61	15
594-5-1, 75	35.45	0.331	178	1.56	61	24
594-5-4, 25	39.45	0.214		1.22	67	29
594-5-4, 75	39.95	1.194	221	1.09	59	5
594-10-2, 25	84.45	0.159	90	1.24	60	39
594-11-1, 75	93.05	0.284	44	1.17	46	21
594-13-4, 125	117.25	0.267	199	1.49	55	28
594-15-5, 25	136.95	0.302	208	1.49	53	25
594-20-3, 125	182.95	0.179	148	1.23	21	34
594-24-5, 25	223.35	0.307	242	0.29	60	5
594-27-5, 25	252.15	0.047	114	0.37	50	40
594-28-1, 125	256.75	0.175		0.35	19	10
594-34-4, 125	318.85	0.374	219	0.28	75	4
594-40-3, 25	373.95	0.432	306	0.26	49	3
594-50-1, 125	467.95	0.174	>600	4.00	136	115

Susceptibility and Q′ Ratio

Initial, low-field magnetic susceptibility measurements were made on most specimens using a Digico bulk susceptibility bridge system. Susceptibilities were commonly dominated by the diamagnetic contributions from water and calcium carbonate. To compensate, an average diamagnetic contribution of $-1.00\ \mu G\ Oe^{-1}$, based on 50% by volume of water and calcium carbonate, respectively, was subtracted from observed susceptibilities, (i.e., the values discussed herein, denoted by χ', refer to the dry noncarbonate component of the sediment). The modified Koenigsberger ratio used is defined as $Q' =$ NRM intensity/χ'.

Orientation and Declination Scatter

Although the Kuster tool used for absolute orientation of cores was moderately successful in producing legible photographic disks, the orientation information generally was inconsistent with paleomagnetic declinations. In agreement with other authors (e.g., Leg 68, Kent and Spariosu, 1982a, b), we conclude that the orientation system is of little or no value. This is a serious handicap for equatorial sites such as Site 586.

Even allowing for the lower precision in measuring declination discussed previously, declination scatter was much greater than for inclination and must be attributed partly to twisting of the sediment column and partial remagnetization during coring, slicing, and handling. For these reasons polarity determination is based almost entirely on inclination data.

AF DEMAGNETIZATION

Alternating magnetic field (AF) cleaning was performed at a peak field of 150 Oe for Holes 586, 586B, 587, 589, and 594, and at 200 Oe for the remaining holes. A few sequences still remain to be cleaned. Stepwise AF demagnetization of individual specimens is preferable to blanket treatment, but rarely leads to more than minor refinements in polarity data from deep-sea sediments and would have been impractical for the present study.

Typical responses of specimens to progressive demagnetization are illustrated in Figure 2, Parts A–E. Hoffman-Day plots depict directions of the magnetic vector removed during successive demagnetization steps (Hoffman and Day, 1978).

A. Single-component stable remanence with a soft overprint of the same polarity. Virtually all specimens showed some evidence of a small soft viscous remanence;

B. As (A), but with soft overprinting of opposite polarity;

C. Two-component remanence with a harder component of very steep inclination, probably imparted during coring. A number of specimens showed this behavior;

D. As (C), but with the softer component imparted during coring—less common.

E. Poor stability, but of constant polarity. Many specimens fell into this class and were considered sufficiently stable to give usable polarity information;

F. Unstable behavior—usually confined to very weakly magnetized sediments and quite common (not illustrated).

The examples chosen illustrate the classes of behavior more clearly than most specimens. Virtually all specimens showed evidence of varying degrees of VRM overprinting, which was easily removed in fields of less than 150 Oe. Surface high-intensity zones and indurated sediments (chalk) toward the bottom of long sequences gave the highest MDFs and greatest directional stability (Fig. 3). However, the large scatter in directions characteristic of much of the latter suggests either that the remanence is not of primary origin or that material was disturbed during drilling.

SCATTER CAUSED BY COMPACTION

Physical compaction of sediments involves juxtaposition of grains to form a more closely packed structure. Magnetic particles in the sediment with a preferential initial alignment will become dispersed in direction during this process. Generally there are enough magnetic particles contributing to the remanence that, provided the directional dispersion is unbiased during compaction, the resultant magnetic vector will be smaller in magnitude but unchanged in direction. However, in sufficiently weakly magnetized sediments such statistical averaging will no longer apply, and compaction may cause significant changes in direction of the magnetic remanence.

To estimate the scale of the effect in Leg 90 sediments, suppose the intensity of magnetization of a 6.5 cm^3 specimen is 0.01 μG. If we neglect grain interaction, the diameter of one saturated magnetite sphere that would account for this is 6.4 μm, which is within the size range of pseudosingle domain behavior. Thus, it is possible that the remanence of many specimens is carried by a very small number of particles and that compaction accounts for much of the scatter observed in the weakly magnetized sediments despite their carrying a hard stable remanence.

MAGNETOSTRATIGRAPHY

Magnetostratigraphy and sedimentation rate summaries are presented in Figures 4 and 5. Results pertaining to particular sites are discussed later. Prior to the first few most recent magnetic reversals at each site, which were self-evident, biostratigraphies were used as a first-order guide for establishing approximate positions on the polarity time scale. This became increasingly necessary at greater depths. With few exceptions, final interpretations are generally in good agreement with the biostratigraphies and can be used to refine the assigned time scales. Speculative interpretations are omitted and single-point polarity intervals are ignored except in special circumstances (e.g., supporting evidence from a duplicate hole).

Site 586

Duplicate sequences were recovered: Hole 586 plus Hole 586A (0.0–44.4–305.3 m) and Hole 586B from 0 to 240.3 m. It was suspected that the top of Hole 586B was started 1.4 m below the mudline. The surficial oxidized layer is confined to the upper 0.15 m of Hole 586. Pyrite is common throughout the sequence. Biosiliceous material, mostly radiolarians, is only a minor component but is much more common than at most Leg 90 sites.

NRM measurements were completed for both sequences, and Hole 586 and the upper eight cores of Hole 586B were AF cleaned at 150 Oe (Fig. 6). Inclinations are widely scattered about the axial dipole value of $+1.0°$ (Table 1, Fig. 7). There is no bias to suggest a systematic overprint, and the distribution of inclinations in Hole 586 was affected little by AF cleaning.

Intensities of magnetization are high (~ 4 μG) in the upper 16 m of Hole 586B, followed by a rapid decrease to about 0.3 μG over the next meter, then a gradual falloff with depth to extremely low values and a corresponding increase in directional scatter. Intensities increase again below 250 m in Hole 586, but directional scatter remains high. In the absence of inclination information and because of high scatter in declinations, only the Brunhes/Matuyama boundary is identified—between 15.0 and 15.75 m (586B-2-3, 100 cm to 586B-2-4, 25 cm). This lies within the upper three cores of Hole 586 that were disturbed and not sampled. Assuming the top of Hole 586B is 1.4 m below the seafloor, a mean sedimentation rate of 22.5 to 23.5 m/m.y. is given, which is in agreement with the biostratigraphically determined rate.

Below the high-intensity surface zone, stability on progressive AF demagnetization was generally poor and lower than at many other sites, despite an average MDF of 173 Oe (for 13 specimens distributed throughout the sequence).

Carbonate contents are relatively low in the upper part of the sequence and show an inverse relationship with intensity of magnetization (J): less than 85% in the upper 10 m where J is high; 85–93% from 10 to 120 m with intermediate-low J; 93–100% below 120 m where extremely low values of J occur. The simple carbonate dilution model discussed earlier can explain most of the variation, but not the transition from high values at the top of the sequence, which must be a diagenetic effect.

Site 587

A single hole was cored at Site 587. Paleomagnetic data were obtained from Cores 587-3 to 587-11 (Fig. 8). Cores 587-1 and 587-2 were completely disturbed and some of the other cores were partially disturbed. Because of this and the high scatter in the data below 40 m, the magnetostratigraphy is poorly defined prior to the Olduvai Subchron. The sequence is devoid of siliceous fossils, and disseminated inclusions of fine-grained authigenic iron sulfide (presumably pyrite) occur occasionally throughout.

The usual surface high-intensity zone presumably was missed in the first two cores. Cores 587-4 and 587-5 contain a high-intensity zone that coincides with high carbonate content (96%). Inclination distributions barely show the expected bipolarity even after AF cleaning (Fig. 9), which is a measure of the poor quality of the data from this site. The normal bias is partly an artifact of the short record length, but probably also indicates incomplete removal of a normal overprint. Median destructive fields are fairly high (217 $\pm$81 Oe ($\pm$s.d.) for four specimens) with moderate stability, so the high-directional scatter observed appears to be an intrinsic property of the characteristic remanence. Magnetic susceptibilities of the dry noncarbonate component followed the general trend of NRM intensity variations. Values of Q' were noticeably higher (typically 0.1–0.9) in the more strongly magnetized sediments above 40 m, which give the best paleomagnetic record. Below this level, Q' was generally less than 0.1. Such values are higher than at most sites. Six specimens remained diamagnetic even after the susceptibility correction for water and carbonate content.

Because of the incidence of coring disturbance and generally poor magnetic properties, the polarity interpretation is not made with a high degree of confidence. AF cleaning significantly improved the stratigraphy. Preferred polarity assignments are summarized in Figure 10, Scheme A. To conform with NN21/NN19 nannofossil interval (587-3-3, 20 cm to 587-3-4, 20 cm), normal polarities in Core 587-3 must be assigned to the lower part of the Brunhes Chron. Both the Jaramillo and the Olduvai subchrons are therefore lost in Core 587-4, which was badly disturbed, and only three specimens were recovered. Hence, we cannot pinpoint the Pliocene/Pleistocene boundary. Biostratigraphically, the boundary is determined to be either at Samples 587-4,CC to 587-5-1, 44 cm (planktonic foraminifers), or at 587-4-4, 4 cm to 587-4-5, 4 cm (nannofossils). Occurrence of the Matuyama–Gauss reversal at the top of Core 587-5 favors the latter. The base of the Gauss at the bottom of Core 587-5 agrees well with the NN15/NN16 nannofossil zone boundary at Samples 587-5-5, 4 cm to 587-5-6, 4 cm.

Below this the magnetostratigraphy is less clear. The four normal subchrons in the Gilbert are either missing or inadequately resolved (single data points). Optimum consistency with the biostratigraphy is obtained if the lower half of Core 587-7 is assigned to Chron 5 (Magnetic Anomaly 3A), and reversed polarities in the upper half of Core 587-7 represent the upper half of Chron 6. No interpretation is yet made below Core 8. Paleomagnetic placement of the Miocene/Pliocene boundary, which occurs just above Magnetic Anomaly 3A (Chron 5), again favors the nannofossil scheme that puts the boundary at 587-7-4, 4 cm to 587-7-5, 4 cm. This preferred polarity interpretation produces fairly uniform, low sedimentation rates except within the Brunhes and Matuyama chrons. An alternative interpretation (Fig. 10, Scheme B) is to assign the normal interval in Core 587-3 to the Olduvai Subchron. This produces more uniform sedimentation rates during the major intervals, but is a poorer match with the biostratigraphy.

Site 588

Record HPC penetration was achieved: Hole 588 from 0.0 to 236.0 m (9.6-m length cores) followed by Hole 588A from 236.0 to 315.0 m (5 m-length cores from Cores 588A-2 to 588A-15). The remaining three cores of Hole 588A were rotary drilled with the XCB to 344.4 m sub-bottom depth. Duplicate HPC cores obtained to 277.4 m in Hole 588B provided an invaluable cross check on the paleomagnetic results. Rotary drilling was continued in Hole 588C to 488.1 m, but no paleomagnetic data are available yet.

The sequence at Site 588 is characterized by the usual surface layer of brown oxidized material (Unit IA). Siliceous microfossils are almost completely absent down to 469 m (Units IB and IC), but relatively abundant thereafter. Iron sulfides are persistent throughout the section and disseminated volcanic ash and glass occur in Units IB and IC. Light green–gray altered ash layers tend to occur above gray sulfide streaks, suggesting that ash concentrations provide a source of iron during diagenesis. The level of bioturbation is relatively low.

Calcium carbonate content exerts a strong influence on the remanent magnetic properties of the sediments: higher contents correspond to lower NRM intensity (and susceptibility) and high directional scatter. Highest intensities are from 0 to 35 m and 205 to 315 m sub-bottom depth, where carbonate contents are relatively low—approximately 92%. Where the paleomagnetic signal is most scattered (about 70–130 m), intensities are the lowest and carbonate contents are 96–97%. As discussed previously, a simple carbonate dilution model predicts such high sensitivity to small compositional changes in carbonate-rich sediments.

The downcore pattern of intensity variation is: high values ($\sim 1\ \mu$G) for the first four cores, 0 to 35 m; a fairly rapid decay with depth down to very low values from 75 to 170 m; rise to high values (1 μG) in Core 22 around 207 m; and a gradual increase with depth to about 25 μG at 336 m, which is the limit of current paleomagnetic measurements. Dry noncarbonate susceptibilities (measured for Hole 588 only) were all positive and followed the same pattern of variation as intensities. Modified Q' ratios were higher than in most sequences, typically 0.3 to 1.0 from 0 to 37 m; 0.01 to 0.2 from 37 to 190 m; and 0.1 to 0.8, increasing with depth below 190 m. These

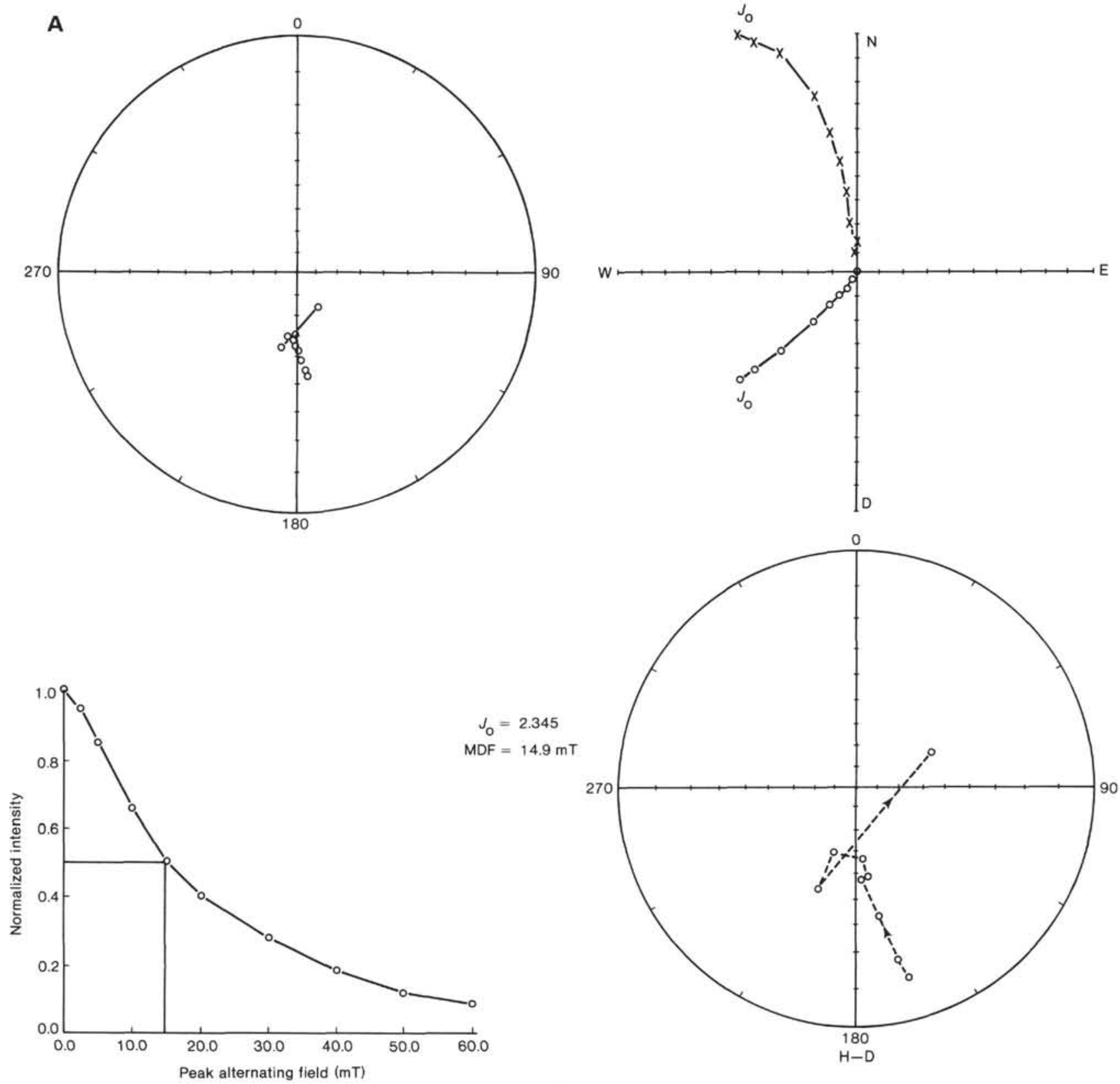

Figure 2. Progressive demagnetization plots for various classes of behavior. On the stereo (top left) and Hoffman-Day (H-D) (bottom right) plots, crosses denote positive inclination. On the Zijderveld plots crosses denote projections on the vertical east-west plane, and circles denote projections on the horizontal plane. The classes of behavior are discussed in the text. A. Sample 588-25-3, 125 cm; depth = 230.65 m. B. Sample 593-1-1, 10 cm; depth = 0.10 m. C. Sample 593-40-4, 75 cm; depth = 375.15 m. D. Sample 594-24-5, 25 cm; depth = 223.35 m. E. Sample 594-6-3, 75 cm; depth = 48.05 m.

relatively high values are reflected in the better quality of the paleomagnetic record and probably result partly from higher concentrations of volcanic material in the sequence.

Inclination distributions (Fig. 11) fail to show the bimodality of a stable primary remanence and reflect the large number of intermediate directions. It is interesting that AF cleaning produces an overall reduction in reverse directions—again indicating a reverse overprint acquired during drilling. The bias toward inclinations steeper than the axial dipole seen in NRM data for Hole 588A further supports the idea of a drilling-induced remanence, but suggests that it may have either polarity.

Progressive AF demagnetization of eight specimens from Hole 588 gave an average MDF of 175 ±99 Oe (± s.d.) Harder magnetic remanence and greatest stability are associated with the more strongly magnetized sediments at the top and bottom of the sequence. Small, soft components removed at fields of 50 to 100 Oe were common.

AF cleaning (Hole 588 data only) was performed in a peak field of 200 Oe, but produced no substantial

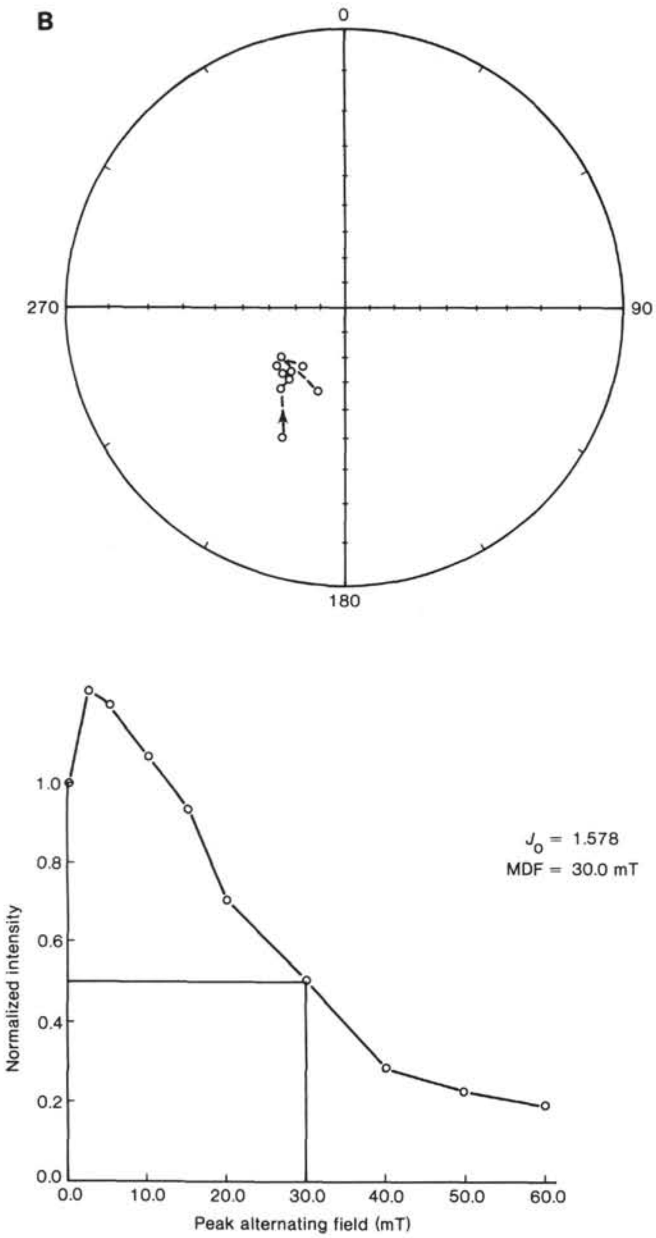

Figure 2. (Continued).

change in the polarity record. In the more weakly magnetized zones, directional scatter was noticeably reduced. A small reverse overprint was evident in the upper 30 m and probably was acquired during coring.

A complete polarity sequence has been identified for Hole 588. This is tentatively extended to the upper five cores (30 m) of Hole 588A for which we only have NRM data (Figs. 12, 13). The polarity sequence is consistent with, and further refines, the planktonic nannofossil stratigraphy with the exception of the placement on the polarity time scale of the long normal interval in Cores 588-24 and 588-25. There is a corresponding long normal zone in Cores 588B-24 through 588B-27 and perhaps 588B-28. The length of the zone in Hole 588B indicates that Hole 588A started closer to 242 m sub-bottom rather than 236 m as recorded during drilling operations. Unless the zone coincides precisely with an interval of unusually high deposition, it must correspond to Chron 9 (8.92 to 10.42 Ma) in the early late Miocene, which is the only very long normal polarity interval anywhere near the expected age. (The next best candidate is Chron 19 in the early Miocene.) Our interpretation requires that the middle to late Miocene boundary be placed in the region of Core 588A-5 (265 m) rather than at about 214 m in Core 588-23 as determined from the NN9/NN10 nannofossil zone boundary. Further support for our interpretation lies in the fact that below Chron 9 there is a one-to-one correspondence with the polarity time scale without invoking hiatuses or large departures from uniform sedimentation.

It is not clear why Site 588 produces the longest paleomagnetic record. Biogenic siliceous content is not above

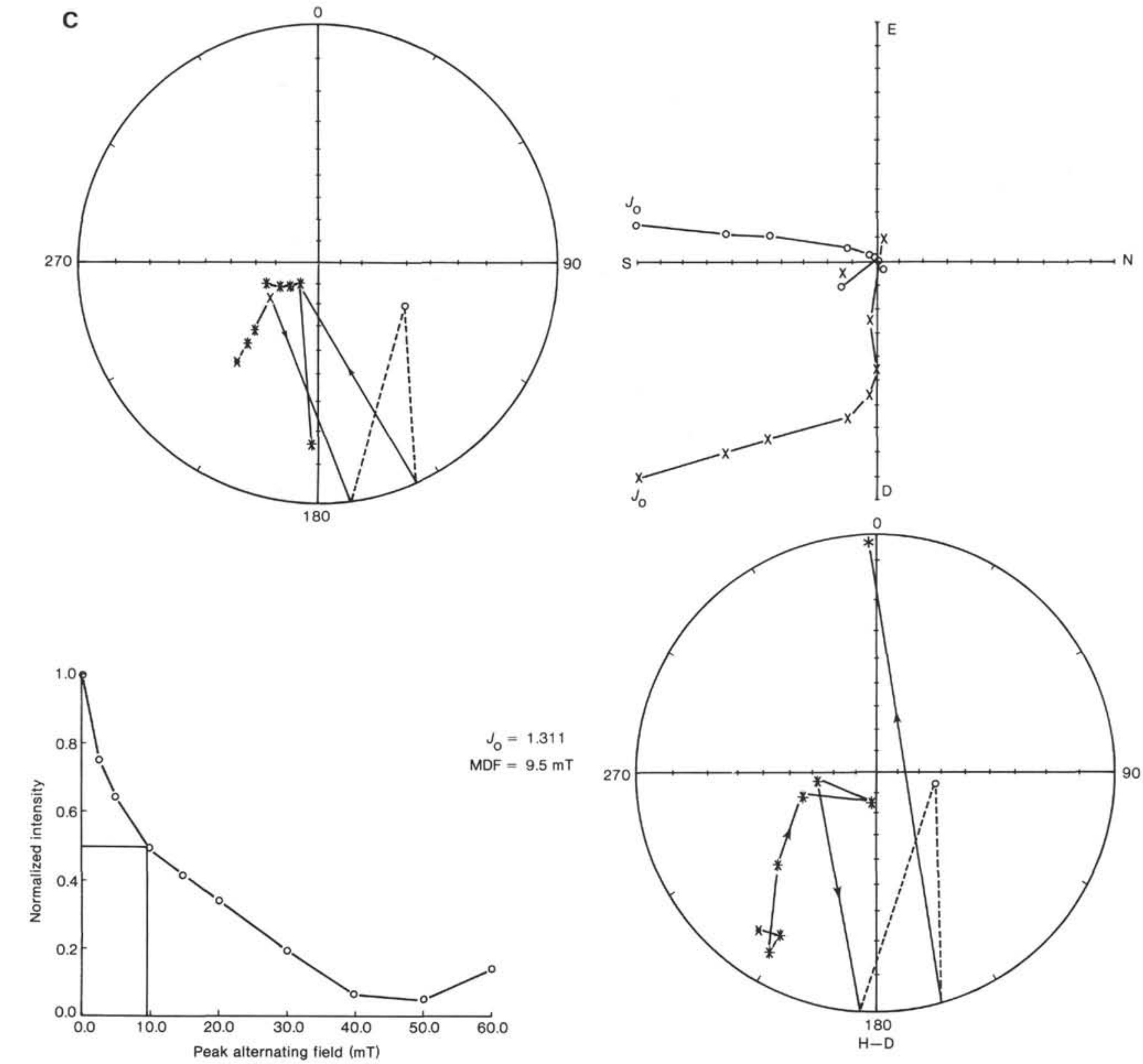

Figure 2. (Continued).

average for the relevant part of the sequence (though it is lower down in Unit II); above the lower high-intensity zone (~200 m) intensities are not noticeably stronger; and behavior during progressive demagnetization did not show any unusual characteristics (although the sample size of eight is not adequate). The only key factor appears to be the above-normal incidence of volcanic ash layers.

Site 589

Four HPC cores were recovered, reaching a sub-bottom depth of 36.1 m. Sediments are similar to those at Site 588 with a surface oxidized layer from 0 to 0.4 m. Median destructive fields at 4.75 and 23.15 m were 431 and 133 Oe, respectively. Q′ ratios were lower than at Site 588: typically 0.07 to 1.75 above 4.8 m and 0.03 to 0.12 below this depth.

The inclination distribution becomes more bimodal after AF cleaning at 150 Oe (Fig. 14), but the vector results (Fig. 15) are not changed significantly. Two polarity interpretations are possible (Fig. 16), depending on whether the normal zone from 31.5 to 34.0 m is assigned to the Olduvai Subchron (Scheme A) or to the normal interval of the upper Gauss (Scheme B), with the Olduvai not recorded. Scheme A gives the better fit to the biostratigraphy, although Scheme B is consistent with more uniform sedimentation. The former is used in Figures 4 and 5.

Site 590

Holes 590 (from 0 to 26.2 m) and 590A gave continuous HPC recovery to a depth of 280.8 m; we have a complete set of AF-cleaned data at 200 Oe. NRM data are available to 335 m in duplicate Hole 590B (HPC to

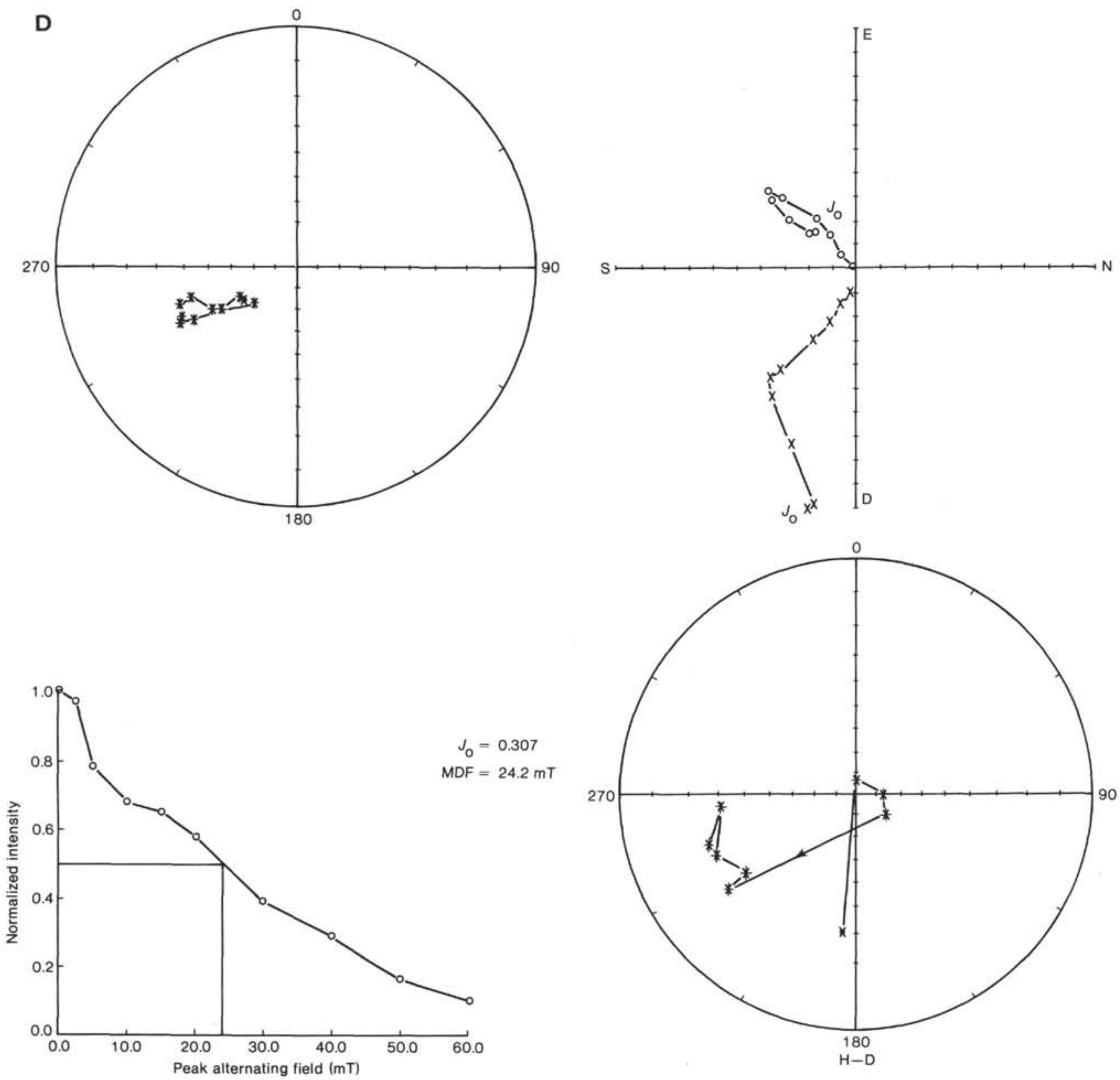

Figure 2. (Continued).

250.7 m then XCB rotary drilling to 499.1 m). This is the shallowest site cored and is not far from Site 589.

The lithology is fairly typical of Leg 90 sites. The surface oxidized layer (Unit IA) occupies the upper 0.4 m of the sequence, whereas the high-intensity zone (~ 1 μG) extends throughout Core 590-1. A rapid step down to values around 0.1 μG in Core 590-2 suggests that diagenetic alteration of primary iron oxides was unusually rapid at this site. Biosiliceous material is generally absent and authigenic iron sulfides occur throughout in burrows, foraminifer tests, and finely dispersed medium gray streaks and halos. Neither the altered volcanic ash concentrations nor the concretions containing pyrite that are distributed throughout the sequence carry a NRM that is noticeably stronger than that of the surrounding sediments. Bioturbation is slight down to about 200 m, moderate to about 300 m, and intense thereafter.

Progressive demagnetization data for six specimens show MDFs tending to decrease with depth from 421 Oe in the surface oxidized layer to about 116 Oe at 215 m. A very soft VRM is present in most specimens, and there is evidence for a somewhat harder quasivertical overprint, probably acquired during coring. To illustrate more systematically the presence of a fairly soft overprint (e.g., present-day or drilling remanence), a downcore plot was generated of the vector removed by AF cleaning. This difference vector was highly scattered, but showed a normal bias in certain zones: 0–13 m, 30–35 m, 45–62 m, 155–190 m, and 213–240 m. There were only a few short intervals in which the difference vector was systemati-

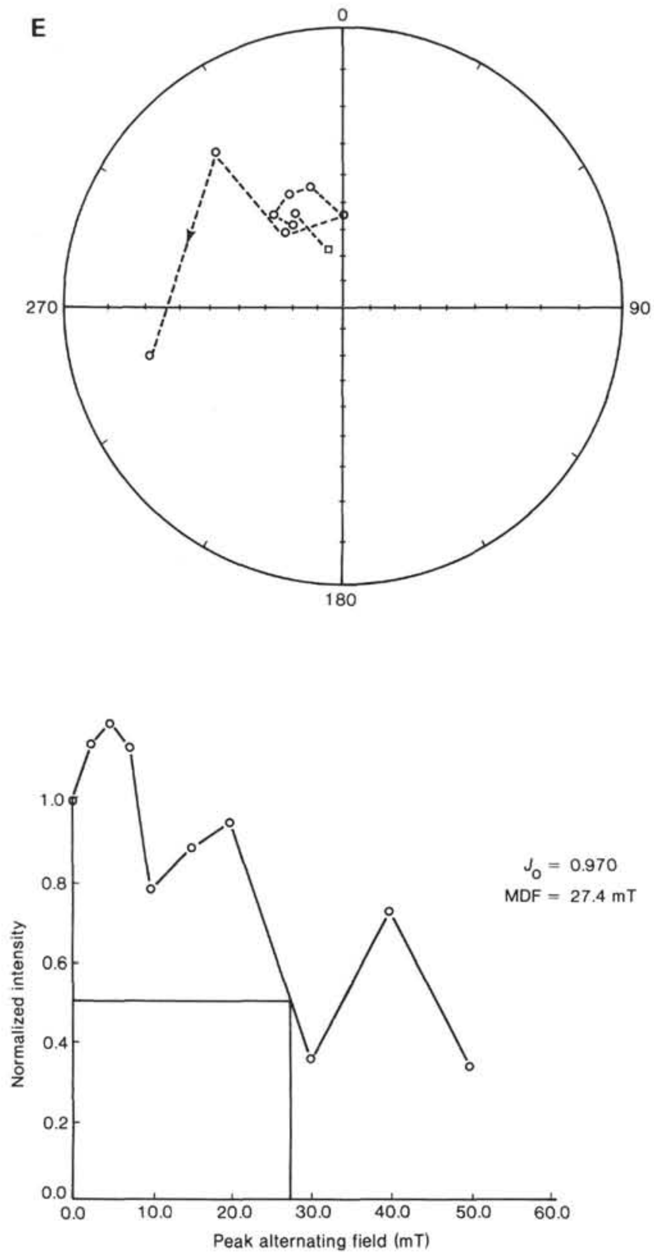

Figure 2. (Continued).

cally reversed. The ratio of the magnitude of the difference vector to the NRM vector (J_D/J_N) varied between about 0.3 to 1.0 within the upper 100 m. This suggests that although a substantial part of the natural remanence is soft, and probably of viscous origin, it is not sufficient to entirely mask the hard (primary?) component. Lower in the sequence, J_D/J_N was slightly higher on the average and more variable. VRM acquisition test results (Table 2) indicate that viscous effects are unlikely to dominate the natural remanence except in the most weakly magnetized sediments.

Above the beginning of the late Pliocene at about 90 m there is a subtle change in lithology, from uniform light gray to white nannofossil ooze to alternating layers of a very pale gray foraminifer-bearing nannofossil ooze and light gray foraminifer–nannofossil ooze (increased current winnowing). The interpretable part of the paleomagnetic record (Fig. 17) is confined to this upper section, where intensities are moderate: typically 0.08 to 0.1 μG, mean MDF is 263 Oe (three specimens) and Q′ is typically 0.02 to 0.15. The polarity sequence down to the base of the Gauss is duplicated in the NRM data from Hole 590B. Evidence for the Cochiti Subchron near the bottom of Core 590A-8 is not confirmed yet in the duplicate core. Prior to this, directions are highly scattered. A more lithified zone of moderate intensity (0.05–0.2 μG) occurs between 270 and 335 m in Hole 590B, which contains a well-defined long interval of nor-

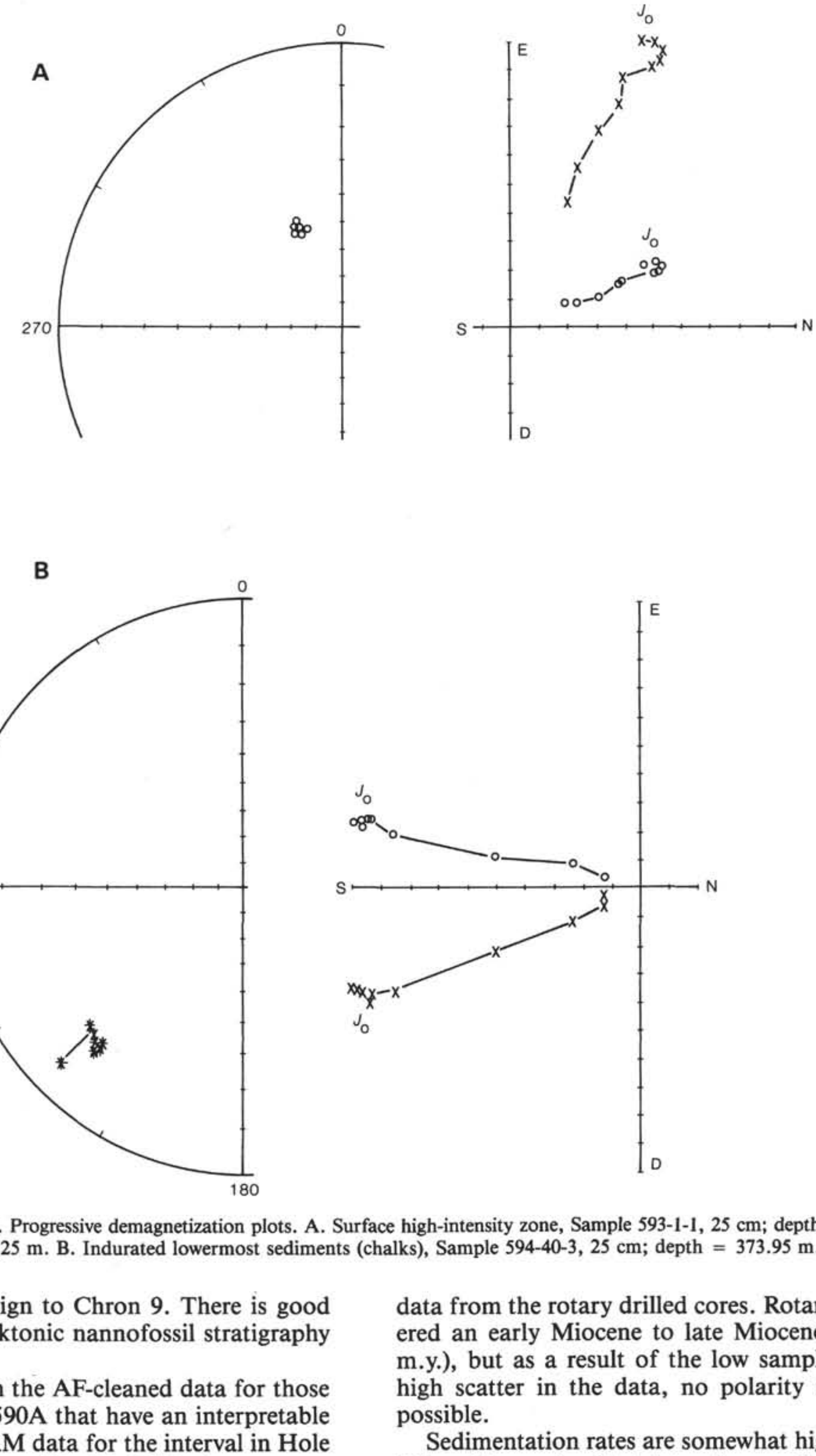

Figure 3. Progressive demagnetization plots. A. Surface high-intensity zone, Sample 593-1-1, 25 cm; depth = 0.25 m. B. Indurated lowermost sediments (chalks), Sample 594-40-3, 25 cm; depth = 373.95 m.

mal polarity that we assign to Chron 9. There is good agreement with the planktonic nannofossil stratigraphy for the site.

Tables 3 and 4 contain the AF-cleaned data for those parts of Holes 590 and 590A that have an interpretable polarity stratigraphy. NRM data for the interval in Hole 590B spanning Chron 9 are listed in Table 5.

Site 591

Although on an eastern spur of the central Lord Howe Rise, Site 591 is in the same general area as Sites 589 and 590. We have AF-cleaned data (at 150 Oe) for the first HPC—Hole 591, 0.0 to 283.1 m; NRM data for the duplicate HPC—Hole 591, 0.0 to 246.5 m; and some NRM data from the rotary drilled cores. Rotary drilling recovered an early Miocene to late Miocene section (17–11 m.y.), but as a result of the low sampling density and high scatter in the data, no polarity interpretation is possible.

Sedimentation rates are somewhat higher than at Site 590 and the surface high-intensity zone is narrower. Otherwise, the magnetic properties of the sequence are similar to Site 590. The zone of enhanced intensity in the middle Miocene at site 588 does not appear at this site. Median destructive fields were fairly high in the surface high-intensity layer (260 Oe) and moderate to low (120–155 Oe) in the very weakly magnetized midhole region. Inclination distribution for Hole 591 became more bi-

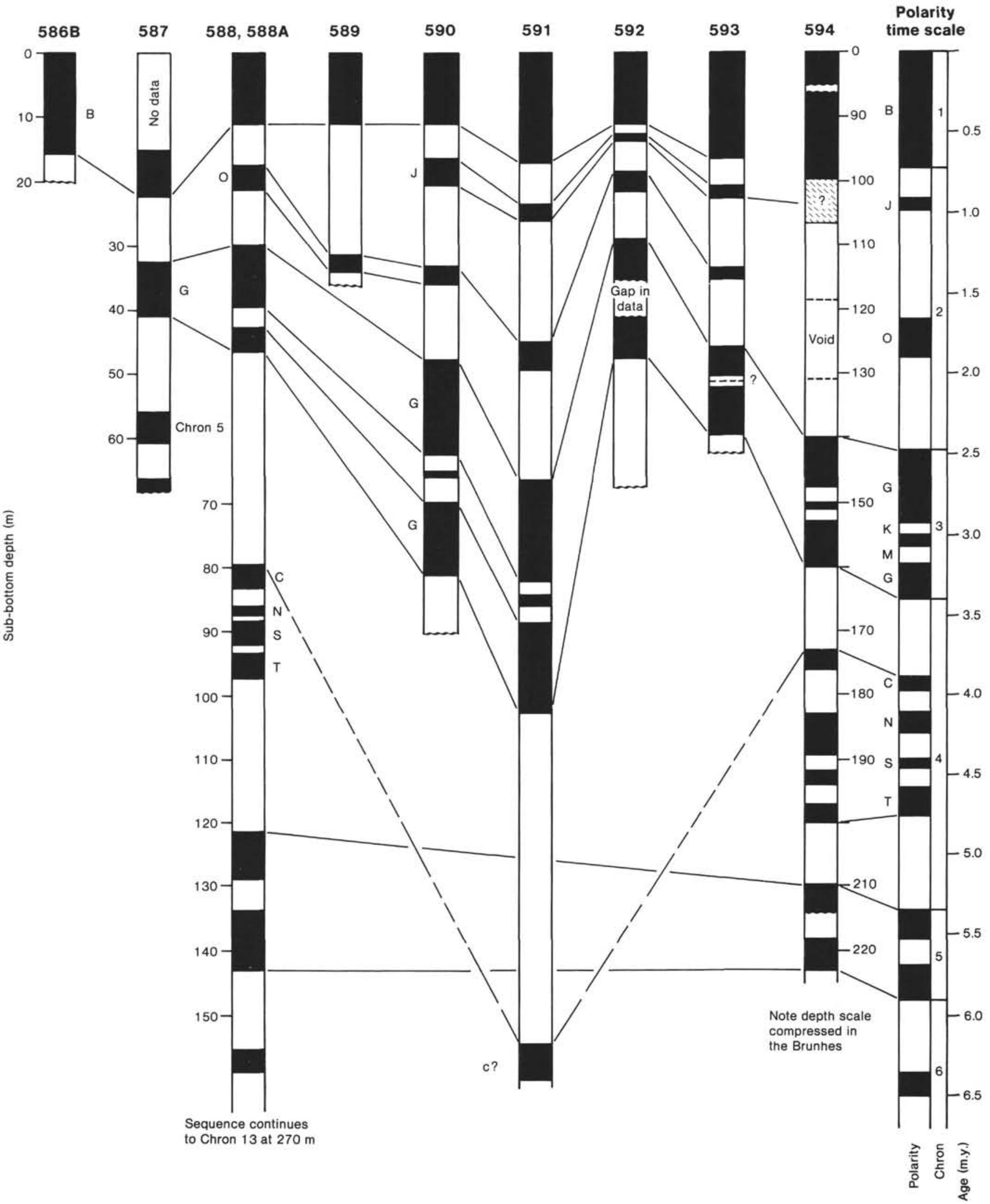

Figure 4. Magnetostratigraphy summary. B = Brunhes, J = Jaramillo, O = Olduvai, G = Gauss, N = Nunivak, S = Sidufjall, T = Thvera. Columns are terminated at levels beyond which no interpretation has yet been possible. The polarity time scale on the right is that of Berggren et al. (1983).

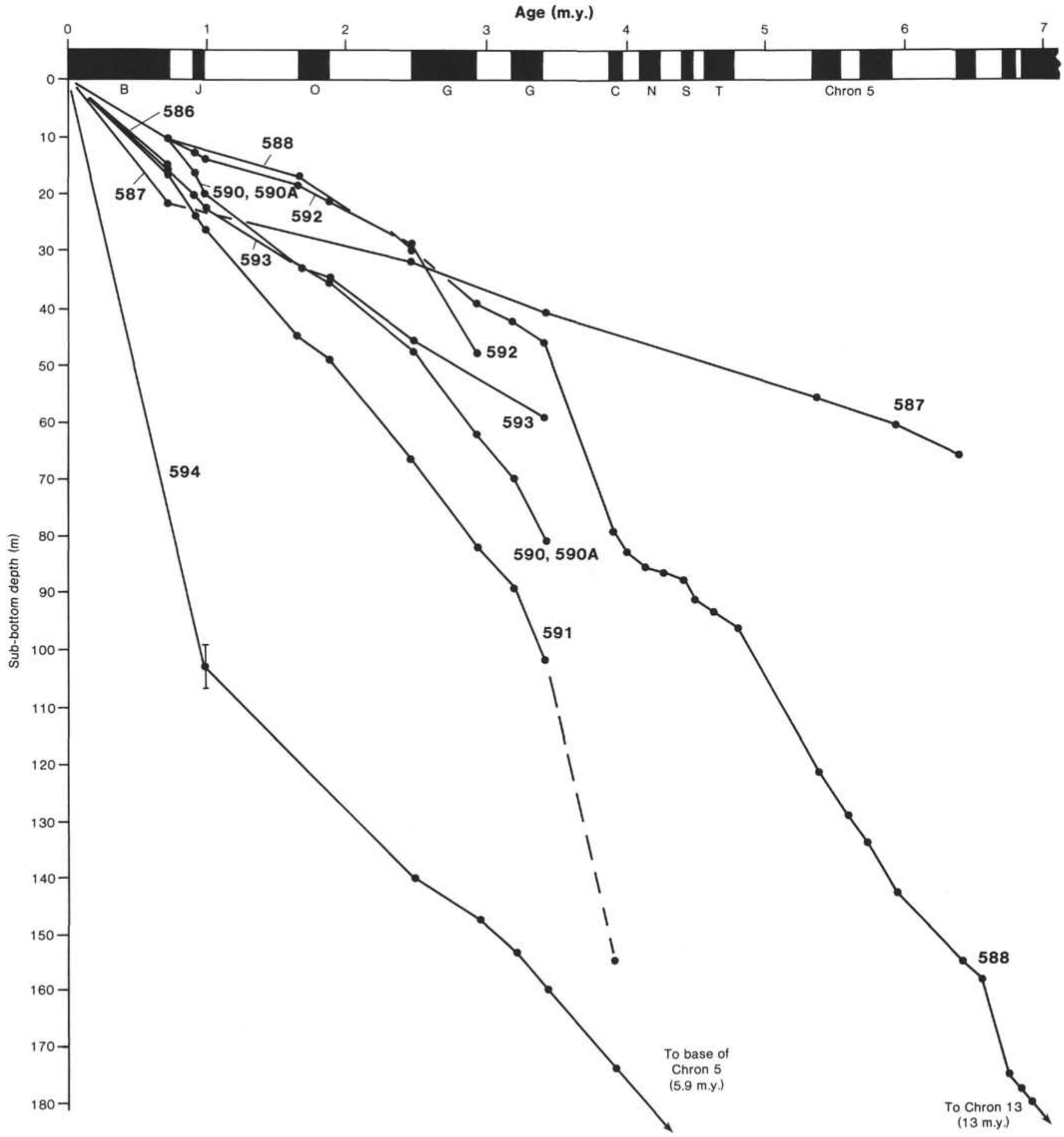

Figure 5. Sedimentation rate summary based on paleomagnetic data.

modal after AF cleaning (Fig. 18), but there remains a very high proportion of intermediate directions. In the upper 150 m the distribution is better grouped about the normal and reversed axial dipole directions. Within this region the inclination of the difference vector, $\overrightarrow{\mathrm{NRM}-\mathrm{AF}}$, tracked variations in the AF-cleaned vector (indicating single-component remanence), except in the upper Matuyama where it had normal polarity. Throughout the Brunhes Chron, J_D/J_N varies between 10 and 30%, increasing with depth to typically 50 to 80%, although values of 100% are not uncommon. This illustrates the softer and more viscous nature of the weaker sediments.

A polarity sequence in Hole 591 is recognized as far as the upper Gilbert (Fig. 19, the AF-cleaned are given in Table 6), which is reproduced in the NRM data for Hole 591A. Below this, high scatter obscures any corre-

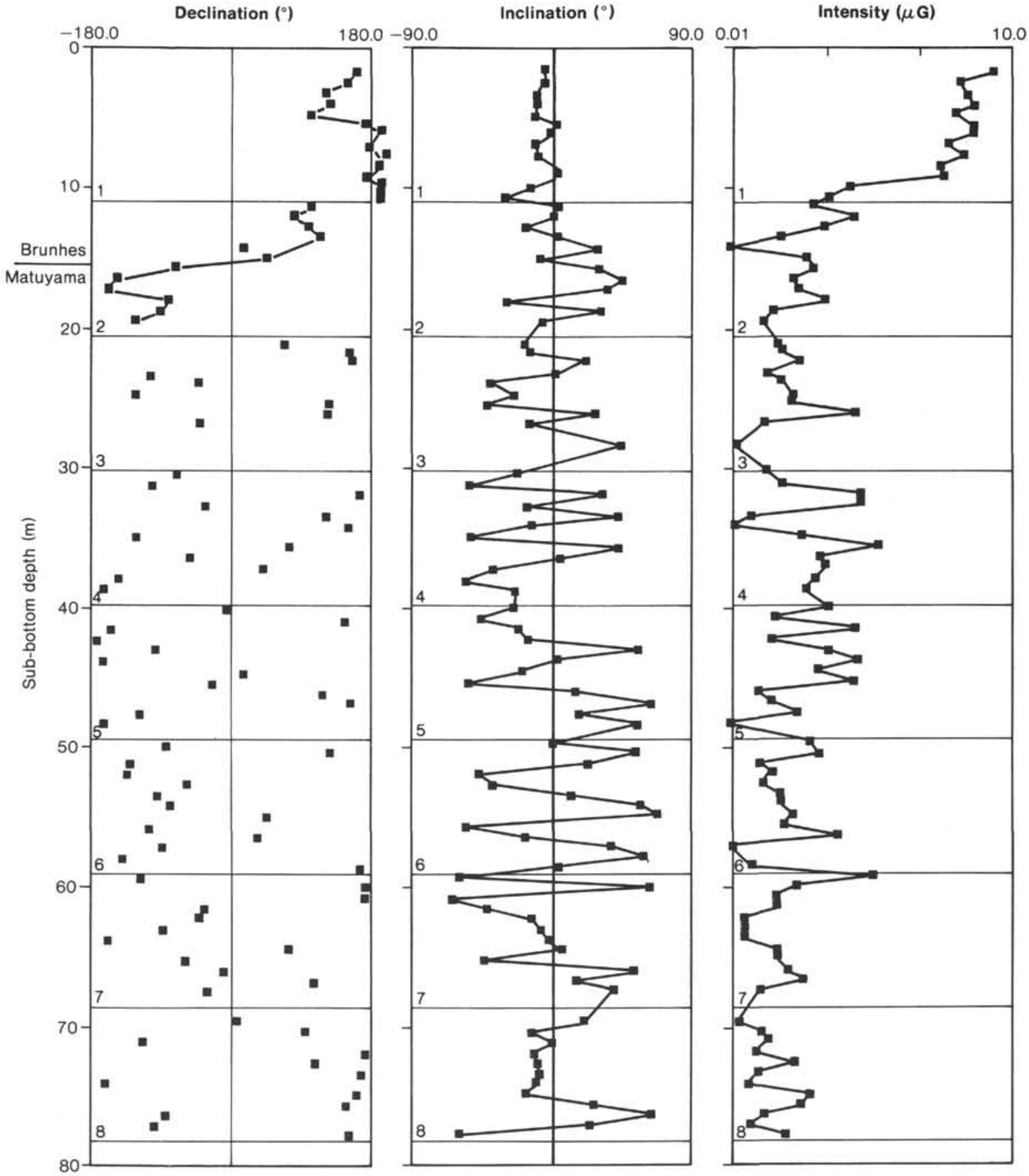

Figure 6. Paleomagnetic data for Hole 586B after AF cleaning at 150 Oe and filtering. Horizontal lines mark core boundaries, numbered in the bottom left; depths are in units of 10 m. Intensities in μG are plotted on a log 10 scale. Declination origins within each core section are arbitrary (i.e., no azimuthal corrections are attempted).

spondence between the two holes. From about 105 m down to 235 m (Cores 591-12 to 591-26), the polarity is predominantly reversed, which is consistent with an extremely high sedimentation rate during the mid- to late-early Pliocene (upper Gilbert) inferred from the nannofossil data. A few normal data points occur during this interval, but these are generally single-point reversals that may not be real. The most probable candidate for the Cochiti Subchron is a 4-point normal interval at 154.7 to 159.5 m.

Site 592

At the single hole cored at this site the HPC was used down to 234.9 m (Core 25) and the XCB thereafter to 388.5 m. Three specimens per core section were collected throughout. Results after AF cleaning at 200 Oe are available for the first 20 cores (to 186.9 m), with NRM data only thereafter.

Magnetic properties are generally similar to those at the previous three sites, but with a somewhat stronger

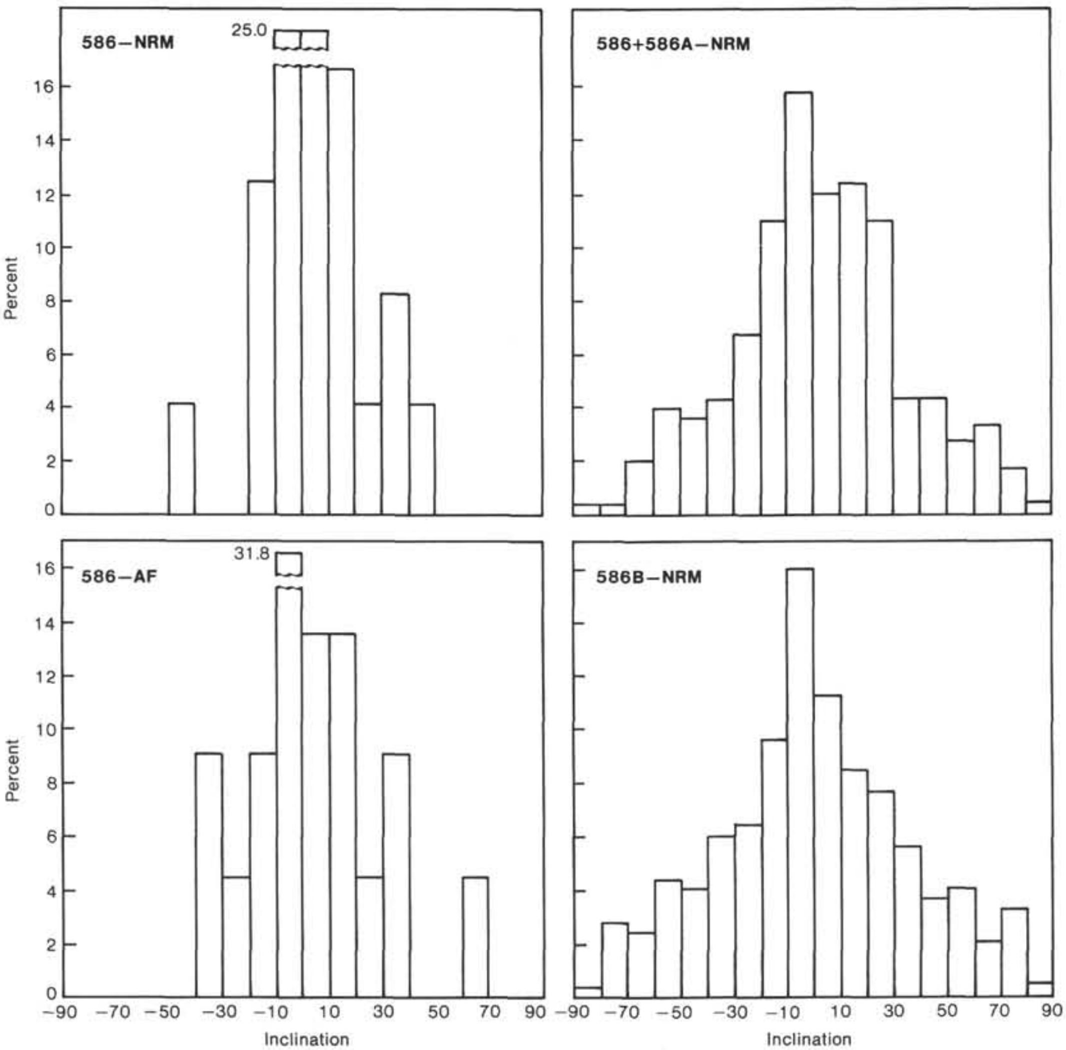

Figure 7. Distribution of inclinations at Site 586. Axial dipole inclination = −1.0°. Histograms for the pre- and postcleaned data are denoted by NRM and AF, respectively.

bias toward intermediate inclinations than in Hole 591 (Fig. 18). Vector difference (NRM-AF) inclinations did not correlate with the NRM vector as at Site 591 and were randomly scattered except between Cores 592-8 and 592-11 (from about 65 to 100 m; Core 8 is largely disturbed), reflecting a VRM component acquired during storage. The ratio J_D/J_N was very scattered and high, with many values greater than 1.0 and poor magnetic stability.

Variations in the dry noncarbonate susceptibility (and Q′) followed the general pattern of intensity changes. Values are typically in the range 0.2–1.0 (Q′ ~0.01–0.1), and 11 out of the 595 measurements were still negative (diamagnetic) despite the correction applied.

We identify a polarity sequence down to the upper Gilbert Chron (Fig. 20), which is in good agreement with the nannofossil data. The AF-cleaned data covering this interval are given in Table 7. A notable feature is the very slow sedimentation during the upper Matuyama. Below the Gauss, down to about 65 m, sediments are generally reversely magnetized, but it is not possible to identify subsequent reversal boundaries unambiguously. From 65 to 100 m magnetic stability is poor, as indicated by high values (often 100%) of the ratio J_D/J_N.

A zone of predominantly normal polarity exists within Cores 592-14 and 592-15 (120–140 m) spanning the boundary between nannofossil zones NN11b and NN12 (Miocene/Pliocene boundary), but this is again a region of poor magnetic stability, and without a duplicate HPC for confirmation the interpretation remains tentative. Records in Cores 592-16 to 592-19 are essentially noise, and Cores 592-20 to 592-24 (180–220 m) are predominantly normal but with poor stability so they are probably overprinted. Below 260 m (Core 592-28) intensities are higher (0.05–2 μG) and magnetic stability properties are better, although the data are still very scattered. There is a strong, stably magnetized zone (0.3–2.4 μG) from 263 to 305.8 m containing the early to mid-Miocene chalk Unit IC, which appears to retain a polarity record. However, the NRM data are rather sparse, many of the polarity intervals being supported by one or two data points only, and the interpretation is ambiguous.

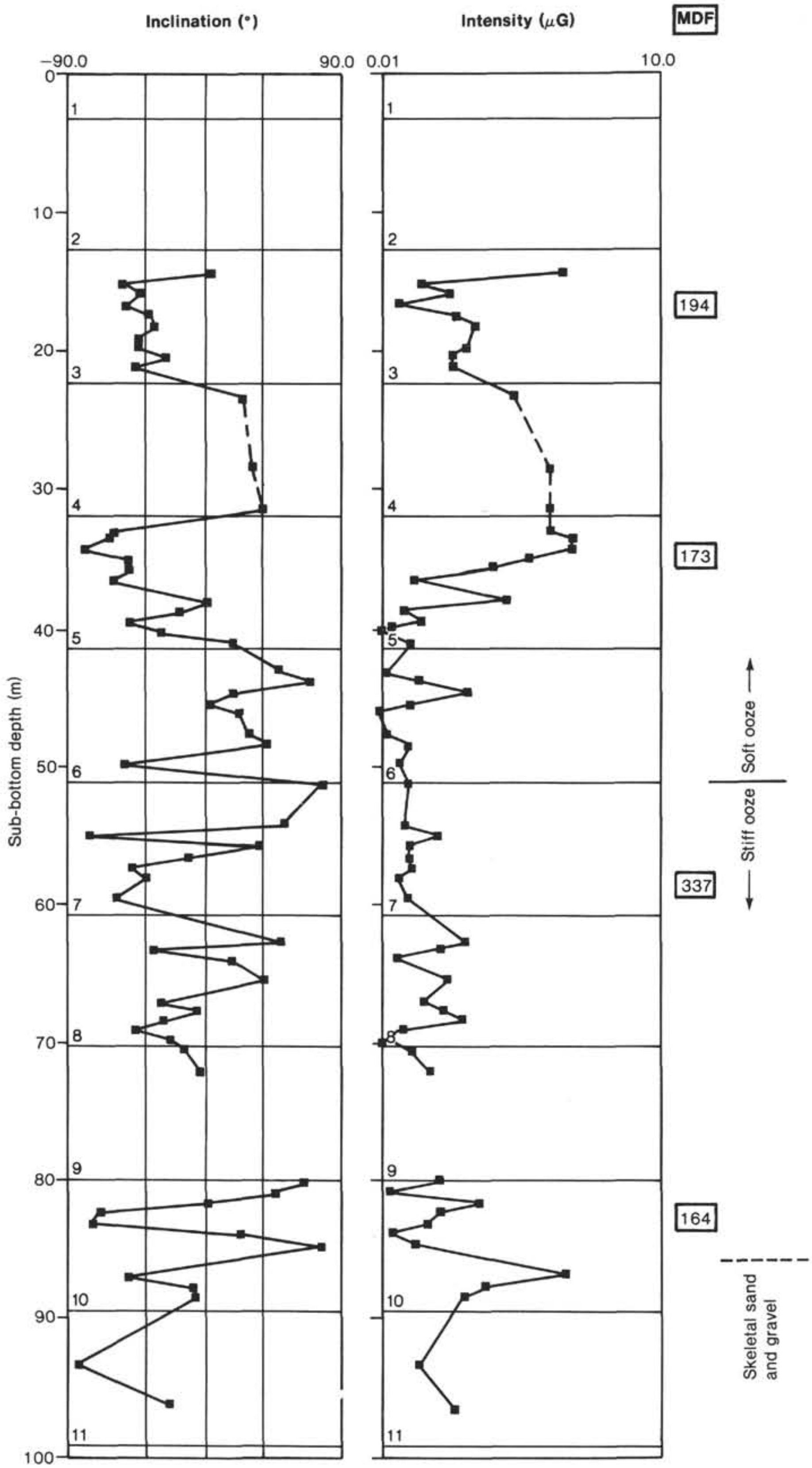

Figure 8. Paleomagnetic results for Hole 587 after AF cleaning at 150 Oe and filtering. Figures on the right-hand side of the intensity plot show MDFs of pilot specimens. Vertical lines on the inclination plot show normal and reverse axial dipole values. Core boundaries are marked by horizontal lines and are numbered in the lower left corner. Subsequent stratigraphic plots follow the same convention.

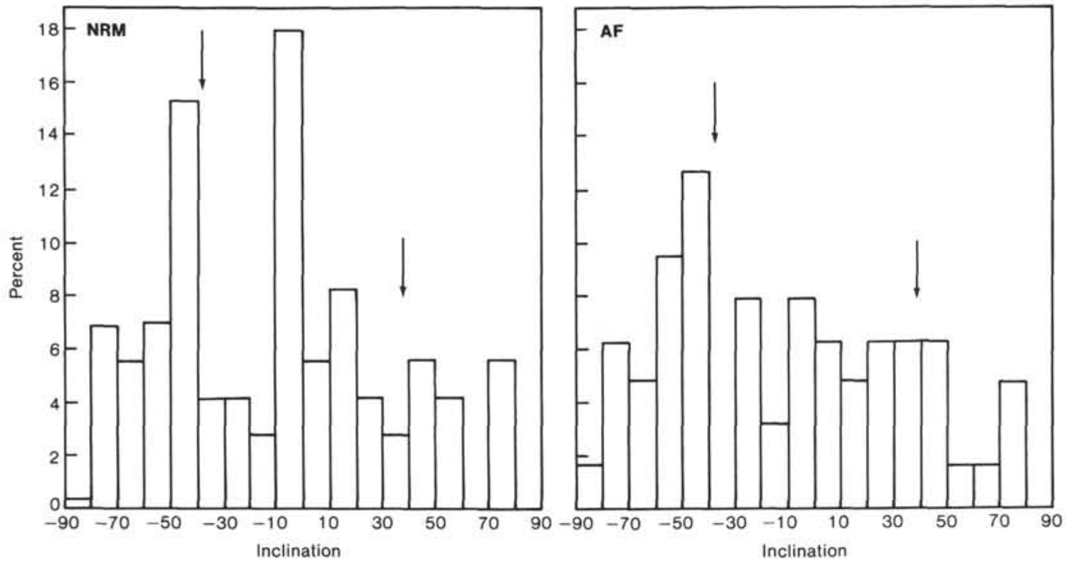

Figure 9. Distribution of inclinations in Hole 587. The axial dipole inclination = −37.8° (arrows).

Site 593

A large data set, AF cleaned at 200 Oe, was obtained from Hole 593: three specimens per section from the 24 HPC cores (0.0–225.9 m) and from the remaining cores recovered by XCB rotary drilling (225.9–571.5 m). Duplicate Hole 593A provided HPC recovery from 0.0 to 103.7 m (Cores 593A-1 to 593A-11, with Cores 593A-8 and 593A-9 being fluid) for which we have AF-cleaned data, and XCB recovery from 448.8 to 257.3 m.

Sediments are similar in character to those at earlier sites. Traces of biosiliceous material occur in a few intervals and foraminifer abundances are lower. Oxidized yellowish gray Subunit IA goes down to 1.5 and 6.0 m in Holes 593 and 593A, respectively. Paleomagnetic inclination and intensity profiles indicate that the vertical offset between the holes is probably no greater than 2 m, hence there must be considerable local variation in thickness of the unit. A unique feature of this sequence is Subunit IC, a pale orange to yellow oxidized nannofossil ooze characterized by unusually high remanent intensities (1.5–3.5 μG). The colored interval (393.8–418 m) is considerably narrower than the interval of elevated intensity (about 360–465 m). The second unique feature is Unit II, Section 593-58-3 to Core 593-60 (545.5–571.5 m), which consists of a black volcanogenic turbidite.

Inclination distributions (Fig. 21) show the highest concentration of intermediate values of any site (except Site 586!), which is a measure of the disappointing quality of this record. The distinct positive bias after AF cleaning arises from a reverse overprint that affects most of the lower half of the sequence (~315–520 m) and was probably acquired during drilling. Evidence for this comes from a consideration of the NRM, AF-cleaned, and vector difference plots, and from AF stability and VRM acquisition tests (see Table 2). This reversely overprinted section encompasses the strongly magnetic Zone D (Table 8) and Subunit IC. Within Zone D magnetic susceptibility, and also Q′, were high, indicating that an increase in the magnetic mineral content is largely responsible for the high magnetization, rather than growth of viscous remanence.

Twenty-four specimens distributed throughout the sequence were subjected to progressive AF demagnetization. Average MDF values are given in Table 8. Specimens with MDF values less than about 150 Oe generally display poor directional stability. In the upper half of the sequence AF cleaning improves the resolution of the polarity sequence, but does not change the overall pattern of reversals. In magnetic Zones A and B the inclination of the NRM–AF difference vector tracked variations in NRM inclination, with a superimposed noise component. Thus, overprinting in the present-day field is not a serious problem. The ratio J_D/J_N increases from about 0.25 at the surface to about 0.75 at about 100 m, with considerable scatter and occasional values greater than 1.0. Below about 100 m values oscillate between about 0.4 and 1.0 with a tendency toward higher values with increasing depth (i.e., the sediments tend to become magnetically softer and/or more viscous with depth). Particularly high values of J_D/J_N occur in certain intervals within the reversely overprinted zone: 357–360 m, 364–369 m, 385–401 m, and 449–454 m. VRM acquisition test results (Table 2) indicate that throughout most of the sequence VRM is unlikely to contribute substantially to the NRM, except at the surface (28% of the NRM acquired in 1000 hr.) and in magnetic Zone D where the VRM contribution can be very large and also magnetically quite hard (MDFs up to 153 Oe). An interesting feature of the VRM acquisition curves (VRM versus log t) was the nature of the departures from linearity. Specimens with low susceptibilities to VRM were quasilinear or slightly convex upward, whereas the highly viscous specimens were clearly concave upward (U-shaped). This demonstrates that the highly magnetic Zone D is associated with a change in magnetic mineralogy and/or grain size and shape.

The magnetic record is generally poorer than at Site 592, but, nevertheless, polarities can be traced back to the base of the Gauss, which are reproducible in both

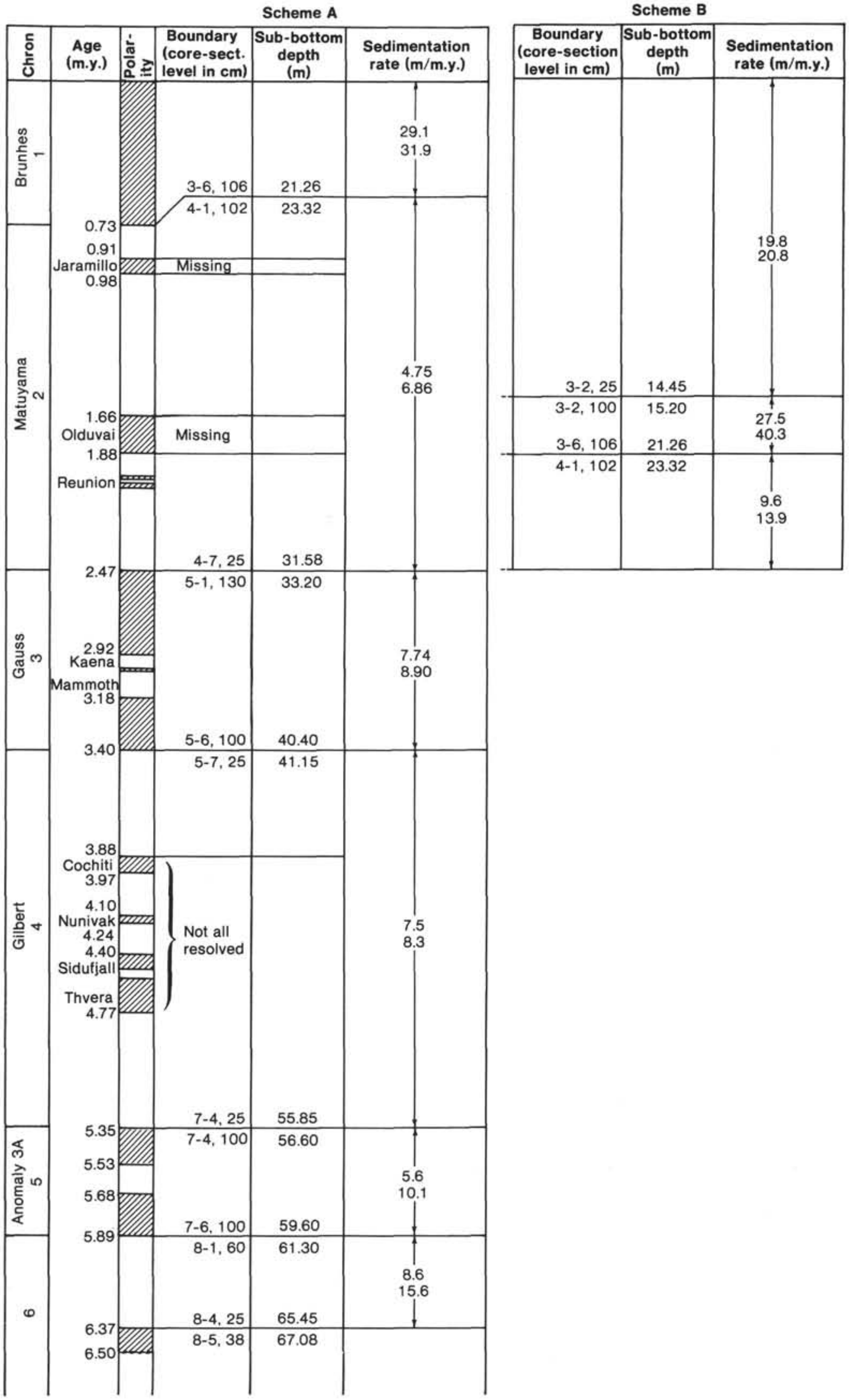

Figure 10. Reversal boundaries identified at Site 587. Numbers within the vertical arrows show maximum and minimum sedimentation rates in m/m.y. corresponding to the boundary limits given. Scheme B is an alternative to the preferred Scheme A for the Brunhes and Matuyama.

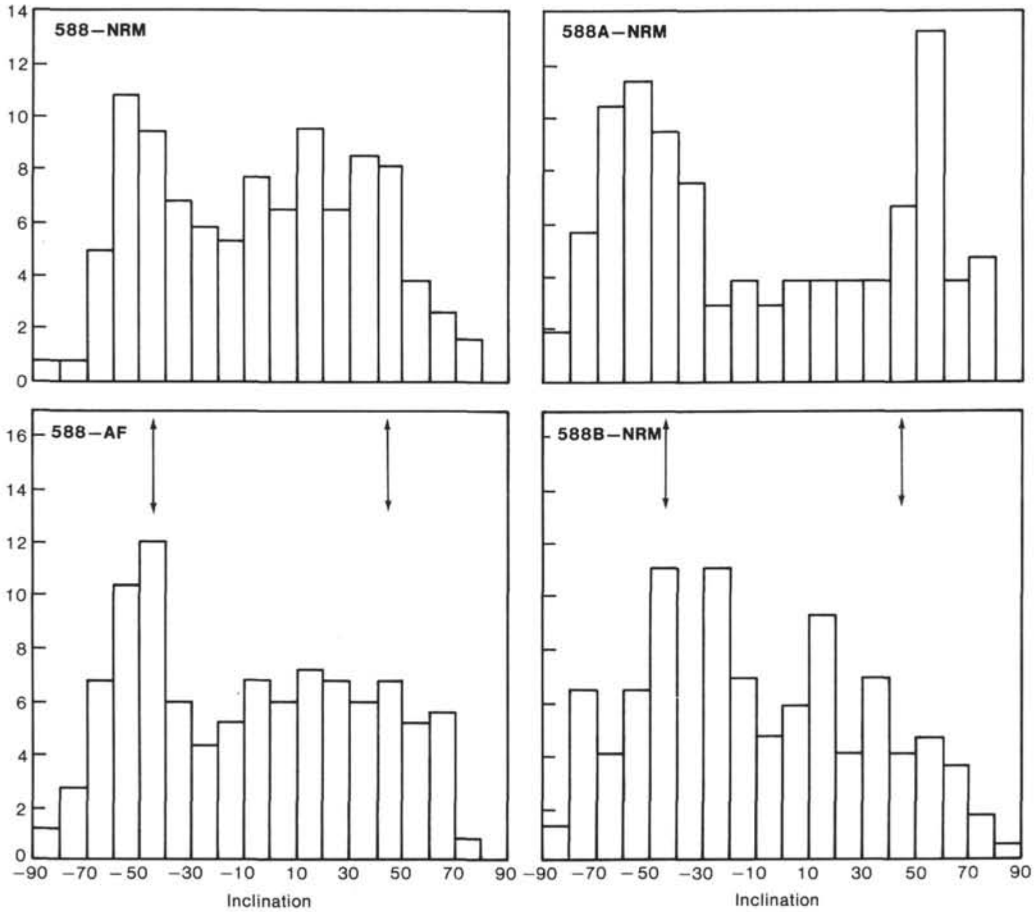

Figure 11. Distribution of inclinations at Site 588. The axial dipole inclination = −44.4° (arrows).

Holes 593 and 593A (Fig. 22). Where the sampled sections overlap below this there is lack of agreement. There is weak evidence for the occurrence of the Kaena and Mammoth subchrons within the Gauss, but it is based only on single-data points of low inclination in each sequence. Table 9 contains the raw data for the upper part of Hole 593.

Volcanogenic Turbidite—Unit II, Hole 593

Special attention was paid to this unit at 545.5–561.9 m in Hole 593, as it is closely associated with the Eocene/Oligocene boundary. Although NRM intensities are high (up to 10 μG), median destructive fields are very low, ranging from 68 to 95 Oe with one specimen at 166 Oe (593-59-4, 128 cm—black, very fine grained material). Shipboard and laboratory remeasurements of NRM showed a substantial decrease over a period of 18 months, suggesting that much of the NRM is a VRM. The isolated band of volcanogenic material below the main unit and the sediments below this level have a harder, more stable remanence—MDF = 158 Oe at 564.15 m, and 190 Oe at 566.15 m.

Results after AF cleaning (Fig. 23) indicate that the unit is predominantly of reversed polarity, which is consistent with the placement of the Eocene/Oligocene boundary within Chron C13R (following the nomenclature of LaBrecque et al., 1983). Sediments below Unit II have a spongy consistency that is usually an indicator of coring disturbance. It is, therefore, not clear whether the normal polarity zones in Core 593-60 correspond to Chron C15N. If so, then either there is a short hiatus below the turbidites or the turbidites were deposited prior to the Eocene/Oligocene boundary. Given the poor magnetic stability characteristics of the volcanogenic sediments, the suggested interpretations can only be regarded as speculative. Table 9 contains the raw data for this interval.

Site 594

The site differs from previous sites in that its proximity to New Zealand produced a larger input of terrigenous material. Good HPC recovery extended to 130.7 m in Hole 594 followed by XCB rotary drilling with poor recovery to 207.5 m. Nine HPC cores were recovered from the duplicate Hole 594A from 41.3 to 127.7 m, followed by XCB recovery of the missing intervals in Hole 594 and continuous recovery from 495.5 to 639.5 m.

The lower unit of the sequence (Unit II) is a pelagic foraminifer-nannofossil ooze grading to chalk around 470 m in the middle Miocene, with olive gray turbidite layers below 534 m. This unit is generally similar to the pelagic oozes and chalks at other sites except for a higher biosiliceous component. After the Kaikoura Orogeny, about 6 m.y. (about 169 m in the sequence), the sedi-

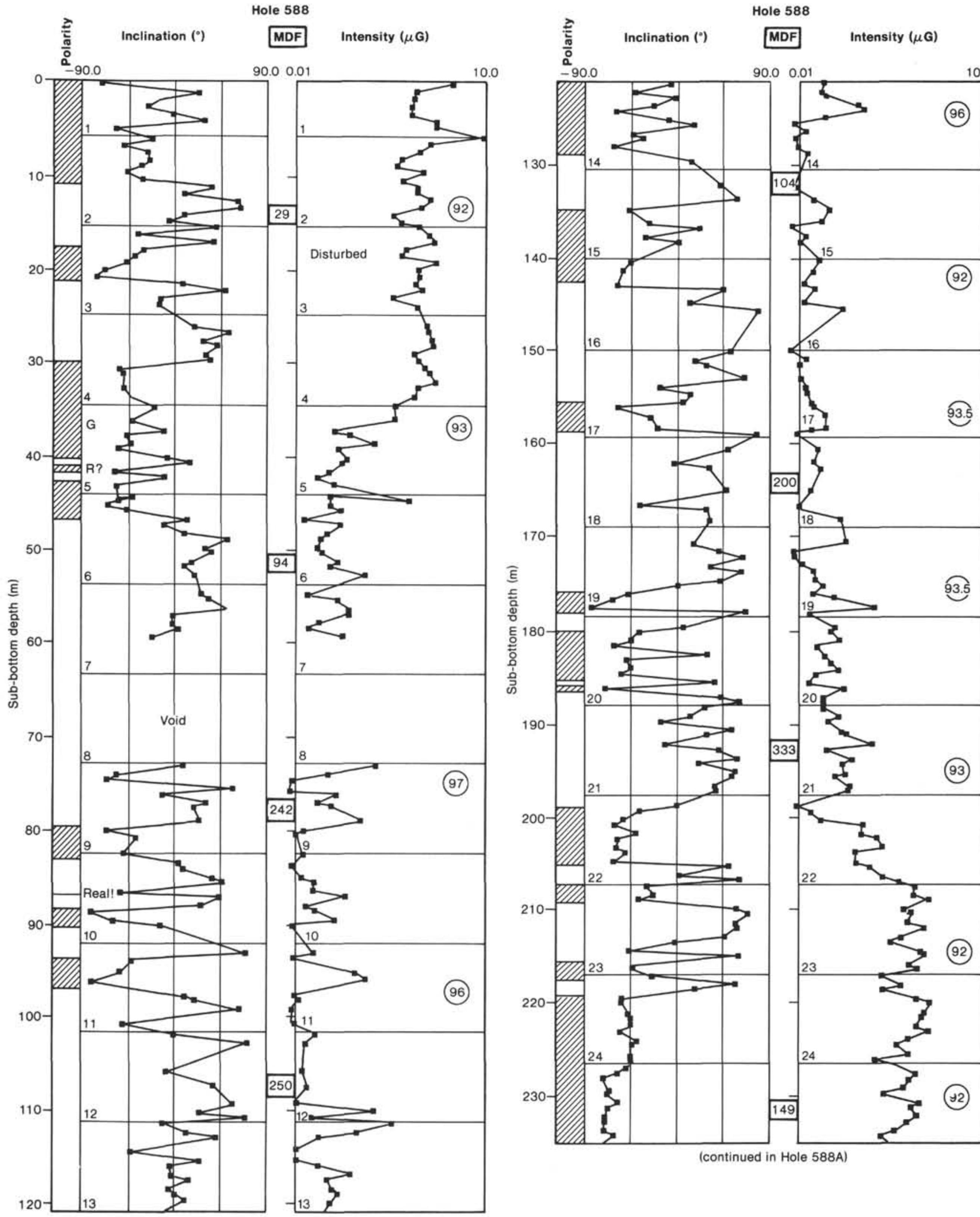

Figure 12. Paleomagnetic results for Hole 588A after AF cleaning at 200 Oe and filtering. Figures in boxes are MDF values and in circles are the carbonate percentages.

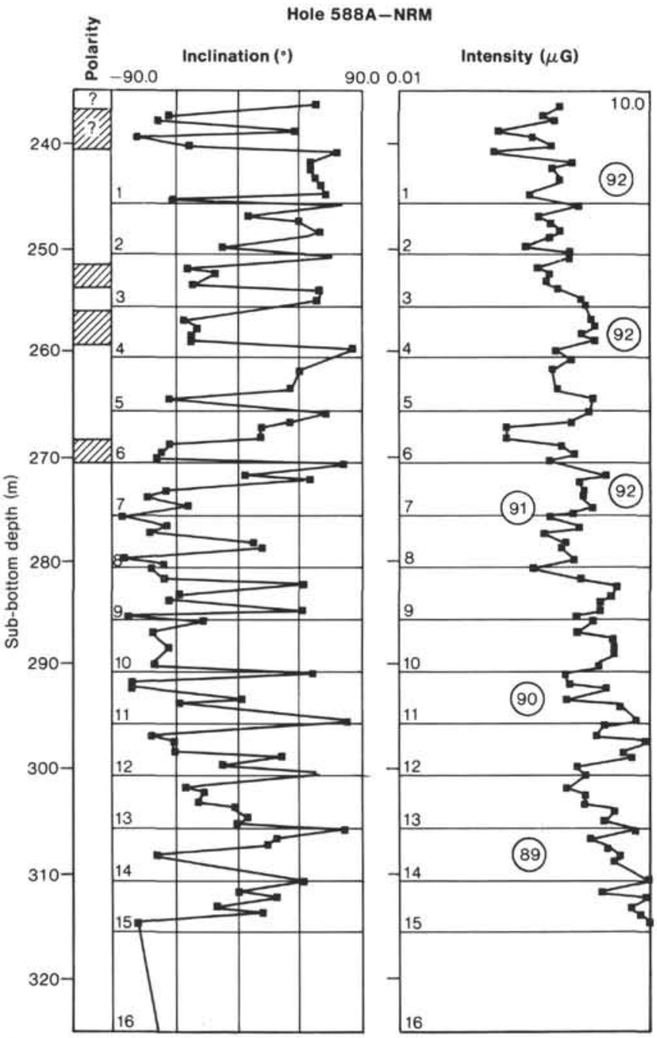

Figure 12. (Continued).

mentation pattern changed with time to alternating pelagic and hemipelagic facies, corresponding to interglacial and glacial conditions, respectively. Enhanced input of terrigenous material is reflected in higher NRM intensities; biosiliceous contents are higher, especially in the hemipelagics; and pyritized streaks and blebs occur throughout the unit.

The distribution of inclinations (Fig. 24) is skewed strongly toward negative (normal polarity) values, with a very large proportion of intermediate inclinations. The former is partly due to the occurrence of a very long normal Brunhes interval (11 cores) and partly to a normal overprint. This is supported by the soft, normal overprint observed in reversely magnetized specimens and by the inclination distribution in the AF-cleaned data that is skewed to a lesser degree than for the NRM data. AF cleaning reduces the proportion of intermediate inclinations, but it still remains high, reflecting the generally poor quality of the paleomagnetic record. Arithmetic mean inclinations for NRM and AF-cleaned data are -16.9 and $-15.9°$, respectively.

Within Unit I (0–169.1 m), intensities are considerably higher than at similar depths at other sites and show a trend toward lower values with depth (from about 2 to 0.1 μG at the bottom of the unit). The usual surficial layer of a few tens of cm of highly magnetized, oxidized material is not present in Hole 594 and may well be missing since it was suspected that coring started below the mudline. (Duplicate HPCs from Hole 594B have not been opened.) Within the pelagic sediments of Unit II, intensities fall to the usual low values, about 0.01 μG at 260 to 290 m, and thereafter increase somewhat with depth as the sediments become compacted, reaching about 0.05 μG at 490 m.

The long-period variations in susceptibility were of low amplitude and followed a similar pattern to those of NRM intensity, with notably higher values in Unit I (2–15 $\mu G\ Oe^{-1}$), with a small bulge at 400 to 470 m (2–4 $\mu G\ Oe^{-1}$). There is correspondingly little variation in the Q′ ratio: typically 0.01 to 0.04 in Unit I and about 0.01 to 0.20 in Unit II. Generally higher values of Q′ in Unit II are indicative of a larger fraction of fine-grained, single-domain magnetic particles of terrigenous origin.

Downcore variations in inclination of the NRM–AF difference vector and the NRM vector were similar for the upper 250 m of the section. The correspondence is much poorer between the difference vector and the AF-cleaned vector. This indicates that the NRM suffers from a substantial soft overprint at this site. Forty-six pilot specimens were subjected to progressive AF demagnetization. Despite moderate MDF values (mean = 179 $\pm$99 Oe [$\pm$s.d.]), stability was generally poor to bad with widespread evidence for a vertical secondary remanence (up and down) probably imparted during core recovery. AF stability is poorer than at most previous sites, although it improves below 300 m where MDF values are higher. VRM test results (Table 2) indicate that a substantial fraction of the natural remanence could be of viscous origin.

Poor magnetic stability properties combined with unconformities within the section render our interpretation of the paleomagnetic record somewhat tentative, particularly prior to the Pleistocene. Despite this there is sufficient correspondence with the polarity time scale to justify an interpretation.

AF-cleaned data for Hole 594 and our preferred identification of reversed boundaries are illustrated in Figures 25 and 26; (the raw data are given in Table 10). Below Core 594-38 (about 360 m) the record is as yet uninterpretable and is omitted. It is clear from the paleomagnetic data alone that the sequence must contain hiatuses. Except for one short interval (41.95–43.95 m), all cores down to Core 594-11 are normally magnetized. Gaps in the record in Cores 594-7, 594-8, and 594-10 correspond to normal polarity in Hole 594A. According to the radiolarian and diatom stratigraphy there is a hiatus from about 1.6 to 0.74 Ma. If so, the bottom of the long normal interval (101.9 m) corresponds to the base of the Olduvai. An alternative interpretation, which is more consistent with the calcareous nannofossil scheme, is to invoke a very much shorter hiatus and to equate the bottom of the long normal interval with the base of the Jaramillo. This latter alternative is illustrated in Figure 26. It can be argued that the bottom of the normal in-

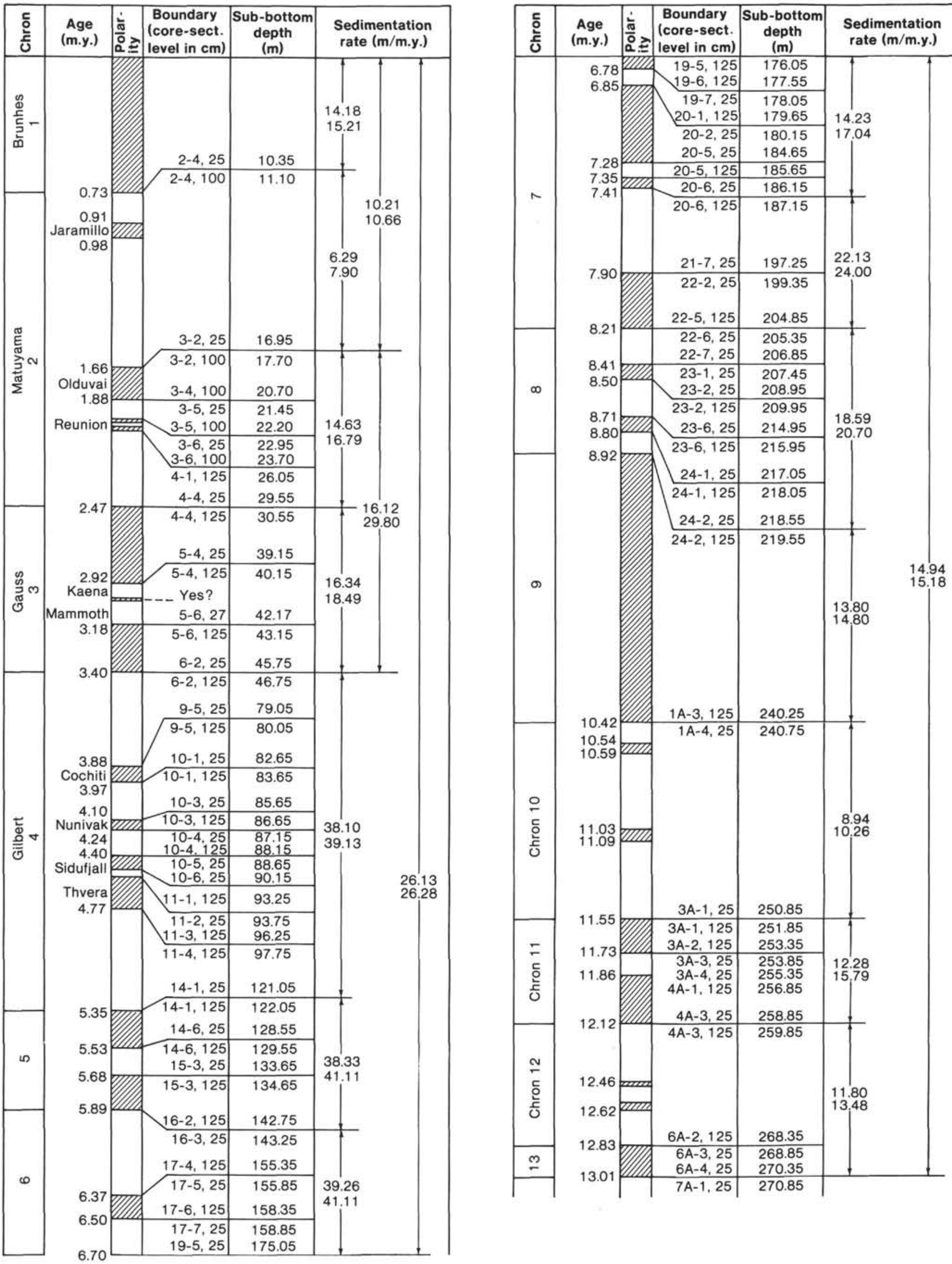

Figure 13. Reversal boundaries for Holes 588 plus 588A.

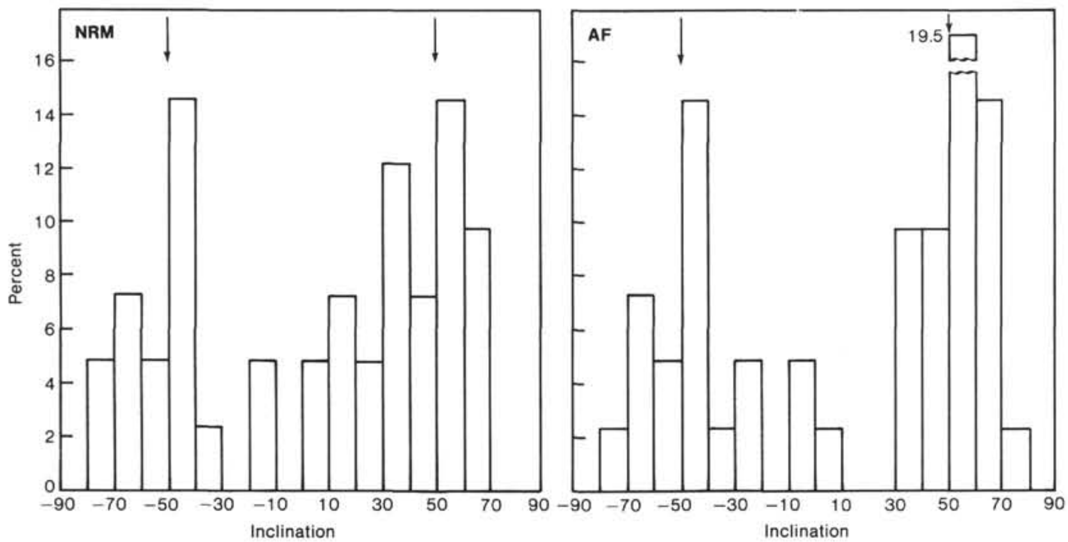

Figure 14. Distribution of inclinations for Hole 589. The axial dipole inclination = −49.9° (arrows).

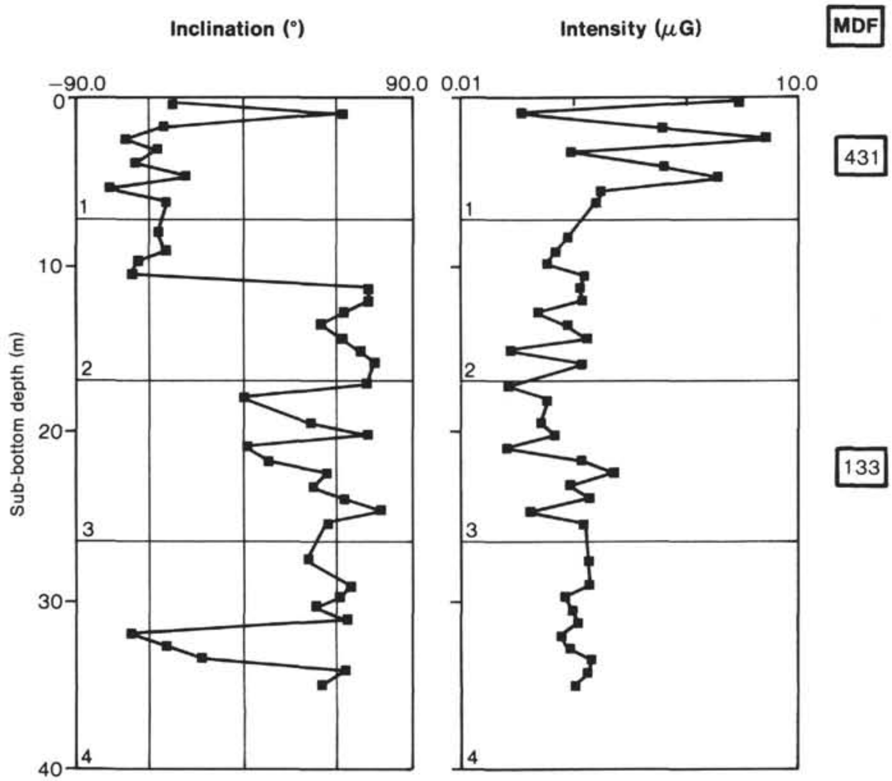

Figure 15. Paleomagnetic results for Hole 589, data AF cleaned at 150 Oe and filtered.

terval corresponds to the base of the Brunhes and the Jaramillo is missing.

Time scales for the biostratigraphic schemes based on calcareous nannofossils (Site 594 chapter; Martini et al., this volume) and on diatoms and radiolarians (Site 594 chapter; Ciesielski, this volume) disagree. The latter indicates four hiatuses: about 8.3-6.5 Ma, about 5.4-4.5 Ma, about 3.85-2.70 Ma, and about 1.6-0.74 Ma. Despite the mediocre quality of the paleomagnetic data, an intercomparison between the two schemes and the magnetic data is possible (Fig. 27).

In the case of the diatom-radiolarian scheme, the optimum match with the paleomagnetics is plausible except for depth intervals 190-230 m and 245-265 m. In the case of the nannofossil scheme, the match down to the mid-late Miocene boundary is consistent with more uniform sedimentation. The Miocene/Pliocene boundary comes at about 210 m on the magnetic interpreta-

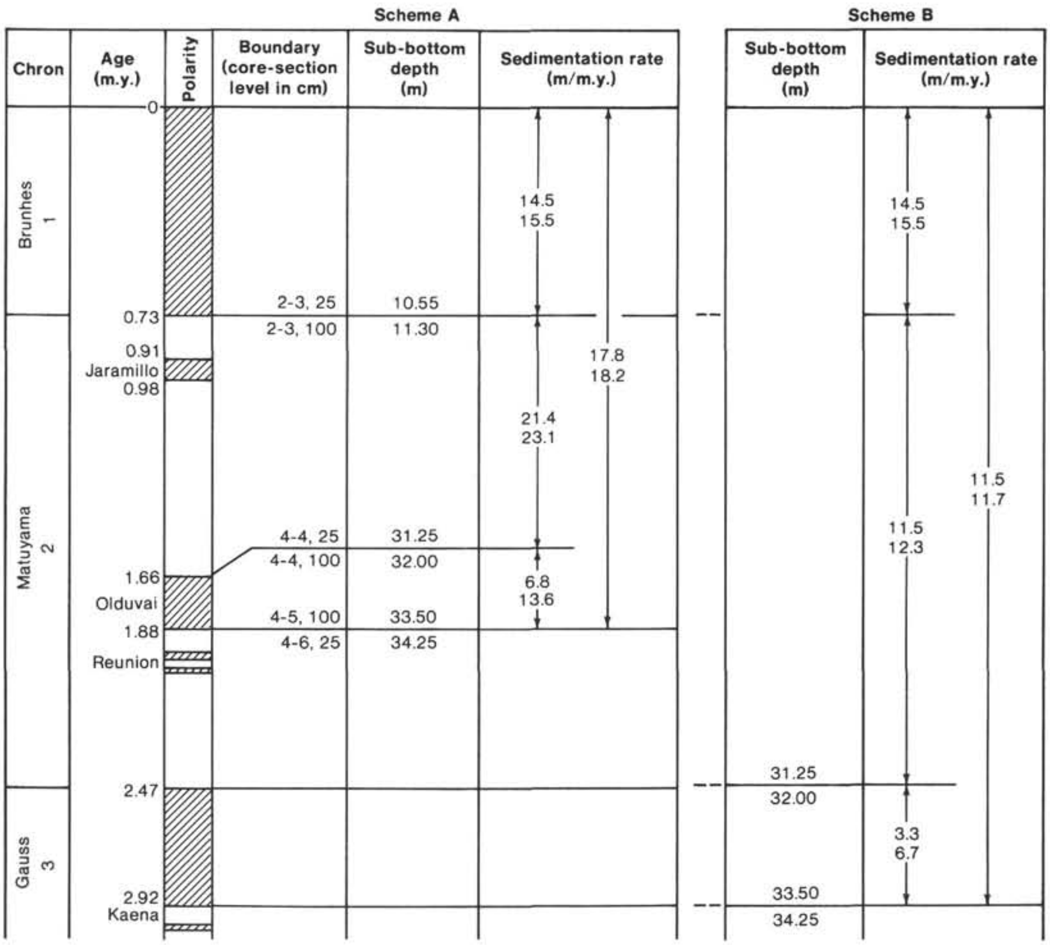

Figure 16. Reversal boundaries for Hole 589—AF. Two interpretations are possible. Scheme A best fits the biostratigraphy.

tion instead of 215 m as on the nannofossil scheme, and the middle Miocene interval on the polarity time scale must be largely missing. Because of its greater simplicity we prefer the combined magneto-nannofossil time scale.

CONCLUSION

The primary objective of this paleomagnetic study is to provide a magnetostratigraphic framework for the transect of sites cored during Leg 90. Excellent recovery, much of it using the HPC, was obtained in the shallow-water carbonate oozes and chalks encountered, extending back to the lower Miocene at most sites and to the upper Eocene at Sites 592 and 593. Despite this, magnetic reversal sequences are recognizable only as far back as the Gilbert (3.4–5.35 m.y.) at most sites. Exceptions to this are Site 588, where we obtained a complete reversal sequence back to the middle Miocene (13 m.y.), and also Site 594, on the southern margin of the Chatham Rise, where the reversal sequence extends to the base of Chron 5 (about 6 m.y., in the late Miocene). There is a very long sequence of 11 cores of Brunhes-age sediments at Site 594. Site 586 on the Ontong-Java Plateau is too close to the equator to use inclination to determine magnetic polarity; the lack of core orientation information was a severe handicap at this site, and only the Brunhes/Matuyama boundary could be identified.

With a few exceptions (e.g., the middle to late Miocene boundary at Site 588) the proposed magnetic chronologies and biostratigraphically determined chronologies are compatible. Volcanogenic turbidite Unit II in Hole 593, associated with the Eocene/Oligocene boundary, is predominantly of reverse polarity, which is consistent with placement of the boundary in Chron C13R (new nomenclature). However, the unit displays poor magnetic stability properties so the evidence is not strong. At Site 594, where there is a conflict between the chronological schemes based on siliceous microfossils (diatoms and radiolarians) and calcareous nannofossils, the magnetic record is in better agreement with the latter.

It is not clear why the paleomagnetic record at Site 588 is so much longer than at other Leg 90 sites on the Lord Howe Rise, all of which are similar sedimentologically. We note that carbonate oozes with a siliceous component studied during previous DSDP Legs give better paleomagnetic records than the almost pure carbonate oozes recovered during Leg 90. This could be related to the stabilizing influence of skeletal siliceous material in the sediment matrix. Such a matrix would be more conducive to the development of a stable postdepositional detrital remanence during compaction. However, sediments from Site 588 were not noticeably more siliceous than from other sites on the Lord Howe Rise.

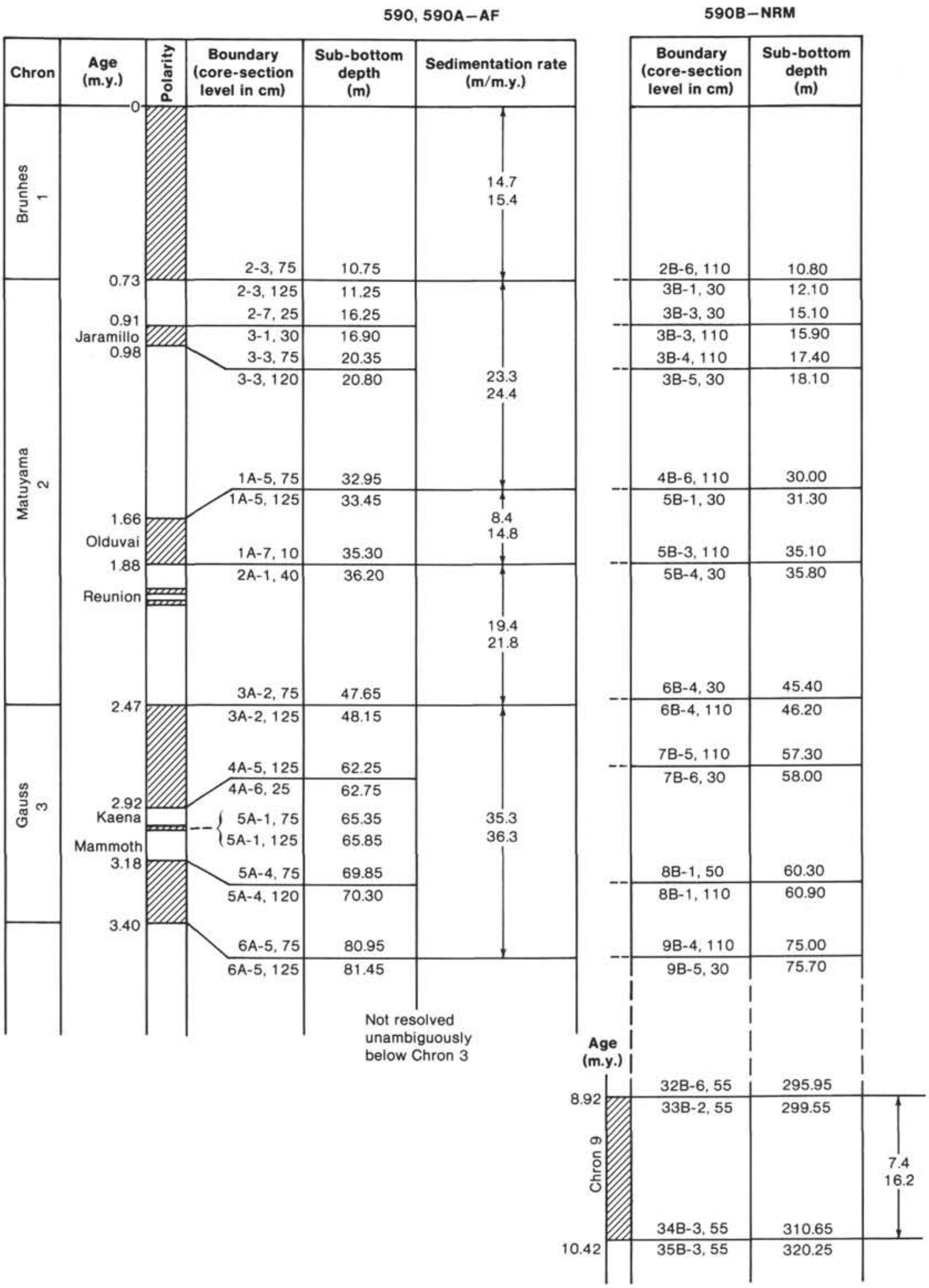

Figure 17. Reversal boundaries identified for Holes 590, 590A, and 590B. Results for Holes 590 and 590A are based on AF-cleaned (200 Oe) and filtered data.

Sequences recovered during Leg 90 were characterized by very high carbonate contents and correspondingly low magnetic remanence, except for a relatively strongly magnetic surficial layer of oxidized material. There is a systematic degradation of the paleomagnetic signal with depth and an associated decrease of magnetic remanence which is pronounced in the surface sediments. This is attributed to the combined effects of removal of primary magnetic oxides during sulfate reduction processes (streaks and blebs of pyrite are common), and nonrandom disorientation of magnetic particles in very dilute dispersions during compaction (giving scattered directions with fairly high MDFs). When carbonate contents are very high (close to 100%), a simple car-

Table 3. AF-cleaned data, Hole 590.

Core-Section (interval in cm)	Sub-bottom depth (m)	Declination (°)	Inclination (°)	Intensity (μG)
1-1, 75	0.75	339.4	−17.1	0.231
1-1, 125	1.25	3.2	−74.0	0.596
1-2, 25	1.75	42.8	−76.8	0.402
1-2, 75	2.25	280.2	−52.3	0.161
1-2, 125	2.75	341.1	−66.8	0.806
1-3, 25	3.25	328.7	−50.2	3.503
1-3, 75	3.75	266.7	−59.5	0.191
1-3, 125	4.25	276.6	−51.5	0.046
1-4, 25	4.75	263.4	−53.9	1.458
1-4, 75	5.25	268.8	−29.5	0.400
1-4, 125	5.75	246.6	−71.9	2.493
1-5, 25	6.25	317.3	−54.5	2.287
1-5, 75	6.75	332.7	−65.9	0.107
2-1, 130	8.30	23.2	−55.0	0.076
2-2, 25	8.75	194.8	−57.1	0.090
2-2, 75	9.25	198.5	−56.8	0.095
2-2, 125	9.75	319.5	−57.2	0.090
2-3, 25	10.25	260.6	−52.8	0.124
2-3, 75	10.75	273.9	−63.0	0.195
2-3, 125	11.25	58.6	52.1	0.045
2-4, 25	11.75	94.2	51.8	0.062
2-4, 75	12.25	48.1	−19.8	0.025
2-4, 125	12.75	71.8	−4.8	0.072
2-5, 25	13.25	345.0	45.7	0.090
2-5, 75	13.75	263.4	21.6	0.092
2-5, 125	14.25	289.3	−2.0	0.106
2-6, 25	14.75	197.3	72.1	0.064
2-6, 75	15.25	132.0	43.0	0.069
2-6, 125	15.75	140.4	4.3	0.061
2-7, 25	16.25	193.2	0.3	1.306
3-1, 30	16.90	338.6	−63.8	0.110
3-1, 75	17.35	268.8	−48.0	0.055
3-1, 125	17.85	320.0	−21.0	0.123
3-2, 25	18.35	258.4	−83.9	0.083
3-2, 75	18.85	325.3	−24.5	0.099
3-2, 125	19.35	348.2	−29.0	0.050
3-3, 25	19.85	298.2	−42.0	0.108
3-3, 75	20.35	243.7	−72.6	0.055
3-3, 120	20.80	303.6	29.0	0.061
3-4, 25	21.35	326.7	−33.4	0.072
3-4, 75	21.85	339.2	10.7	0.029
3-4, 125	22.35	126.3	0.2	0.231
3-5, 25	22.85	28.6	61.2	0.032
3-5, 75	23.35	6.8	−62.3	0.057
3-5, 115	23.75	343.1	−36.2	0.067
3-7, 25	25.85	62.4	17.6	0.086

bonate dilution model is sufficient to account for large variations in NRM intensity without invoking any change in the rate of input of magnetic material.

Stratigraphic plots of the vector removed during AF cleaning, inclination histograms, and progressive AF demagnetization and direct VRM tests on selected specimens demonstrate that VRM is common and quite variable within and between sequences, and in some zones is comparable in magnitude to the NRM. A number of specimens contained a vertical component of magnetization, presumably imparted during core recovery, and in some of these this was magnetically the hardest component present. Much of the lower half of the sequence from Hole 593 was affected by a reverse (drilling) overprint. Despite these effects, preliminary polarity results based on NRM data were generally very similar to final ones based on AF-cleaned data. Thus raw NRM data alone may be used for initial shipboard determination of reversal boundaries. Secondly, it was clear that the application of progressive AF demagnetization to all specimens individually, rather than bulk (blanket) AF treat-

Table 4. AF-cleaned data, upper part of Hole 590A.

Core-Section (interval in cm)	Sub-bottom depth (m)	Declination (°)	Inclination (°)	Intensity (μG)
1-1, 100	27.20	287.5	30.6	0.077
1-2, 25	27.95	348.3	16.2	0.052
1-2, 75	28.45	349.7	17.5	0.169
1-2, 125	28.95	40.7	38.0	0.028
1-3, 25	29.45	74.8	66.5	0.065
1-3, 75	29.95	102.4	43.5	0.085
1-3, 125	30.45	100.3	11.8	0.128
1-4, 25	30.95	162.6	65.6	0.116
1-4, 75	31.45	104.7	27.9	0.041
1-5, 25	32.45	113.5	28.6	0.042
1-5, 75	32.95	75.6	45.9	0.043
1-5, 125	33.45	214.2	−28.7	0.105
1-6, 25	33.95	306.1	−42.0	0.203
1-6, 85	34.55	248.9	−30.1	0.100
1-6, 125	34.95	297.8	−56.2	0.093
1-7, 10	35.30	318.1	−27.7	0.089
2-1, 40	36.20	297.5	31.9	0.030
2-1, 120	37.00	291.2	−23.2	0.041
2-2, 25	37.55	281.2	45.0	0.128
2-2, 75	38.05	324.3	18.0	0.037
2-2, 75	38.05	334.4	24.4	0.022
2-2, 125	38.55	263.4	49.2	0.110
2-2, 125	38.55	268.0	43.8	0.119
2-3, 25	39.05	257.7	46.1	0.052
2-3, 25	39.05	248.7	49.2	0.050
2-3, 75	39.55	221.8	−4.8	0.082
2-3, 125	40.05	105.3	35.0	0.030
2-4, 25	40.55	138.2	64.8	0.072
2-4, 75	41.05	4.7	22.1	0.104
2-4, 125	41.55	145.3	42.1	0.086
2-5, 25	42.05	157.6	66.5	0.044
2-5, 75	42.55	165.8	57.9	0.099
2-5, 125	43.05	151.8	20.4	0.048
2-6, 25	43.55	292.2	72.4	0.070
2-6, 75	44.05	122.8	49.0	0.026
2-6, 125	44.55	121.1	65.8	0.059
2-7, 10	44.90	223.6	47.7	0.023
3-1, 25	45.65	313.7	52.8	0.029
3-1, 75	46.15	330.4	−27.5	0.062
3-1, 125	46.65	79.0	55.9	0.053
3-2, 25	47.15	8.6	49.3	0.105
3-2, 75	47.65	317.6	11.6	0.034
3-2, 125	48.15	115.4	−48.8	0.091
3-3, 25	48.65	274.0	−37.4	0.071
3-3, 75	49.15	313.7	−23.5	0.029
3-3, 125	49.65	281.8	−34.2	0.075
3-4, 25	50.15	243.1	−59.0	0.103
3-4, 75	50.65	329.1	−48.2	0.040
3-4, 125	51.15	78.0	4.9	0.027
3-5, 25	51.65	88.7	−80.9	0.103
3-5, 75	52.15	319.4	−76.5	0.067
3-5, 125	52.65	57.2	−77.5	0.091
3-6, 25	53.15	351.5	−41.8	0.077
3-6, 70	53.60	113.5	−57.4	0.121
4-1, 30	55.30	38.3	−27.6	0.119
4-1, 75	55.75	252.4	−74.8	0.082
4-1, 125	56.25	243.7	−83.2	0.075
4-2, 25	56.75	202.7	−19.2	0.076
4-2, 75	57.25	280.1	−47.5	0.078
4-2, 125	57.75	16.7	−40.6	0.060
4-3, 25	58.25	280.7	−33.6	0.072
4-3, 90	58.90	294.7	−28.3	0.087
4-3, 130	59.30	272.3	−49.3	0.105
4-4, 25	59.75	345.3	−37.4	0.188
4-4, 80	60.30	248.6	−34.7	0.042
4-4, 125	60.75	265.7	−16.3	0.058
4-5, 25	61.25	237.5	−39.1	0.059
4-5, 75	61.75	334.5	−40.8	0.029
4-5, 125	62.25	53.6	−10.7	0.050
4-6, 25	62.75	267.2	24.2	0.070
4-6, 85	63.35	282.3	−7.4	0.051
5-1, 75	65.35	264.3	−77.5	0.043
5-1, 125	65.85	259.2	−47.9	0.068
5-2, 25	66.35	286.8	28.1	0.034
5-2, 75	66.85	232.3	53.1	0.029
5-2, 125	67.35	295.0	21.2	0.062
5-3, 25	67.85	215.9	−74.9	0.029

Table 4. (Continued).

Core-Section (interval in cm)	Sub-bottom depth (m)	Declination (°)	Inclination (°)	Intensity (μG)
5-3, 75	68.35	351.7	56.6	0.022
5-3, 125	68.86	252.5	53.1	0.254
5-4, 25	69.35	248.9	46.7	0.043
5-4, 75	69.85	269.3	58.0	0.083
5-4, 120	70.30	184.0	−63.9	0.035
5-5, 25	70.85	86.7	−60.0	0.040
5-5, 75	71.35	137.8	−76.9	0.035
5-5, 125	71.85	45.6	25.3	0.038
5-6, 25	72.35	109.5	−39.5	0.117
5-6, 75	72.85	58.0	−42.4	0.036
5-6, 125	73.35	37.5	−57.4	0.024
6-1, 75	74.95	57.6	−1.0	0.022
6-1, 125	75.45	175.0	−39.8	0.032
6-2, 25	75.95	75.9	−62.5	0.067
6-2, 75	76.45	39.0	−55.5	0.017
6-2, 125	76.95	74.9	−54.2	0.025
6-3, 25	77.45	130.7	32.5	0.141
6-3, 75	77.95	140.4	−78.6	0.012
6-3, 125	78.45	131.7	−49.3	0.027
6-4, 25	78.95	183.8	−67.1	0.012
6-4, 75	79.45	53.6	−80.0	0.031
6-4, 125	79.95	33.1	−41.6	0.023
6-5, 25	80.45	194.9	−39.9	0.045
6-5, 25	80.45	117.1	−73.1	0.037
6-5, 75	80.95	60.6	−36.5	0.025
6-5, 125	81.45	85.4	26.9	0.011
6-6, 25	81.95	298.4	52.7	0.021
6-6, 75	82.45	193.5	43.6	0.038
6-6, 125	82.95	0.5	46.6	0.039
7-1, 25	84.05	12.9	30.0	0.011
7-1, 75	84.55	59.0	43.3	0.009
7-1, 125	85.05	347.7	−69.2	0.063
7-2, 25	85.55	5.1	25.7	0.018
7-2, 75	86.05	0.9	−48.5	0.007
7-2, 125	86.55	191.6	−56.4	0.006
7-3, 25	87.05	316.4	41.7	0.018
7-3, 75	87.55	231.4	81.6	0.050
7-3, 125	88.05	153.9	−2.4	0.060
7-4, 25	88.55	186.9	−8.8	0.018
7-4, 75	89.05	149.1	−18.8	0.018
7-4, 125	89.55	245.4	33.0	0.004
7-5, 25	90.05	29.0	39.7	0.014
7-5, 75	90.55	306.3	20.3	0.012
7-5, 125	91.05	238.8	−10.5	0.010
7-6, 25	91.55	134.5	1.0	0.210
7-6, 75	92.05	28.6	−47.7	0.009
7-6, 125	92.55	215.7	13.5	0.019
8-1, 75	94.15	266.7	−17.8	0.013
8-1, 125	94.65	225.1	15.7	0.023
8-2, 75	95.65	237.1	11.6	0.008
8-2, 125	96.15	277.6	−57.5	0.004
8-3, 25	96.65	309.8	−78.9	0.009
8-3, 75	97.15	307.3	58.2	0.008
8-3, 120	97.60	185.3	−39.4	0.010
8-4, 25	98.15	153.9	54.9	0.007
8-4, 75	98.65	332.6	39.1	0.023
8-4, 125	99.15	227.1	78.9	0.008
8-5, 25	99.65	315.8	49.9	0.112
8-5, 75	100.15	189.3	44.0	0.010
8-5, 125	100.65	232.2	−6.0	0.009
8-6, 25	101.15	103.7	−28.0	0.014
8-6, 75	101.65	104.8	−15.5	0.019
8-6, 125	102.15	114.9	−69.5	0.007
10-1, 25	112.85	182.5	−32.3	0.013
10-1, 75	113.35	188.3	−29.1	0.012
10-1, 125	113.85	275.5	−42.3	0.005
10-2, 25	114.35	148.2	−48.9	0.007
10-2, 75	114.85	300.3	10.5	0.027
10-2, 125	115.35	201.3	57.8	0.011
10-3, 25	115.85	184.2	77.4	0.024
10-3, 75	116.35	50.2	32.8	0.018
10-3, 125	116.85	35.6	−25.4	0.013
10-4, 25	117.35	29.9	47.6	0.185
10-4, 75	117.85	184.7	−0.8	0.013
10-4, 125	118.35	337.9	3.6	0.006
10-5, 25	118.85	339.9	32.7	0.015

Table 4. (Continued).

Core-Section (interval in cm)	Sub-bottom depth (m)	Declination (°)	Inclination (°)	Intensity (μG)
10-5, 75	119.35	71.6	13.6	0.009
10-5, 125	119.85	332.5	21.1	0.004
10-6, 25	120.35	223.7	−13.1	0.010
10-6, 75	120.85	263.4	13.5	0.026

Table 5. NRM data, Hole 590B spanning Chron 9.

Core-Section (interval in cm)	Sub-bottom depth (m)	Declination (°)	Inclination (°)	Intensity (μG)
31-1, 55	278.85	250.1	8.1	0.071
31-2, 55	280.35	261.7	−9.6	0.060
31-3, 55	281.85	263.1	−6.3	0.060
31-4, 55	283.35	262.9	−12.9	0.055
31-5, 55	284.85	257.6	0.7	0.064
32-1, 55	288.45	196.2	3.9	0.088
32-2, 55	289.95	257.8	−2.7	0.061
32-3, 55	291.45	218.7	−9.1	0.049
32-4, 55	292.95	309.9	−14.7	0.024
32-5, 55	294.45	228.0	24.2	0.021
32-6, 55	295.95	246.6	−34.7	0.024
33-1, 55	298.05	247.9	18.4	0.046
33-2, 55	299.55	288.4	−32.8	0.061
33-3, 55	301.05	231.0	−23.9	0.028
33-4, 55	302.55	247.0	−23.7	0.037
33-5, 55	304.05	255.6	−27.5	0.047
33-6, 55	305.55	134.3	−36.4	0.145
34-1, 55	307.65	178.0	−82.5	0.042
34-2, 55	309.15	227.9	−47.5	0.019
34-3, 55	310.65	269.5	−36.4	0.034
34-4, 55	312.15	320.2	25.4	0.045
34-5, 55	313.65	247.8	−29.6	0.028
34-6, 55	315.15	175.1	−13.8	0.048
35-1, 55	317.25	176.6	−14.8	0.018
35-3, 55	320.25	209.0	−8.4	0.025
36-1, 55	326.85	274.0	−14.1	0.855
36-2, 55	328.35	174.9	19.1	0.048
36-3, 55	329.85	275.4	−11.8	0.016
36-4, 55	331.35	212.5	−30.5	0.069
36-5, 55	332.85	246.7	−25.6	0.044
36-6, 55	334.35	356.0	−56.2	0.014

ment such as we used, would lead to only minor refinements in the final polarity interpretation. For studies such as this, involving large collections of specimens, time is better devoted to processing a duplicate core to verify results from the first hole.

The hydraulic piston corer and extended core barrel rotary drilling were very successfully during Leg 90. Although the majority of HPC cores were oriented using the Kuster tool, we found that corrected declination results were no improvement on the raw data for identifying reversal boundaries. We conclude that it is not worthwhile bothering with the Kuster tool in its present form. In comparison with the inclination results, the declination data were more scattered than expected, even allowing for greater experimental uncertainty in the latter. This shows that even with the HPC, large-scale twisting of cores during recovery and/or sampling is common.

ACKNOWLEDGMENTS

We acknowledge with thanks the invaluable role played by the captain and crew of the *Glomar Challenger* during this Christmas voyage, DSDP staff, Peter Aldrich and others for voluntary assistance with

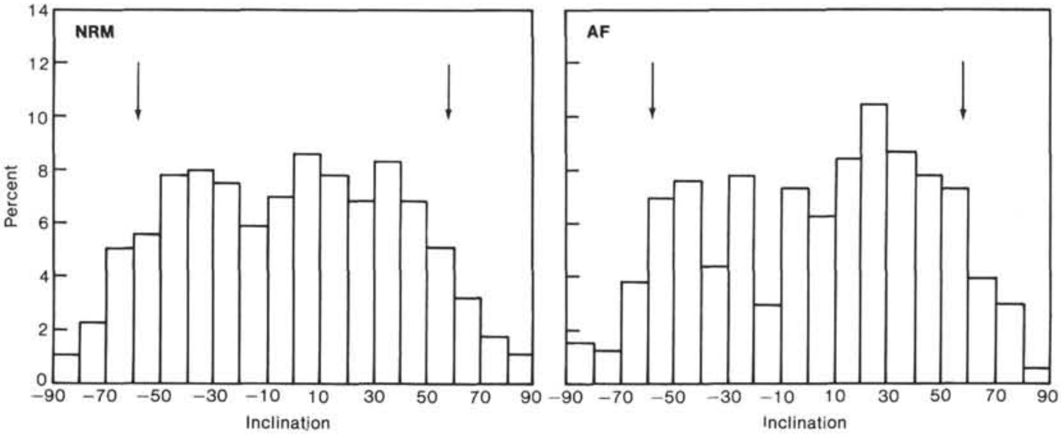

Figure 18. Distribution of inclinations for Hole 591 before and after AF cleaning. The axial dipole inclination = −50.9° (arrows).

laboratory work, and Pat Aldrich for secretarial help. Support came from NSF Grant OCE 8302233.

REFERENCES

Berggren, W. A., Kent, D. V., Flynn, J. F., and Van Couvering, J. A., 1983. Cenozoic geochronology. Woods Hole Oceanogr. Inst., Spec. Publ., Sept. 1983.

________, in press. Cenozoic geochronology. *Geol. Soc. Am. Bull.*

Berggren, W. A., Kent, D. V., and Van Couvering, J. A., in press. Neogene chronology and chronostratigraphy. *In* Snelling, N. J. (Ed.), *Geochronology and the Geological Record*. Geol. Soc. Lond., Spec. Pap.

Berner, R. A., 1964. Stability fields of iron minerals in anaerobic marine sediments. *J. Geol.*, 72:826–834.

Bleil, U., in press. The magnetostratigraphy of NW Pacific sediments, Deep Sea Drilling Project Leg 86. *In* von Huene, R., Aubouin, J., et al., *Init. Repts. DSDP*, 86: Washington (U.S. Govt. Printing Office).

Clement, R. M., and Kent, D. V., 1984. A detailed record of the Lower Jaramillo polarity transition from a southern hemisphere, deep-sea sediment core. *J. Geophys. Res.*, 89:1049–1058.

Hoffman, K. A., and Day, R., 1978. Separation of multicomponent NRM: a general method. *Earth Planet. Sci. Lett.*, 40:433–438.

Karlin, R., and Levi, S., 1983. Diagenesis of magnetic minerals in recent haemipelagic sediments. *Nature*, 303:327–330.

Kent, D. V., and Lowrie, W., 1977. VRM studies in Leg 37 igneous rocks. *In* Aumento, F., Melson, W. G., et al., *Init. Repts. DSDP*, 37: Washington (U.S. Govt. Printing Office), 525–529.

Kent, D. V., and Spariosu, D. J., 1982a. Magnetostratigraphy of Caribbean Site 502 hydraulic piston cores. *In* Prell, W. L., Gardner, J. V., et al., *Init. Repts. DSDP*, 68: Washington (U.S. Govt. Printing Office), 419–433.

________, 1982b. Magnetostratigraphy of equatorial Pacific Site 503 hydraulic piston cores. *In* Prell, W. L., Gardner, J. V., et al., *Init. Repts. DSDP*, 68: Washington (U.S. Govt. Printing Office), 435–440.

LaBrecque, J. L., Hsü, K. J., Carman, M. F., Jr., Karpoff, A., McKenzie, J. A., Percival, S. F., Jr., Petersen, N. P., Pisciotto, K. A., Schreiber, E., Tauxe, L., Tucker, P., Weissert, H. J., and Wright, R., 1983. DSDP Leg 73: Contributions to Paleogene stratigraphy in nomenclature, chronology and sedimentation rates. *Palaeogeogr., Palaeoclimatol., Palaeoecol.*, 42:91–125.

Lowrie, W., and Kent, D. V., 1978. Characteristics of VRM in oceanic basalts. *J. Geophys.*, 44:297–315.

Mayer, L. A., 1982. Physical properties of sediment recovered on Deep Sea Drilling Project Leg 68 with the hydraulic piston corer. *In* Prell, W. L., Gardner, J. V., et al., *Init. Repts. DSDP*, 68: Washington (U.S. Govt. Printing Office), 365–382.

Shimizu, Y., 1960. Magnetic viscosity of magnetite. *J. Geomag. Geoelectr.*, 11:125–138.

Silva, A. J., and Hollister, C. D., 1979. Geotechnical properties of ocean sediments recovered with the giant piston corer: Blake-Bahama Outer Ridge. *Mar. Geol.*, 29:1–22.

Tauxe, L., Tucker, P., and Petersen, N., 1984. Magnetostratigraphy of Leg 73 sediments. *In* Hsü, K. J., LaBrecque, J. L., et al., *Init. Repts. DSDP*, 73: Washington (U.S. Govt. Printing Office), 609–621.

Tauxe, L., Tucker, P., Petersen, N. P., and LaBrecque, J. L., 1983. The magnetostratigraphy of Leg 73 sediments. *Palaeogeogr., Palaeoclimatol., Palaeoecol.*, 42:65–90.

Tucker, P., and Tauxe, L., 1984. The downhole variation of the rock magnetic properties of IPOD Leg 73. *In* Hsü, K. J., LaBrecque, J. L., et al., *Init. Repts. DSDP*, 73: Washington (U.S. Govt. Printing Office), 673–685.

Weinreich, N., and Theyer, F., in press. Paleomagnetism of the Leg 85 sediments: Neogene magnetostratigraphy and tectonic history of the Central Equatorial Pacific. *In* Mayer, L., Theyer, F., et al., *Init. Repts. DSDP*, 85: Washington (U.S. Govt. Printing Office).

Date of Initial Receipt: 25 October 1984
Date of Acceptance: 1 April 1985

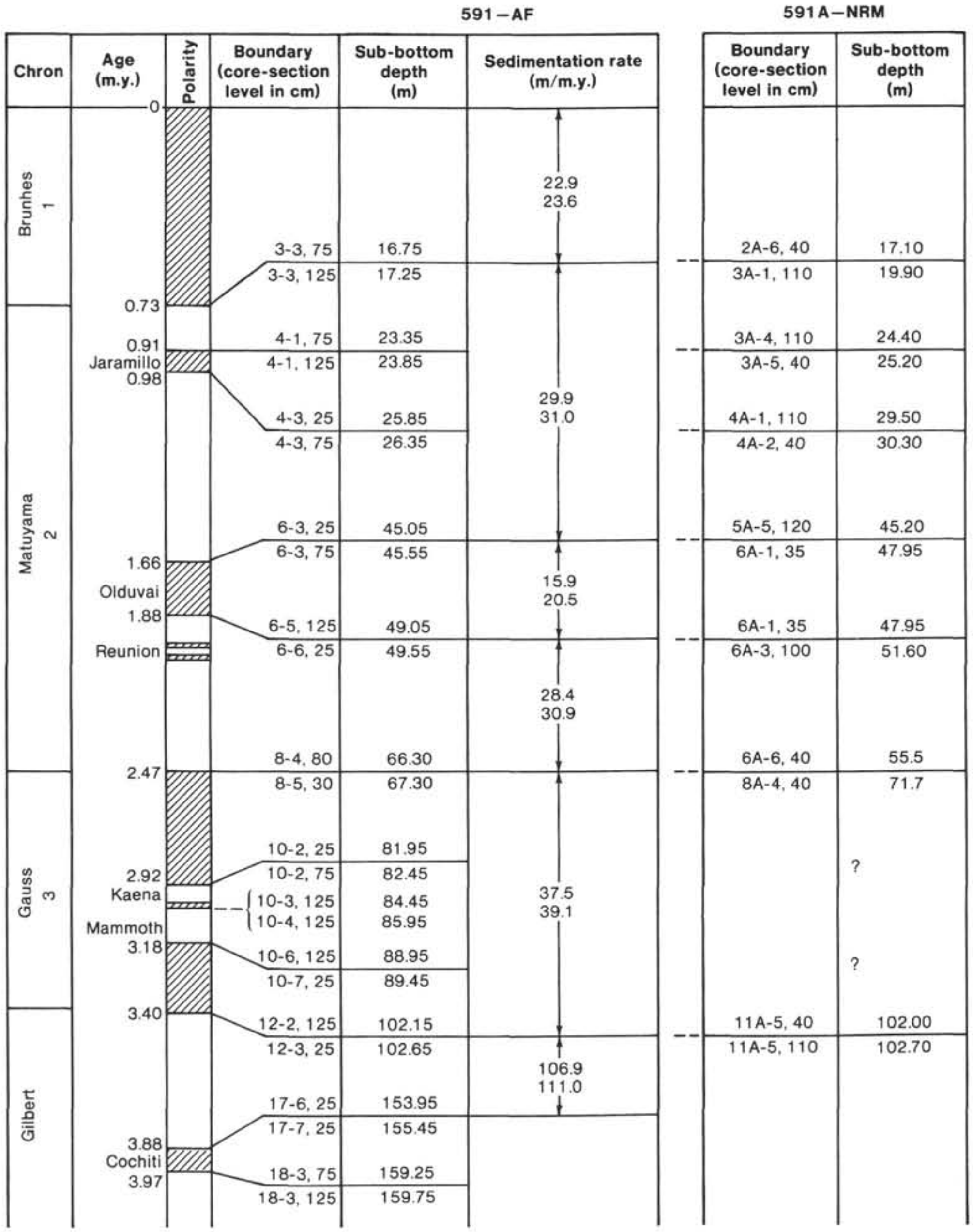

Figure 19. Reversal boundaries for the upper parts of Holes 591 and 591A. Results for Hole 591 are based on AF-cleaned (150 Oe) and filtered data. The polarity sequence is not defined below 167.5 m.

Table 6. AF-cleaned data, upper part of Hole 591.

Core-Section (interval in cm)	Sub-bottom depth (m)	Declination (°)	Inclination (°)	Intensity (μG)
1-1, 80	0.80	58.0	−55.7	3.295
1-1, 125	1.25	253.3	−83.0	0.807
1-2, 25	1.75	56.0	−53.8	4.473
1-2, 80	2.30	41.2	−48.8	7.225
1-2, 125	2.75	64.9	−56.0	0.600
2-1, 25	3.65	36.5	−49.0	2.220
2-1, 25	3.65	36.1	−49.6	2.242
2-1, 75	4.15	43.1	−55.7	0.356
2-1, 125	4.65	93.7	−50.0	0.103
2-2, 25	5.15	105.0	−64.2	0.131
2-2, 75	5.65	96.3	−52.4	0.185
2-3, 25	6.65	58.3	−16.7	0.204
2-3, 75	7.15	91.0	−70.0	0.072
2-3, 125	7.65	83.8	−54.1	0.063
2-4, 25	8.15	62.0	−56.0	0.097
2-4, 75	8.65	55.0	−58.0	0.103
2-4, 125	9.15	62.3	−66.0	0.078
2-5, 25	9.65	40.1	−66.0	0.145
2-5, 75	10.15	27.5	−49.7	0.063
2-5, 125	10.65	341.6	−70.6	0.112
2-6, 25	11.15	45.2	−12.8	0.075
2-6, 75	11.65	337.7	−72.1	0.146
2-7, 25	12.65	61.3	−67.0	0.154
3-1, 25	13.25	165.8	−45.1	0.127
3-1, 75	13.75	189.1	−52.3	0.155
3-1, 125	14.20	198.5	−48.3	0.088
3-2, 25	14.75	188.0	−40.6	0.094
3-2, 75	15.25	196.0	−37.7	0.188
3-2, 125	15.75	140.4	−27.3	0.176
3-3, 25	16.25	205.9	−39.5	0.145
3-3, 75	16.75	250.4	−17.5	0.029
3-3, 125	17.25	324.8	42.7	0.038
3-4, 25	17.75	343.2	47.7	0.096
3-4, 75	18.25	29.9	43.8	0.040
3-4, 125	18.75	359.8	13.6	0.029
3-5, 25	19.25	23.3	57.5	0.057
3-5, 75	19.75	349.3	32.1	0.076
3-5, 125	20.25	282.2	45.9	0.023
3-6, 25	20.75	351.1	26.4	0.035
3-6, 75	21.25	328.6	28.8	0.107
3-6, 125	21.75	131.1	50.8	0.027
4-1, 75	23.35	237.4	−6.9	0.006
4-1, 125	23.85	28.4	−69.7	0.075
4-2, 25	24.35	295.7	−24.2	0.017
4-2, 75	24.85	119.1	−27.2	0.029
4-2, 125	25.35	108.1	−46.7	0.021
4-3, 25	25.85	52.2	−25.5	0.021
4-3, 75	26.35	229.4	41.7	0.032
4-3, 125	26.85	250.1	61.3	0.022
4-4, 25	27.35	191.5	38.4	0.008
4-4, 75	27.85	246.3	35.4	0.006
4-4, 125	28.35	293.7	−23.4	6.906
4-5, 25	28.85	154.2	6.6	0.047
4-5, 75	29.35	212.3	52.6	0.018
4-5, 125	29.85	291.4	7.9	0.010
4-6, 25	30.35	27.2	38.3	0.017
4-6, 75	30.85	23.6	78.5	0.082
4-6, 125	31.35	354.1	30.6	0.020
5-1, 47	32.67	263.7	39.9	0.033
5-1, 75	32.95	144.2	86.6	0.029
5-1, 125	33.45	88.6	63.7	0.032
5-2, 25	33.95	231.3	48.4	0.016
5-2, 75	34.45	253.8	23.3	0.022
5-2, 125	34.95	198.0	−2.3	0.048
5-3, 25	35.45	198.1	51.0	0.027
5-3, 75	35.95	227.7	46.1	0.023
5-3, 125	36.45	221.6	−18.2	0.031
5-4, 25	36.95	167.9	0.0	0.009
5-4, 75	37.45	119.7	83.5	0.027
5-4, 125	37.95	191.4	41.0	0.024
5-5, 25	38.45	115.8	78.2	0.026
5-5, 75	38.95	114.1	63.6	0.036
5-5, 125	39.45	237.4	24.9	0.053
5-6, 25	39.95	243.8	11.3	0.017
5-6, 75	40.45	187.3	32.0	0.038
6-1, 125	43.05	325.7	57.4	0.021

Table 6. (Continued).

Core-Section (interval in cm)	Sub-bottom depth (m)	Declination (°)	Inclination (°)	Intensity (μG)
6-2, 25	43.55	133.5	59.4	0.040
6-2, 75	44.05	113.4	53.9	0.041
6-2, 125	44.55	176.6	14.3	0.034
6-3, 25	45.05	169.3	28.8	0.035
6-3, 75	45.55	154.0	−11.6	0.019
6-3, 125	46.05	229.6	−33.4	0.072
6-4, 25	46.55	266.9	−26.3	0.052
6-4, 75	47.05	253.1	−55.8	0.049
6-4, 125	47.55	290.8	−45.5	0.066
6-5, 25	48.05	280.8	−37.2	0.051
6-5, 75	48.55	277.0	−44.0	0.069
6-5, 125	49.05	261.0	−47.8	0.069
6-6, 25	49.55	283.7	38.0	0.019
6-6, 75	50.05	49.8	58.5	0.020
6-6, 125	50.55	110.9	35.5	0.027
7-1, 75	52.15	13.4	5.6	0.042
7-1, 125	52.65	324.3	37.6	0.029
7-2, 25	53.15	236.5	4.6	0.024
7-2, 75	53.65	172.9	−9.0	0.026
7-2, 125	54.15	305.8	18.0	0.019
7-3, 25	54.65	349.5	39.8	0.013
7-3, 75	55.15	190.6	63.4	0.025
7-3, 125	55.65	210.8	−12.5	0.039
7-4, 25	56.15	348.6	43.6	0.031
7-4, 75	56.65	14.2	55.3	0.011
7-4, 125	57.15	325.7	58.0	0.043
7-5, 25	57.65	256.0	57.2	0.029
7-5, 75	58.15	299.9	44.1	0.017
7-5, 125	58.65	262.8	30.2	0.016
7-6, 25	59.15	293.4	22.5	0.023
7-6, 75	59.65	284.5	37.5	0.039
7-6, 125	60.15	40.8	−31.5	0.008
8-1, 30	61.30	228.1	28.2	0.031
8-1, 80	61.80	78.8	−52.6	0.650
8-1, 130	62.30	263.9	44.8	0.028
8-2, 30	62.80	243.4	38.1	0.034
8-2, 80	63.30	244.0	15.2	0.017
8-2, 130	63.80	109.3	52.6	0.070
8-3, 30	64.30	265.2	4.7	0.069
8-3, 80	64.80	230.9	33.9	0.036
8-3, 130	65.30	210.0	11.5	0.008
8-4, 30	65.80	211.2	30.4	0.022
8-4, 80	66.30	237.7	8.7	0.029
8-5, 30	67.30	278.7	−58.0	0.012
8-5, 80	67.80	6.2	−49.7	0.025
8-5, 130	68.30	105.0	−45.1	0.064
8-6, 30	68.80	304.4	−34.5	0.027
8-6, 80	69.30	158.3	−48.9	0.080
8-6, 130	69.80	298.9	16.0	0.013
9-1, 75	71.35	247.3	−21.5	0.028
9-1, 125	71.85	255.8	25.4	0.009
9-2, 25	72.35	273.1	−37.9	0.031
9-2, 75	72.85	269.3	−34.8	0.015
9-2, 125	73.35	273.4	−31.8	0.042
9-3, 25	73.85	251.1	−36.4	0.029
9-3, 75	74.35	207.6	−6.5	0.037
9-3, 125	74.85	223.3	−7.8	0.017
9-4, 25	75.35	265.6	−64.3	0.016
9-4, 75	75.85	229.6	−41.9	0.026
9-4, 125	76.35	272.8	8.1	0.030
9-5, 25	76.85	199.3	−25.8	0.015
9-5, 75	77.35	238.4	−19.8	0.019
9-5, 125	77.85	265.1	5.2	0.006
9-6, 25	78.35	84.8	−2.0	0.034
9-6, 75	78.85	205.9	−48.7	0.038
9-6, 125	79.35	200.0	−38.3	0.015
10-1, 85	81.05	207.9	0.0	0.006
10-1, 125	81.45	62.9	56.7	0.006
10-2, 25	81.95	220.8	−24.9	0.024
10-2, 75	82.45	336.1	13.3	0.008
10-2, 125	82.95	147.7	61.1	0.009
10-3, 25	83.45	160.3	48.9	0.022
10-3, 75	83.95	317.8	30.2	0.006
10-3, 125	84.45	292.9	−28.6	0.009
10-3, 125	84.45	307.0	−27.7	0.012
10-4, 25	84.95	116.2	−49.2	0.036

Table 6. (Continued).

Core-Section (interval in cm)	Sub-bottom depth (m)	Declination (°)	Inclination (°)	Intensity (μG)
10-4, 75	85.45	93.4	−59.7	0.018
10-4, 125	85.95	187.6	−56.7	0.011
10-5, 25	86.45	248.8	22.8	0.031
10-5, 75	86.95	327.7	12.2	0.009
10-5, 125	87.45	220.6	11.1	0.010
10-6, 25	87.95	266.3	27.4	0.019
10-6, 75	88.45	323.5	14.6	0.023
10-6, 125	88.95	308.1	26.0	0.014
10-7, 25	89.45	298.6	−48.3	0.012
11-1, 75	90.55	325.4	−11.1	0.004
11-1, 125	91.05	215.0	−35.6	0.010
11-2, 25	91.55	350.1	29.4	0.080
11-2, 75	92.05	43.4	−52.7	0.013
11-2, 125	92.55	75.3	−33.6	0.008
11-2, 125	92.55	49.8	−40.9	0.009
11-3, 25	93.05	117.3	−36.4	0.020
11-3, 75	93.55	42.6	−65.0	0.018
11-3, 125	94.05	236.8	16.0	0.062
11-4, 25	94.55	261.3	−35.0	0.022
11-4, 75	95.05	255.5	−59.1	0.048
11-4, 125	95.55	258.2	−57.4	0.013
11-5, 25	96.05	130.2	−5.7	0.016
11-5, 75	96.55	244.7	42.9	0.053
11-5, 125	97.05	167.3	43.3	0.018
11-6, 25	97.55	295.8	−35.3	0.013
11-6, 25	97.55	295.2	−25.3	0.016
11-6, 75	98.05	243.2	2.4	0.009
11-6, 75	98.05	239.0	14.7	0.008
11-6, 125	98.55	295.2	−57.2	0.008
11-6, 125	98.55	333.1	−61.1	0.011
12-1, 125	100.65	319.5	−79.2	0.070
12-2, 25	101.15	142.3	−54.4	0.020
12-2, 75	101.65	157.8	−28.4	0.015
12-2, 75	101.65	166.3	−44.1	0.014
12-2, 75	101.65	157.8	−28.4	0.015
12-2, 125	102.15	1.5	−41.7	0.036
12-3, 25	102.65	118.8	14.5	0.009
12-3, 25	102.65	88.4	27.2	0.006
12-3, 75	103.15	276.6	14.5	0.032
12-3, 125	103.65	268.6	25.2	0.010
12-4, 25	104.15	172.8	48.8	0.007
12-4, 75	104.65	36.6	−11.0	0.006
12-4, 75	104.65	60.3	−5.9	0.006
12-4, 75	104.65	44.1	0.0	0.007
12-4, 125	105.15	115.2	−20.3	0.009
12-4, 125	105.15	107.8	−11.4	0.009
12-5, 25	105.65	172.4	−23.3	0.015
12-6, 25	107.15	202.5	67.5	0.159
12-6, 125	108.15	193.8	53.1	0.105
13-1, 25	109.25	167.0	72.0	0.017
13-1, 75	109.75	347.3	14.3	0.030
13-1, 125	110.25	225.9	37.8	0.018
13-2, 25	110.75	138.0	−19.3	0.011
13-2, 75	111.25	194.0	53.9	0.020
13-2, 125	111.75	263.7	37.6	0.027
13-3, 25	112.25	213.0	10.6	0.019
13-3, 75	112.75	233.1	−12.9	0.026
13-3, 125	113.25	284.7	18.6	0.019
13-4, 25	113.75	230.9	−21.1	0.065
13-4, 75	114.25	283.7	8.0	0.024
13-4, 125	114.75	272.9	2.7	0.024
13-5, 25	115.25	280.4	−47.4	0.068
13-5, 75	115.75	83.4	−4.0	0.016
13-5, 125	116.25	287.9	18.7	0.025
13-6, 25	116.75	300.8	22.9	0.020
13-6, 125	117.75	222.1	20.7	0.110
14-1, 75	119.05	97.7	18.8	0.087
14-1, 125	119.55	271.9	53.3	0.012
14-2, 25	120.05	273.7	62.4	0.041
14-2, 75	120.55	303.4	−9.5	0.024
14-2, 125	121.05	259.4	−27.7	0.024
14-3, 25	121.55	349.8	23.4	0.045
14-3, 75	122.05	322.5	2.5	0.018
14-3, 125	122.55	242.1	6.8	0.020
14-4, 25	123.05	279.0	1.8	0.018
14-4, 75	123.55	269.5	10.1	0.021

Table 6. (Continued).

Core-Section (interval in cm)	Sub-bottom depth (m)	Declination (°)	Inclination (°)	Intensity (μG)
14-4, 125	124.05	263.1	33.2	0.019
14-5, 25	124.55	135.6	8.5	0.022
14-5, 75	125.05	265.0	11.1	0.020
14-5, 125	125.55	249.1	−69.3	0.491
14-6, 25	126.05	316.1	45.6	0.017
14-6, 75	126.55	247.3	26.4	0.019
14-6, 125	127.05	259.2	69.5	0.008
14-7, 25	127.55	90.1	−45.2	0.030
15-1, 75	128.35	323.5	41.9	0.007
15-1, 125	128.85	280.7	10.4	0.096
15-2, 25	129.35	334.7	4.2	0.026
15-2, 75	129.85	298.7	−41.8	0.025
15-2, 125	130.35	84.4	−50.9	0.016
15-3, 25	130.85	301.2	65.7	0.020
15-3, 75	131.35	176.7	−41.3	0.029
15-3, 125	131.85	201.9	44.5	0.017
15-4, 25	132.35	167.1	1.5	0.037
15-4, 75	132.85	212.5	26.6	0.012
15-4, 125	133.35	116.6	21.2	0.012
15-5, 25	133.85	347.1	33.4	0.009
15-5, 75	134.35	223.2	−86.2	0.038
15-5, 125	134.85	32.7	−30.4	0.610
15-6, 25	135.35	277.2	53.4	0.013
15-6, 75	135.85	241.5	−33.4	0.008
15-6, 125	136.35	210.0	52.2	0.012
15-7, 25	136.85	257.3	47.8	0.010
16-1, 30	137.20	312.1	66.5	0.019
16-1, 75	137.65	196.2	61.6	0.011
16-1, 125	138.15	6.8	5.1	0.015
16-2, 25	138.65	178.8	−73.8	0.007
16-2, 75	139.15	88.4	42.8	0.017
16-2, 125	139.65	270.5	72.2	0.061
16-3, 25	140.15	270.0	41.2	0.081
16-3, 75	140.65	110.1	−37.1	0.026
16-3, 125	141.15	182.0	10.8	0.009
16-4, 25	141.65	229.0	−35.5	0.003
16-4, 75	142.15	114.7	−23.5	0.119
16-4, 125	142.65	211.3	−40.0	0.007
16-5, 25	143.15	9.9	30.5	0.039
16-5, 75	143.65	350.5	−62.5	0.246
16-5, 125	144.15	313.3	−23.8	0.009
16-6, 25	144.65	56.0	−8.7	0.033
16-6, 75	145.15	246.5	−3.5	0.028
16-6, 125	145.65	195.4	17.2	0.016
16-7, 25	146.15	140.3	46.1	0.128
17-2, 125	148.95	150.7	43.7	0.025
17-3, 25	149.45	57.7	17.1	0.077
17-3, 75	149.95	193.7	−23.0	0.009
17-3, 75	149.95	181.0	−2.1	0.011
17-3, 125	150.45	9.9	23.0	0.028
17-4, 25	150.95	247.9	−31.1	0.091
17-4, 75	151.45	169.4	54.6	0.010
17-4, 125	151.95	121.3	80.5	0.006
17-5, 25	152.45	336.6	8.8	0.030
17-5, 75	152.95	87.6	17.1	0.052
17-5, 125	153.45	197.9	47.1	0.002
17-6, 25	153.95	205.9	21.5	0.017
17-6, 25	153.95	108.4	72.1	0.018
17-6, 125	154.95	241.9	−67.9	0.005
17-7, 25	155.45	219.1	−64.4	0.009
18-1, 125	156.75	277.8	28.4	0.008
18-2, 75	157.75	28.5	−57.2	0.015
18-3, 25	158.75	258.6	−2.9	0.023
18-3, 75	159.25	257.8	−17.5	0.013
18-3, 75	159.25	254.7	−26.7	0.014
18-3, 125	159.75	195.8	−4.6	0.012
18-4, 25	160.25	355.4	39.5	0.032
18-4, 75	160.75	146.2	2.5	0.009
18-4, 125	161.25	188.2	3.6	0.006
18-4, 125	161.25	177.7	17.1	0.006
18-5, 25	161.75	197.1	34.8	0.006
18-5, 75	162.25	315.9	−6.7	0.055
18-5, 125	162.75	222.7	15.9	0.011
18-6, 25	163.25	228.5	−34.8	0.004
18-6, 75	163.75	329.6	37.4	0.011
18-6, 125	164.25	218.2	−35.3	0.007

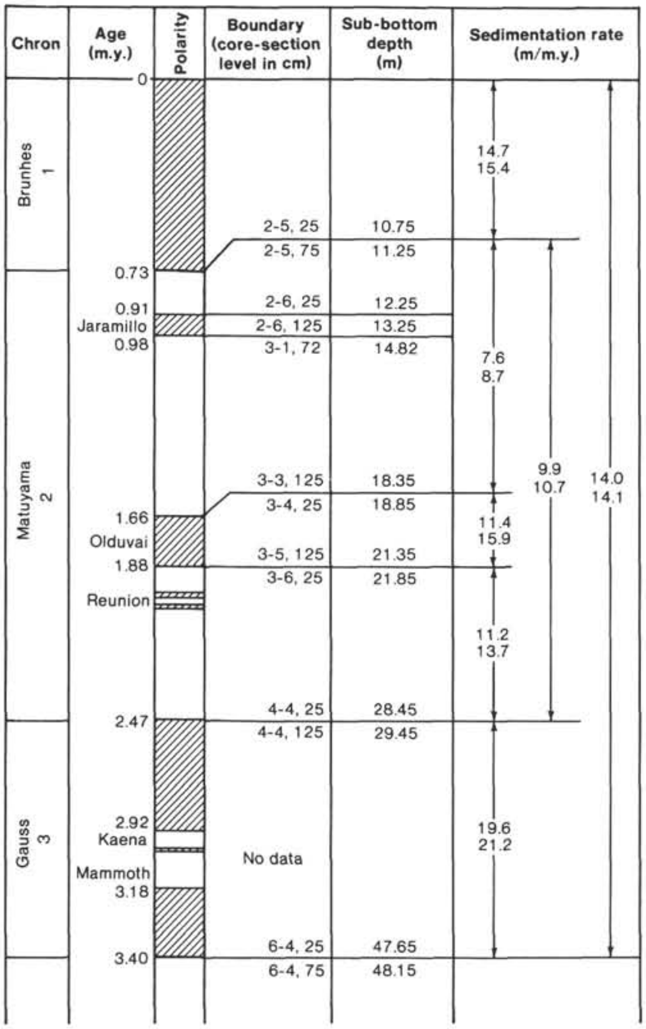

Figure 20. Reversal boundaries for the upper part of Hole 592 based on AF-cleaned (200 Oe) and filtered data. The polarity sequence is not defined below 60.4 m.

Table 7. AF-cleaned data, upper part of Hole 592.

Core-Section (interval in cm)	Sub-bottom depth (m)	Declination (°)	Inclination (°)	Intensity (μG)
1-1, 75	0.75	273.4	−39.4	0.092
1-1, 125	1.25	293.3	−45.1	0.035
1-2, 25	1.75	183.5	−54.2	0.095
1-2, 75	2.25	172.0	−64.6	0.065
1-2, 125	2.75	193.7	−63.6	0.090
1-3, 25	3.25	201.5	−32.4	0.013
1-3, 75	3.75	213.2	−44.3	0.025
1-3, 125	4.25	261.6	−74.8	0.030
2-1, 25	4.75	239.2	−4.1	0.029
2-1, 75	5.25	222.0	−61.2	0.041
2-1, 125	5.75	183.4	−18.4	0.031
2-2, 75	6.75	213.0	−55.4	0.043
2-2, 125	7.25	212.5	−34.7	0.035
2-3, 21	7.71	105.1	−32.8	0.027
2-3, 75	8.25	146.5	−57.8	0.118
2-3, 75	8.25	149.4	−54.0	0.131
2-3, 125	8.75	126.5	23.1	0.044
2-3, 125	8.75	131.4	17.7	0.048
2-4, 25	9.25	175.7	−49.6	0.060
2-4, 125	10.25	341.3	−16.3	0.014
2-5, 75	11.25	0.0	77.0	0.026
2-5, 125	11.75	300.1	44.4	0.023
2-6, 25	12.25	305.5	5.6	0.020
2-6, 125	13.25	159.8	−78.2	0.032
3-1, 72	14.82	189.7	63.9	0.032
3-1, 125	15.35	191.8	54.4	0.024
3-2, 25	15.85	341.9	47.8	0.056
3-2, 75	16.35	349.6	48.3	0.016
3-2, 125	16.85	186.2	49.5	0.125
3-3, 25	17.35	3.0	48.3	0.024
3-3, 75	17.85	36.1	46.2	0.039
3-3, 125	18.35	105.5	54.3	0.017
3-4, 25	18.85	30.5	−20.1	0.031
3-4, 75	19.35	78.5	−35.6	0.030
3-4, 125	19.85	6.9	−6.8	0.024
3-5, 25	20.35	354.7	3.3	0.024
3-5, 75	20.85	113.7	−36.6	0.015
3-5, 125	21.35	234.8	−13.6	0.016
3-6, 25	21.85	6.5	10.2	0.013
3-6, 75	22.35	73.4	36.5	0.026
3-6, 125	22.85	272.6	66.3	0.105
4-1, 75	24.45	319.7	61.9	0.034
4-1, 125	24.95	5.7	53.3	0.018
4-2, 75	25.95	16.1	58.5	0.024
4-2, 125	26.45	74.5	66.5	0.040
4-3, 125	27.95	41.1	12.6	0.027
4-4, 25	28.45	74.9	16.1	0.019
4-4, 125	29.45	243.4	−23.1	0.013
4-5, 75	30.45	169.3	−60.8	0.021
4-5, 125	30.95	283.4	−70.0	0.015
4-5, 125	30.95	281.8	−49.4	0.013
4-6, 25	31.45	254.9	−16.4	0.025
4-6, 75	31.95	195.3	−62.8	0.031
4-6, 125	32.45	274.7	−81.6	0.032
6-1, 75	43.65	188.0	−27.6	0.031
6-1, 125	44.15	143.4	−69.0	0.033
6-2, 25	44.65	258.1	−12.4	0.015
6-2, 75	45.15	248.2	38.2	0.023
6-2, 125	45.65	56.3	−76.5	0.005
6-3, 75	46.65	57.5	−76.7	0.013
6-3, 125	47.15	108.8	−55.8	0.008
6-4, 25	47.65	34.5	−19.7	0.011
6-4, 75	48.15	19.8	12.9	0.009
6-4, 125	48.65	179.2	−39.2	0.015
6-5, 25	49.15	265.2	9.7	0.015
6-5, 75	49.65	59.5	25.9	0.019
6-5, 125	50.15	160.5	37.2	0.010
6-6, 25	50.65	258.3	11.8	0.020
6-6, 75	51.15	158.1	7.7	0.022
6-6, 125	51.65	7.0	23.1	0.015
7-1, 25	52.75	146.9	58.6	0.012
7-1, 75	53.25	302.4	−18.3	0.122
7-1, 125	53.75	85.2	−40.0	0.011
7-2, 25	54.25	252.5	11.6	0.053
7-2, 75	54.75	104.0	−4.5	0.010
7-2, 125	55.25	344.6	−18.1	0.040
7-3, 25	55.75	93.0	17.5	0.008
7-3, 75	56.25	227.1	−0.7	0.017
7-3, 125	56.75	238.4	−46.5	0.016
7-4, 25	57.25	217.8	25.2	0.035
7-4, 75	57.75	162.8	−1.9	0.018
7-4, 125	58.25	144.7	13.2	0.031
7-5, 25	58.75	129.4	58.1	0.019
7-5, 75	59.25	158.8	15.2	0.030
8-1, 25	62.35	236.3	5.1	0.009
8-1, 30	62.40	287.0	−32.4	0.005
8-1, 75	62.85	269.3	−70.4	0.036
8-1, 125	63.35	193.2	26.1	0.014
8-3, 75	65.85	108.4	−86.8	0.013
8-4, 25	66.85	276.8	22.8	0.012
8-4, 125	67.85	107.8	26.0	0.022
8-5, 25	68.35	172.7	7.0	0.019
8-5, 125	69.35	198.6	−55.6	0.021
8-6, 25	69.85	300.2	−59.7	0.012
8-6, 75	70.35	140.6	−80.4	0.130
8-6, 125	70.85	149.4	32.5	0.015

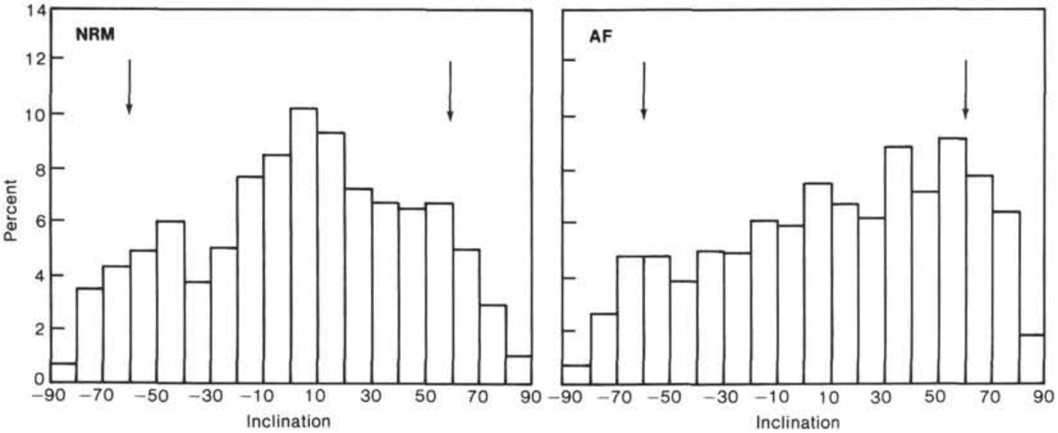

Figure 21. Distribution of inclinations for Hole 593 before and after AF cleaning at 200 Oe. The axial dipole inclination at the site is −59.7° (arrows). The positive bias after AF cleaning is caused by a long interval of reversed overprinting.

Table 8. Magnetic properties, Hole 593.

Magnetic zone	Depth (m)	Ranges J_N (μG)	χ' (μG Oe^{-1})	Q′ (Oe)	Mean MDF (Oe)	Comment
A	0.0–0.45	1.4–2.3	2.2–3.2	0.63–0.89	~450	Strongly magnetized oxidized surface layer, Subunit IA
B	0.45–75	0.01–0.1	falls to 1	0.01–0.1	265 ± 168	J_N and χ' decrease gradually with depth, Q′ initially drops to 0.035 at 0.75 m
C	75–360	0.005–0.02	0.5–1.5	.015–0.2	194 ± 111	Extremely weak magnetization
D	360–470	2–4	1–6	0.2–0.8	231 ± 115	Strongly magnetic, includes colored Subunit IC, very poor magnetic stability, high VRM coefficient
E	>470	0.01–0.1	0.5–1.5	0.02–0.5	221 ± 108	J_N, χ', and Q′ increase with depth

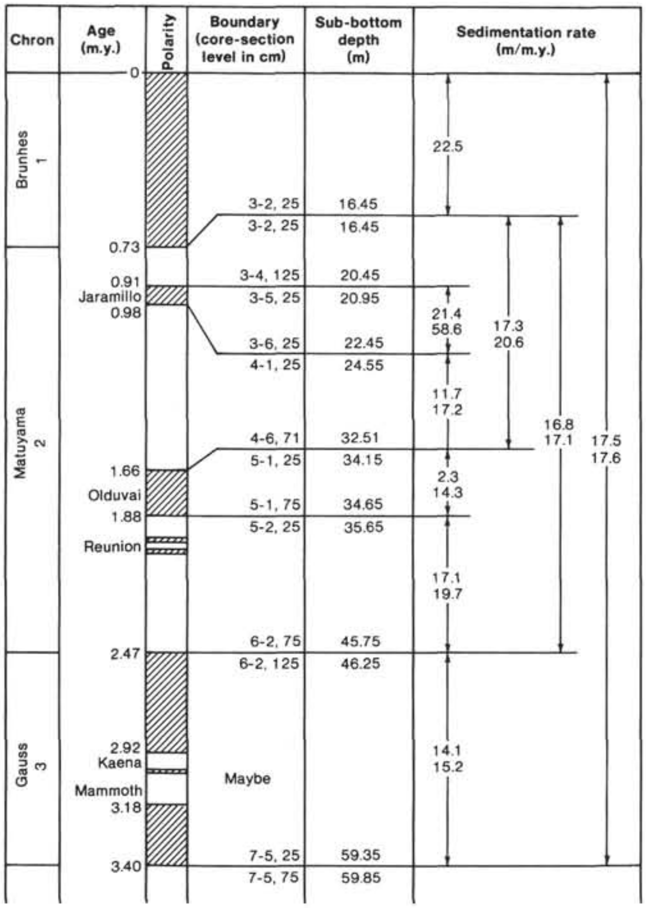

Figure 22. Reversal boundaries for the upper part of the sequence in Hole 593, based on AF-cleaned (200 Oe) and filtered data. The pattern is duplicated in Hole 593A down to 63 m sub-bottom depth.

Table 9. AF-cleaned data, upper part of Hole 593 and Unit II.

Core-Section (interval in cm)	Sub-bottom depth (m)	Declination (°)	Inclination (°)	Intensity (μG)
1-1, 10	0.10	230.6	−57.6	1.107
1-1, 25	0.25	277.4	−49.2	1.530
1-1, 45	0.45	340.5	−51.4	1.088
1-1, 75	0.75	80.5	−76.8	0.050
1-1, 95	0.95	66.5	−39.8	0.023
1-1, 110	1.10	213.0	−9.4	0.080
1-2, 10	1.60	327.3	−57.8	0.018
1-2, 25	1.75	143.0	−57.6	0.046
1-2, 45	1.95	118.6	−79.5	0.041
1-2, 95	2.45	122.6	2.2	0.138
1-2, 110	2.60	146.4	−61.0	0.113
1-2, 125	2.75	111.6	−55.4	0.077
1-3, 25	3.25	314.8	−21.9	0.051
1-3, 25	3.25	310.6	−23.6	0.048
1-3, 50	3.50	170.3	−57.9	0.038
1-3, 75	3.75	171.2	−40.9	0.043
1-3, 95	3.95	194.9	−40.3	0.166
1-3, 125	4.25	189.6	−48.6	0.067
1-4, 25	4.75	178.0	−62.0	0.051
1-4, 25	4.75	248.4	−76.7	0.033
1-4, 50	5.00	190.5	−39.4	0.048
2-1, 75	5.85	353.9	−50.8	0.038
2-1, 125	6.35	94.4	−32.2	0.020
2-2, 25	6.85	184.8	−80.4	0.019
2-2, 75	7.35	150.7	−2.9	0.023
2-3, 25	8.35	304.8	−54.3	0.032
2-3, 75	8.85	274.1	−33.4	0.074

Table 9. (Continued).

Core-Section (interval in cm)	Sub-bottom depth (m)	Declination (°)	Inclination (°)	Intensity (μG)
2-3, 125	9.35	332.0	−64.1	0.046
2-4, 25	9.85	318.9	−37.0	0.032
2-4, 75	10.35	37.7	−51.7	0.015
2-4, 125	10.85	312.4	−15.6	0.038
2-5, 25	11.35	302.6	−31.3	0.019
2-5, 75	11.85	269.1	−41.0	0.040
2-5, 125	12.35	318.2	−21.3	0.044
2-6, 25	12.85	323.5	−6.2	0.034
2-6, 75	13.35	323.6	6.3	0.005
2-6, 125	13.85	339.6	−23.1	0.022
3-1, 75	15.45	135.5	−55.0	0.034
3-2, 25	16.45	200.7	−30.4	0.028
3-2, 75	16.95	308.4	−7.6	0.013
3-2, 125	17.45	310.4	37.5	0.017
3-3, 25	17.95	288.6	37.5	0.033
3-3, 75	18.45	268.9	12.6	0.023
3-3, 125	18.95	280.7	43.0	0.082
3-4, 25	19.45	193.7	54.5	0.016
3-4, 75	19.95	1.7	47.8	0.018
3-4, 125	20.45	339.2	68.2	0.013
3-5, 25	20.95	72.2	−64.6	0.039
3-5, 68	21.38	182.8	−57.7	0.096
3-5, 125	21.95	164.7	−67.1	0.024
3-6, 25	22.45	78.6	−63.4	0.027
3-6, 75	22.95	183.0	−57.2	0.016
3-6, 125	23.45	146.6	−35.4	0.014
4-1, 25	24.55	269.4	61.4	0.163
4-1, 75	25.05	112.6	−8.1	0.179
4-1, 125	25.55	225.6	63.7	0.022
4-2, 25	26.05	249.0	73.0	0.030
4-2, 75	26.55	223.2	32.9	0.042
4-2, 125	27.05	315.2	74.7	0.029
4-3, 25	27.55	282.9	35.0	0.025
4-3, 75	28.05	129.7	66.3	0.020
4-3, 125	28.55	81.4	10.5	0.170
4-4, 25	29.05	103.7	55.8	0.038
4-4, 75	29.55	136.2	33.5	0.031
4-4, 125	30.05	77.3	47.7	0.049
4-5, 25	30.55	305.3	39.4	0.047
4-5, 25	30.55	320.5	34.8	0.057
4-5, 75	31.05	330.6	48.9	0.024
4-5, 75	31.05	341.6	52.7	0.025
4-5, 125	31.55	319.8	62.2	0.015
4-5, 125	31.55	319.7	65.2	0.016
4-6, 25	32.05	356.2	23.1	0.034
4-6, 71	32.51	330.1	39.6	0.043
5-1, 25	34.15	322.1	−18.9	0.042
5-1, 75	34.65	254.4	−53.9	0.036
5-2, 25	35.65	71.2	76.8	0.009
5-2, 75	36.15	115.3	49.9	0.031
5-2, 125	36.65	233.8	28.8	0.019
5-3, 25	37.15	310.2	−13.7	0.015
5-3, 75	37.65	103.9	68.1	0.032
5-3, 125	38.15	159.5	68.8	0.022
5-4, 25	38.65	114.7	−57.9	0.029
5-4, 75	39.15	106.2	68.0	0.022
5-4, 125	39.65	166.2	62.4	0.023
5-5, 25	40.15	284.7	68.7	0.021
5-5, 75	40.65	148.3	63.7	0.037
5-5, 125	41.15	277.9	21.4	0.031
5-6, 25	41.65	41.8	−39.5	0.007
5-6, 75	42.15	155.8	74.9	0.011
5-6, 125	42.65	138.6	6.2	0.169
6-1, 75	44.25	293.3	39.7	0.015
6-1, 125	44.75	26.7	70.5	0.063
6-2, 25	45.25	293.4	2.0	0.039
6-2, 75	45.75	359.1	23.2	0.010
6-2, 125	46.25	336.8	−2.3	0.128
6-3, 25	46.75	275.4	−37.3	0.046
6-3, 75	47.25	261.7	−16.3	0.053
6-3, 121	47.71	224.3	−63.7	0.030
6-3, 125	47.75	164.6	36.1	0.015
6-4, 25	48.25	328.9	−69.9	0.040
6-4, 75	48.75	153.9	−67.6	0.042
6-4, 125	49.25	110.7	−62.3	0.022
6-4, 125	49.25	110.9	−61.6	0.024
6-5, 25	49.75	304.4	−60.5	0.024

Table 9. (Continued).

Core-Section (interval in cm)	Sub-bottom depth (m)	Declination (°)	Inclination (°)	Intensity (μG)
6-5, 75	50.25	135.8	-45.7	0.030
6-5, 125	50.75	231.5	-4.5	0.022
6-6, 25	51.25	242.2	-37.7	0.025
6-6, 75	51.75	205.7	2.2	0.010
6-6, 125	52.25	236.2	-53.3	0.039
7-1, 75	53.85	1.0	-26.1	0.038
7-2, 75	55.35	250.1	-74.5	0.021
7-3, 75	56.85	294.1	-25.9	0.014
7-4, 75	58.35	318.4	-61.2	0.015
7-4, 124	58.84	27.8	-26.0	0.018
7-5, 25	59.35	262.5	-12.7	0.022
7-5, 75	59.85	279.8	40.7	0.026
7-5, 125	60.35	279.7	54.7	0.013
7-6, 25	60.85	85.7	-23.9	0.051
7-6, 75	61.35	283.6	34.0	0.020
7-6, 125	61.85	215.1	18.8	0.013
8-2, 25	64.45	180.0	-66.1	0.009
8-2, 75	64.95	245.0	-50.3	0.012
9-1, 75	73.05	207.7	-23.4	0.011
9-1, 125	73.55	271.7	-4.3	0.013
9-2, 25	74.05	162.6	67.8	0.074
9-2, 75	74.55	140.6	40.1	0.008
9-2, 125	75.05	215.0	23.1	0.008
9-3, 75	76.05	246.0	45.4	0.006
8-3, 125	76.55	229.3	47.7	0.016
9-3, 125	76.55	200.5	29.4	0.012
9-4, 25	77.05	102.3	-55.6	0.174
9-4, 75	77.55	231.8	3.1	0.011
9-4, 125	78.05	18.2	-75.0	0.806
9-5, 25	78.55	164.8	29.8	0.003
9-5, 25	78.55	169.1	37.1	0.004
9-5, 75	79.05	212.2	-13.8	0.009
9-5, 125	79.55	29.4	19.4	0.029
9-6, 25	80.05	141.5	6.5	0.065
58-1, 25	542.95	158.5	-60.2	0.618
58-1, 75	543.45	40.0	17.3	0.008
58-1, 125	543.95	93.1	-5.7	0.029
58-2, 25	544.45	293.1	13.6	0.024
58-2, 85	545.05	224.7	-12.9	0.025
58-2, 125	545.45	212.1	-28.0	0.044
58-3, 72	546.42	66.0	51.0	2.039
59-1, 94	553.24	353.0	67.0	9.320
59-2, 132	555.12	315.0	79.0	8.102
59-3, 50	555.80	340.0	81.0	5.545
59-3, 132	556.62	132.0	61.0	4.734
59-5, 65	558.95	33.0	-62.0	0.179
59-5, 100	559.30	343.0	30.0	0.303
59,CC 10	560.20	126.0	18.0	0.030
60-1, 25	562.15	253.4	6.9	0.016
60-1, 78	562.68	99.3	-20.9	0.034
60-1, 125	563.15	99.4	-55.0	0.071
60-2, 25	563.65	281.4	-59.5	0.265
60-2, 75	564.15	232.0	-39.0	0.078
60-2, 84	564.24	258.8	-17.7	0.024
60-2, 125	564.65	272.0	75.5	0.009
60-3, 25	565.15	102.9	10.4	0.019
60-3, 75	565.65	175.5	-28.1	0.006
60-3, 125	566.15	258.0	33.7	0.022
60-4, 25	566.65	209.5	59.7	0.015
60-4, 70	567.10	69.9	11.9	0.014
60-4, 125	567.65	190.7	-13.3	0.012
60-5, 75	568.65	111.8	-67.5	0.008
60-5, 125	569.15	195.2	-47.0	0.011
60-6, 25	569.65	84.7	1.4	0.077

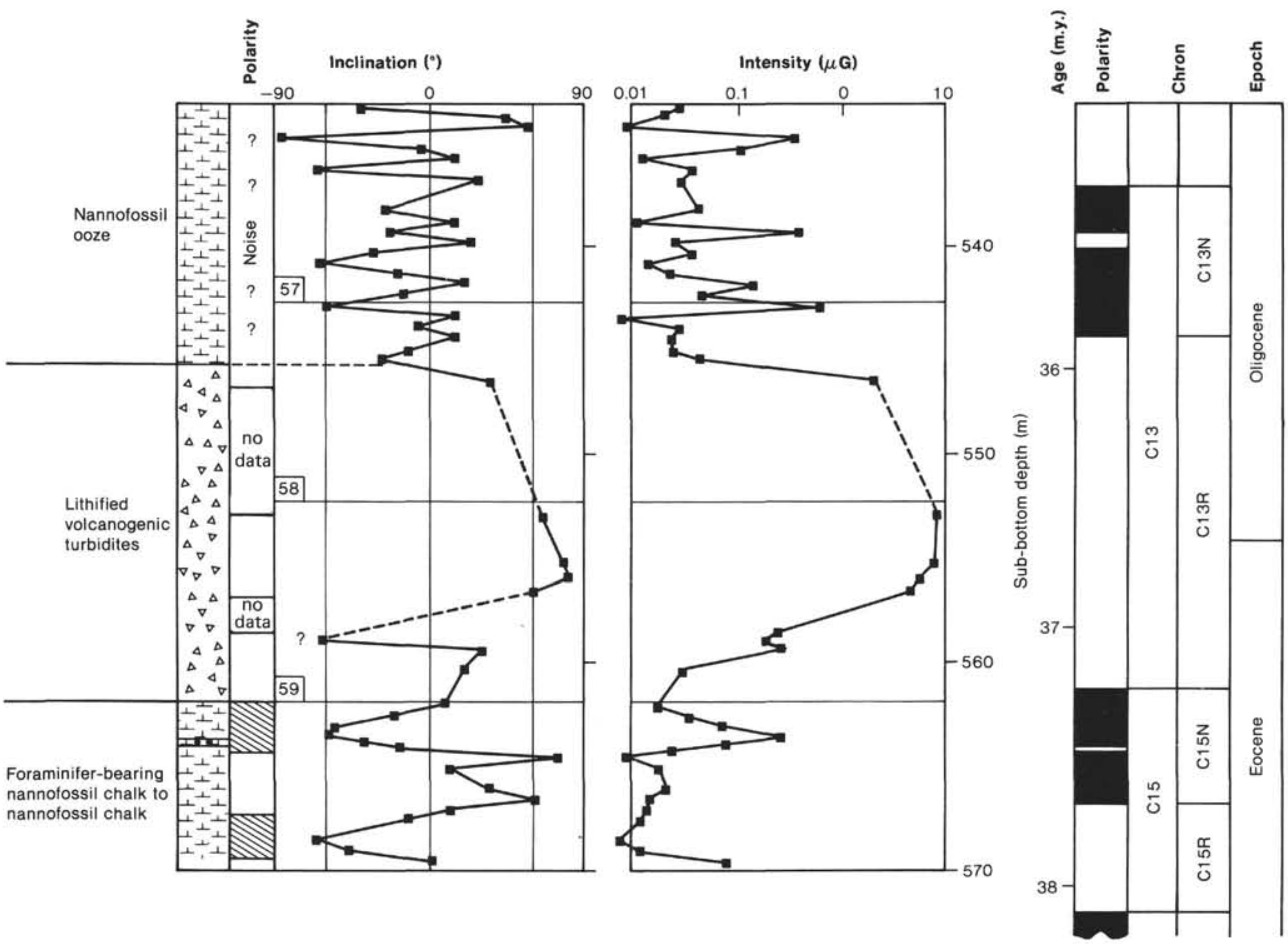

Figure 23. Inclination and intensity data in the vicinity of the volcanogenic turbidite beds in Hole 593, which are thought to mark the Eocene/Oligocene boundary. Core numbers are shown in boxes. Shaded regions are normal polarity. The magnetic polarity time scale is that of Berggren et al. (in press).

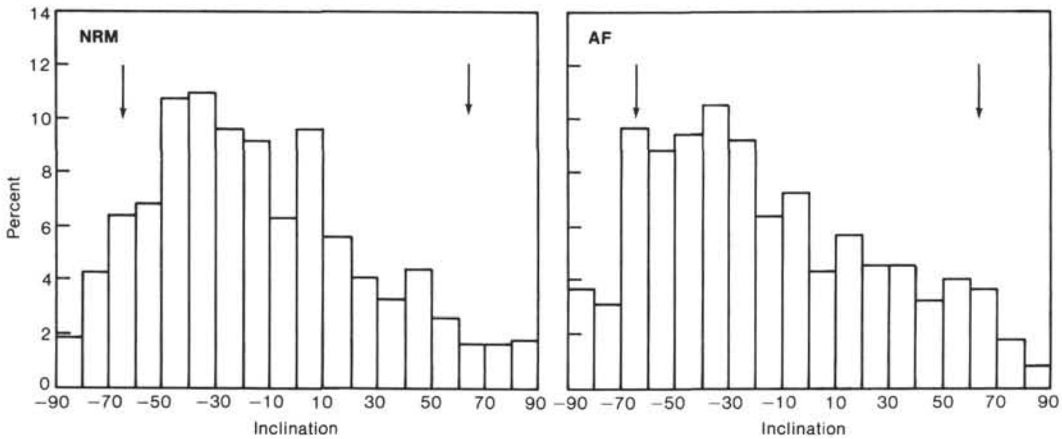

Figure 24. Distribution of inclinations for Hole 594 before and after AF cleaning at 150 Oe. The axial dipole inclination for the site is −63.8° (arrows).

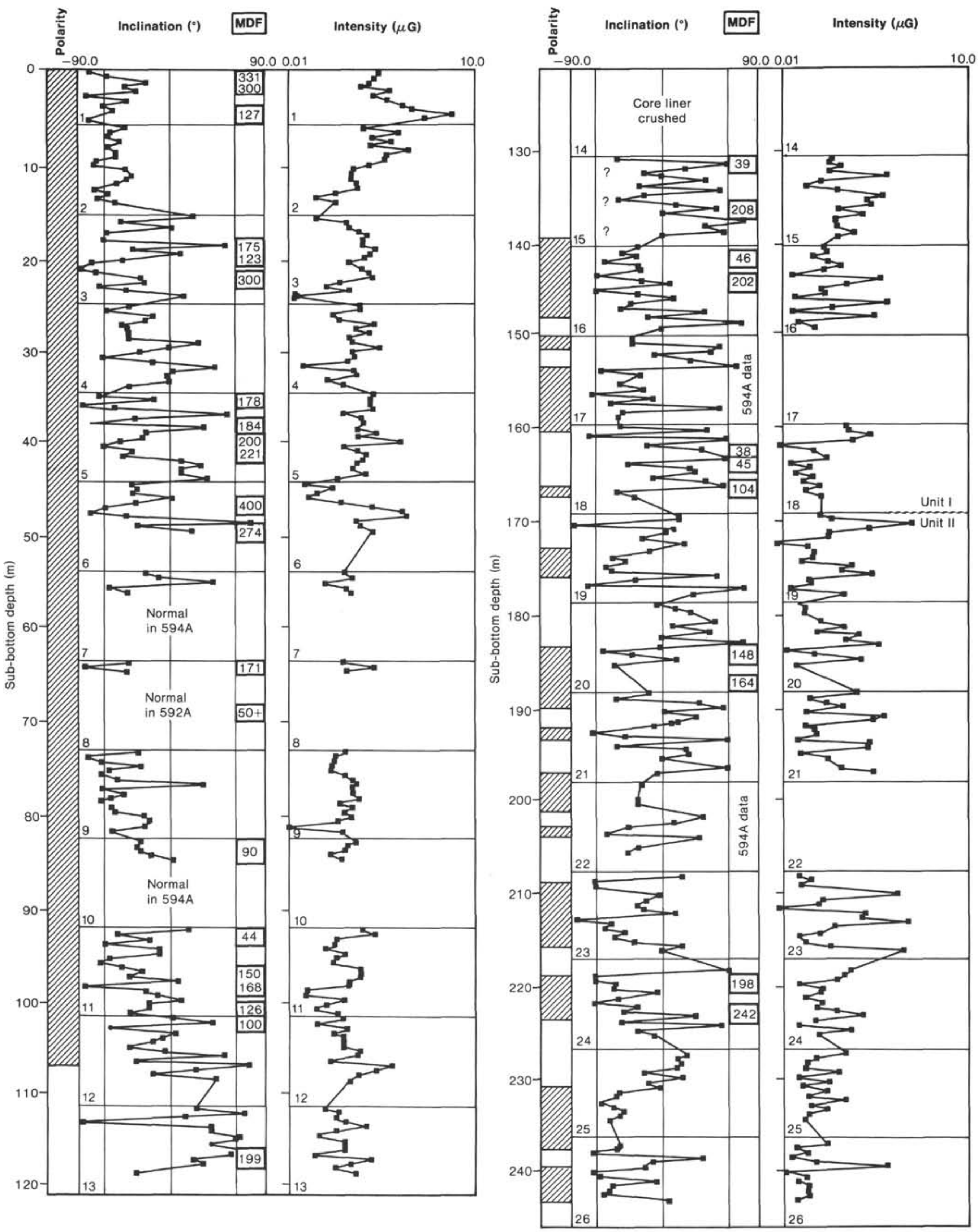

Figure 25. Inclination and intensity data for Hole 594, after AF cleaning at 150 Oe. The polarity record below 360 m is unresolved. Data from Hole 594A have been used to fill in some of the gaps in the record from Hole 594.

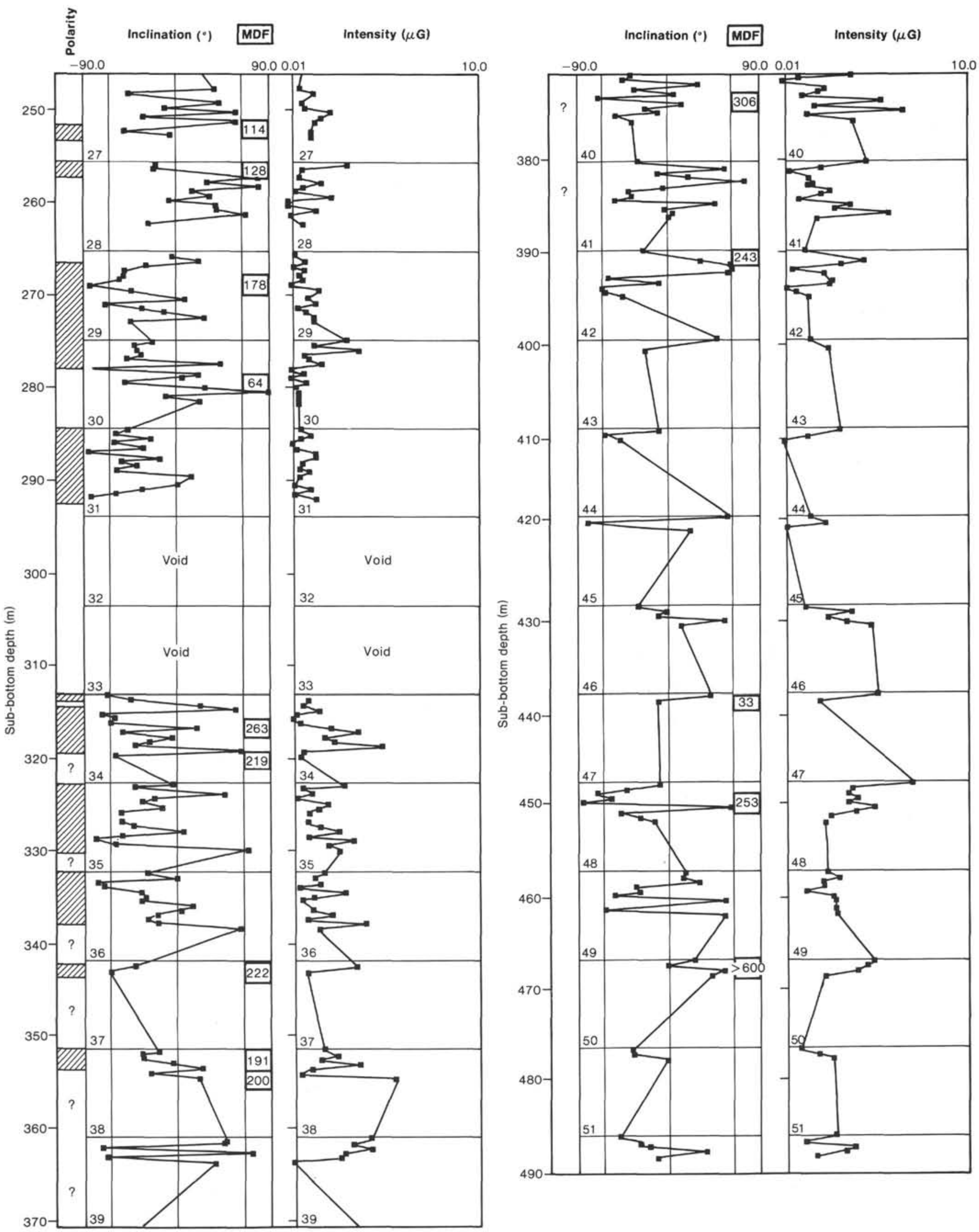

Figure 25. (Continued).

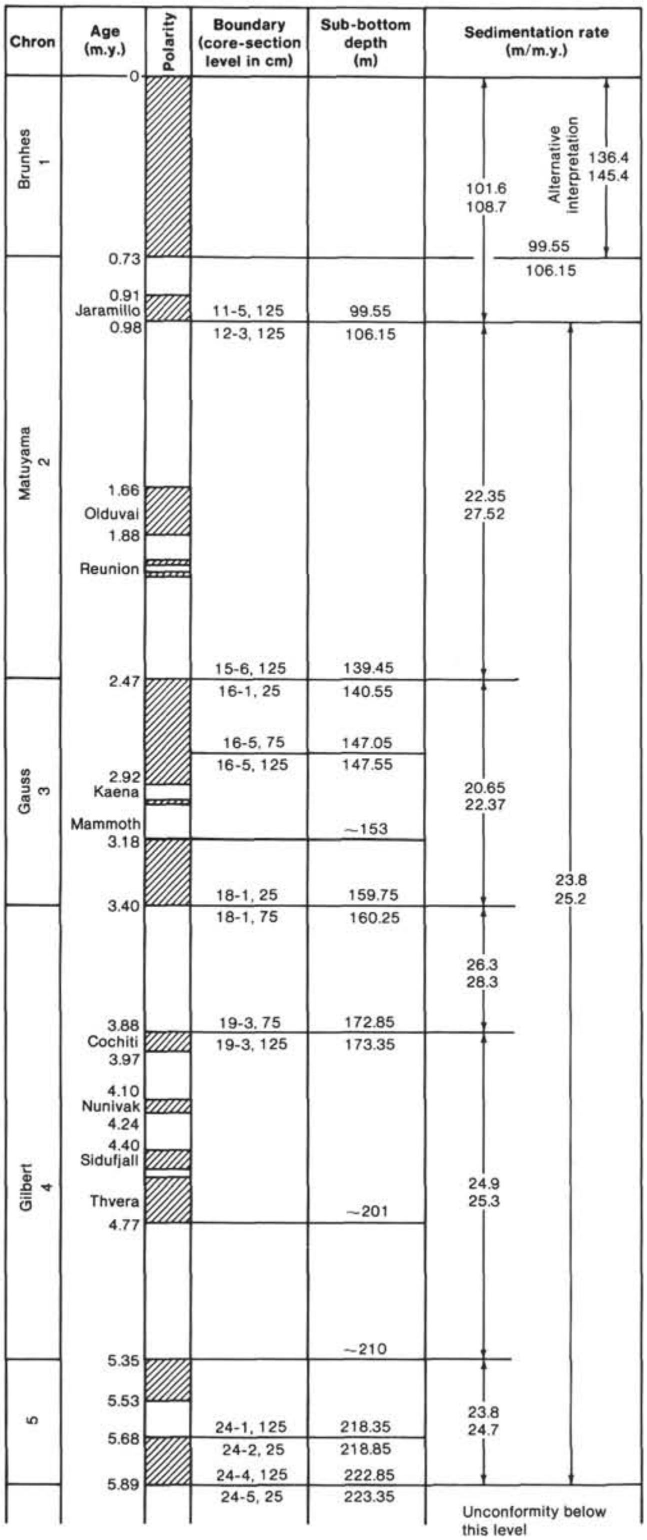

Figure 26. Reversal boundaries and sedimentation rates for Hole 594.

Table 10. AF-cleaned data, upper 38 cores of Hole 594.

Core-Section (interval in cm)	Sub-bottom depth (m)	Declination (°)	Inclination (°)	Intensity (μG)
1-1, 25	0.25	126.0	−75.4	0.284
1-1, 75	0.75	212.0	−61.0	0.257
1-1, 125	1.25	218.1	−20.6	0.200
1-2, 25	1.75	206.1	−46.6	0.146
1-2, 75	2.25	246.8	−33.6	0.457
1-2, 125	2.75	127.4	−84.4	0.238
1-3, 25	3.25	202.2	−41.7	0.389
1-3, 75	3.75	187.5	−67.3	0.658
1-3, 125	4.25	245.0	−56.1	0.895
1-4, 25	4.75	202.3	−67.3	4.482
1-4, 75	5.25	215.4	−83.1	1.496
1-4, 75	5.25	215.0	−83.0	1.496
2-1, 25	6.15	291.8	−43.5	0.152
2-1, 75	6.65	288.2	−58.8	0.623
2-1, 125	7.15	348.4	−63.6	0.207
2-2, 25	7.65	353.4	−49.5	0.444
2-2, 75	8.15	294.2	−61.5	0.176
2-2, 125	8.65	245.1	−53.2	0.850
2-3, 25	9.15	147.1	−52.8	0.318
2-3, 75	9.65	358.6	−74.1	0.341
2-3, 125	10.15	279.0	−76.1	0.191
2-4, 25	10.65	270.9	−44.0	0.100
2-4, 75	11.15	321.5	−38.3	0.090
2-4, 125	11.65	333.5	−42.0	0.092
2-5, 25	12.15	239.4	−51.3	0.111
2-5, 75	12.65	334.1	−74.6	0.129
2-5, 125	13.15	195.9	−60.9	0.051
2-6, 25	13.65	102.6	−73.7	0.026
2-6, 75	14.15	196.9	−53.8	0.053
3-1, 25	15.75	168.7	22.5	0.027
3-1, 75	16.25	189.2	−48.5	0.078
3-1, 125	16.75	158.1	0.9	0.083
3-2, 25	17.25	289.8	−61.2	0.131
3-2, 75	17.75	121.8	−62.4	0.176
3-2, 125	18.25	100.6	−66.7	0.144
3-3, 25	18.75	160.6	55.1	0.138
3-3, 75	19.25	105.0	−35.0	0.216
3-3, 125	19.75	231.9	15.1	0.192
3-4, 25	20.25	108.6	−43.7	0.150
3-4, 75	20.75	128.9	−79.9	0.090
3-4, 125	21.25	12.1	−89.1	0.147
3-5, 25	21.75	151.2	−72.8	0.182
3-5, 75	22.25	187.4	−26.4	0.213
3-5, 125	22.75	142.6	−22.7	0.065
3-6, 25	23.25	245.3	−69.9	0.040
3-6, 75	23.75	336.9	−41.9	0.094
3-6, 125	24.25	286.9	18.6	0.011
4-1, 25	25.35	145.2	−40.1	0.145
4-1, 75	25.85	168.2	−63.2	0.139
4-1, 125	26.35	225.4	−16.6	0.048
4-2, 25	26.85	169.7	−24.3	0.064
4-2, 75	27.35	158.1	−47.6	0.241
4-2, 125	27.85	178.3	−42.2	0.115
4-3, 25	28.35	186.0	−40.8	0.184
4-3, 75	28.85	273.8	−41.3	0.086
4-3, 125	29.35	355.2	30.5	0.099
4-4, 25	29.85	303.3	−3.5	0.304
4-4, 75	30.35	209.7	−29.6	0.094
4-4, 125	30.85	261.9	−65.3	0.106
4-5, 25	31.35	251.9	−17.6	0.079
4-5, 75	31.85	88.2	42.5	0.015
4-5, 125	32.35	211.6	2.0	0.104
4-6, 25	32.85	247.7	−5.1	0.124
4-6, 75	33.35	45.5	−1.0	0.043
4-6, 122	33.82	40.6	−39.6	0.072
5-1, 25	34.95	55.7	−70.1	0.206
5-1, 75	35.45	124.6	−15.8	0.198
5-1, 125	35.95	328.3	−88.7	0.184
5-2, 22	36.42	262.7	−57.2	0.205
5-2, 75	36.95	202.5	55.8	0.072
5-2, 125	37.45	137.1	−35.8	0.136
5-3, 25	37.95	284.7	−80.6	0.149
5-3, 75	38.45	199.8	35.6	0.127
5-3, 125	38.95	282.5	−23.1	0.252
5-4, 25	39.45	121.0	−26.0	0.114
5-4, 75	39.95	64.0	−51.0	0.638
5-4, 125	40.45	180.5	−65.9	0.069

Table 10. (Continued).

Core-Section (interval in cm)	Sub-bottom depth (m)	Declination (°)	Inclination (°)	Intensity (μG)
5-5, 25	40.95	95.9	−36.9	0.121
5-5, 75	41.45	57.3	−46.4	0.171
5-5, 125	41.95	85.4	13.0	0.146
5-6, 25	42.45	114.9	31.1	0.112
5-6, 75	42.95	219.4	9.6	0.101
5-6, 125	43.45	308.1	9.2	0.162
5-7, 25	43.95	295.7	36.8	0.057
6-1, 28	44.58	18.0	−37.9	0.016
6-1, 75	45.05	184.2	−32.4	0.049
6-1, 125	45.55	98.5	−38.2	0.027
6-2, 25	46.05	213.3	3.8	0.020
6-2, 75	46.55	295.9	−34.5	0.065
6-2, 125	47.05	281.6	−64.7	0.199
6-3, 25	47.55	308.0	−81.0	0.720
6-3, 75	48.05	345.0	−43.0	0.854
6-3, 125	48.55	137.5	82.4	0.109
6-4, 25	49.05	222.3	−33.4	0.129
6-4, 74	49.54	249.2	21.2	0.210
7-1, 25	54.15	201.3	−23.9	0.069
7-1, 75	54.65	210.4	−10.5	0.105
7-1, 125	55.15	210.1	42.9	0.032
7-2, 25	55.65	9.7	−61.9	0.084
7-2, 75	56.15	101.8	−42.5	0.102
8-1, 25	63.75	358.5	−39.9	0.065
8-1, 75	64.25	58.7	−84.2	0.253
8-1, 125	64.75	274.0	−42.0	0.078
9-1, 25	73.35	7.0	−29.8	0.072
9-1, 75	73.85	348.6	−80.0	0.055
9-1, 125	74.35	349.5	−68.3	0.053
9-2, 25	74.85	47.9	−27.9	0.046
9-2, 75	75.35	312.9	−61.9	0.045
9-2, 125	75.85	40.6	−67.1	0.077
9-3, 25	76.35	220.7	−52.7	0.106
9-3, 75	76.85	121.5	32.0	0.119
9-3, 125	77.35	354.3	−66.7	0.100
9-4, 25	77.85	286.4	−43.2	0.099
9-4, 75	78.35	240.9	−59.1	0.140
9-4, 125	78.85	92.0	−66.0	0.062
9-5, 25	79.35	293.1	−55.8	0.106
9-5, 75	79.85	280.6	−53.7	0.074
9-5, 125	80.35	235.1	−23.9	0.105
9-6, 25	80.85	232.2	−18.9	0.058
9-6, 75	81.35	163.7	−24.6	0.008
9-6, 125	81.85	159.5	−58.7	0.067
10-1, 25	82.95	157.7	−27.3	0.117
10-1, 75	83.45	217.6	−31.8	0.086
10-1, 125	83.95	310.7	−31.1	0.081
10-2, 25	84.45	239.1	−19.5	0.044
10-2, 75	84.95	67.7	3.5	0.063
11-1, 25	92.55	161.6	18.0	0.155
11-1, 75	93.05	234.4	−51.3	0.247
11-1, 125	93.55	292.6	−17.3	0.053
11-2, 25	94.05	313.2	−63.4	0.052
11-2, 75	94.55	250.1	−10.4	0.037
11-2, 125	95.05	145.7	−8.7	0.073
11-3, 25	95.55	116.0	−57.8	0.054
11-3, 75	96.05	326.1	−68.6	0.049
11-3, 125	96.55	312.7	−46.4	0.132
11-4, 25	97.05	198.7	−26.4	0.137
11-4, 75	97.55	232.3	−40.0	0.144
11-4, 125	98.05	143.0	9.0	0.089
11-5, 25	98.55	109.0	−84.5	0.093
11-5, 75	99.05	120.9	−23.3	0.018
11-5, 125	99.55	29.4	−12.5	0.017
11-6, 25	100.05	219.6	11.8	0.081
11-6, 75	100.55	222.7	−20.7	0.038
11-6, 125	101.05	172.6	−20.3	0.026
11-7, 25	101.55	272.8	−38.5	0.056
12-1, 25	102.15	199.0	2.8	0.079
12-1, 75	102.65	160.0	43.0	0.027
12-1, 125	103.15	349.1	−60.5	0.079
12-2, 25	103.65	238.5	5.6	0.053
12-2, 75	104.15	20.3	−7.9	0.075
12-2, 125	104.65	236.8	−16.4	0.072
12-3, 25	105.15	244.2	−40.7	0.082
12-3, 75	105.65	179.3	−3.8	0.134
12-3, 125	106.15	213.2	51.9	0.123

Table 10. (Continued).

Core-Section (interval in cm)	Sub-bottom depth (m)	Declination (°)	Inclination (°)	Intensity (μG)
12-4, 25	106.65	247.4	−34.8	0.044
12-4, 75	107.15	226.4	77.9	0.421
12-4, 125	107.65	226.4	24.1	0.242
12-5, 25	108.15	213.6	−21.8	0.121
12-5, 75	108.65	189.3	44.9	0.092
13-1, 25	111.75	251.0	25.3	0.035
13-1, 75	112.25	275.9	74.5	0.061
13-1, 125	112.75	270.2	14.6	0.050
13-2, 25	113.25	107.0	−86.6	0.072
13-2, 75	113.75	237.7	39.4	0.185
13-2, 125	114.25	235.0	39.3	0.053
13-3, 25	114.75	130.9	65.4	0.028
13-3, 75	115.23	130.6	62.5	0.074
13-3, 125	115.75	55.3	37.0	0.076
13-4, 25	116.25	20.7	69.5	0.074
13-4, 75	116.75	123.4	61.5	0.023
13-4, 125	117.25	331.8	22.5	0.220
13-5, 25	117.75	221.3	32.4	0.095
13-5, 75	118.25	267.0	0.9	0.047
13-5, 125	118.75	318.3	−34.3	0.115
15-1, 25	130.95	122.5	−48.4	0.060
15-1, 75	131.45	117.7	72.8	0.056
15-1, 125	131.95	157.8	23.4	0.087
15-2, 25	132.45	344.8	−17.5	0.052
15-2, 75	132.95	148.5	−0.4	0.510
15-2, 125	133.45	207.6	44.9	0.039
15-3, 25	133.95	205.6	−23.4	0.022
15-3, 75	134.45	280.9	57.7	0.073
15-3, 125	134.95	322.1	−16.5	0.470
15-4, 25	135.45	357.3	−42.5	0.226
15-4, 75	135.95	1.7	15.0	0.287
15-4, 125	136.45	102.9	54.5	0.076
15-5, 25	136.95	339.1	−1.5	0.214
15-5, 75	137.45	267.2	61.4	0.068
15-5, 125	137.95	130.7	78.8	0.069
15-6, 25	138.45	198.7	40.3	0.075
15-6, 75	138.95	310.5	63.1	0.140
15-6, 125	139.45	226.1	−0.9	0.074
16-1, 25	140.55	262.1	−23.6	0.044
16-1, 75	141.05	279.0	−38.1	0.049
16-1, 125	141.55	176.8	−24.1	0.032
16-2, 25	142.05	222.2	−59.0	0.056
16-2, 75	142.55	300.1	−22.2	0.082
16-2, 125	143.05	72.0	−20.0	0.048
16-3, 25	143.55	39.7	−62.2	0.015
16-3, 75	144.05	167.5	−19.3	0.402
16-3, 125	144.55	285.4	8.0	0.105
16-4, 25	145.05	0.1	−64.8	0.042
16-4, 75	145.55	301.0	−23.5	0.048
16-4, 125	146.05	111.4	11.9	0.015
16-5, 25	146.55	277.6	−31.3	0.518
16-5, 75	147.05	85.2	−42.4	0.064
16-5, 125	147.55	149.2	38.7	0.014
16-6, 25	148.05	96.8	−12.8	0.329
16-6, 75	148.55	70.1	79.1	0.017
16-6, 125	149.05	272.3	−3.4	0.032
18-1, 25	159.75	194.5	−41.0	0.104
18-1, 75	160.25	353.0	42.6	0.118
18-1, 125	160.75	95.4	−70.9	0.264
18-2, 25	161.25	116.3	62.4	0.134
18-2, 75	161.75	256.5	−15.3	0.009
18-2, 125	162.25	272.3	35.8	0.031
18-3, 25	162.75	241.5	−40.7	0.005
18-3, 75	163.25	155.7	66.9	0.053
18-3, 125	163.75	179.5	−34.3	0.012
18-4, 25	164.25	236.7	27.4	0.026
18-4, 75	164.75	284.4	34.6	0.014
18-4, 125	165.25	100.3	−10.2	0.027
18-5, 25	165.75	154.3	40.3	0.021
18-5, 75	166.25	169.2	59.4	0.041
18-5, 125	166.75	132.4	−44.8	0.023
18-6, 25	167.25	161.6	−28.8	0.041
19-1, 25	169.35	210.9	14.3	0.040
19-1, 75	169.85	105.7	14.7	0.061
19-1, 125	170.35	315.7	−86.4	1.215
19-2, 25	170.85	265.6	13.6	0.233
19-2, 75	171.35	97.8	3.3	0.057

Table 10. (Continued).

Core-Section (interval in cm)	Sub-bottom depth (m)	Declination (°)	Inclination (°)	Intensity (μG)
19-2, 125	171.85	326.5	−24.7	0.050
19-3, 25	172.35	309.8	21.6	0.008
19-3, 75	172.85	257.7	−2.2	0.026
19-3, 125	173.35	332.2	−13.6	0.030
19-4, 25	173.85	161.0	−51.7	0.028
19-4, 75	174.35	334.6	−35.5	0.021
19-4, 125	174.85	73.9	−58.1	0.129
19-5, 25	175.35	125.9	−51.7	0.086
19-5, 75	175.85	170.7	52.4	0.297
19-5, 125	176.35	80.3	−29.9	0.023
19-6, 25	176.85	114.0	−74.8	0.028
19-6, 75	177.35	289.9	78.8	0.012
19-6, 125	177.85	236.2	31.8	0.101
20-1, 25	178.95	0.3	−5.6	0.016
20-1, 75	179.45	231.7	10.8	0.022
20-1, 125	179.95	241.8	29.4	0.020
20-2, 25	180.45	351.6	−34.8	0.006
20-2, 75	180.95	148.8	48.4	0.043
20-2, 125	181.45	44.2	11.2	0.095
20-3, 25	181.95	102.2	46.8	0.031
20-3, 75	182.45	168.2	−4.3	0.163
20-3, 125	182.95	131.0	77.6	0.088
20-4, 25	183.45	233.9	−2.9	0.416
20-4, 75	183.95	256.5	−62.9	0.010
20-4, 125	184.45	98.7	−31.1	0.028
20-5, 25	184.95	146.5	14.8	0.189
20-5, 75	185.45	209.7	−47.6	0.015
21-1, 25	188.55	338.8	−12.4	0.153
21-1, 75	189.05	251.8	−52.1	0.025
21-1, 125	189.55	63.8	35.0	0.045
21-2, 25	190.05	139.0	57.7	0.094
21-2, 75	190.55	187.9	−3.2	0.020
21-2, 125	191.05	274.3	31.5	0.487
21-3, 25	191.55	179.2	13.3	0.266
21-3, 75	192.05	257.6	−11.5	0.021
21-3, 125	192.55	191.8	−71.8	0.032
21-4, 25	193.05	352.1	−35.9	0.033
21-4, 75	193.55	179.7	61.1	0.016
21-4, 125	194.05	207.0	−47.5	0.250
21-5, 25	194.55	226.9	21.0	0.210
21-5, 75	195.05	216.5	23.7	0.018
21-5, 125	195.55	17.0	−2.9	0.052
21-6, 75	196.55	174.2	63.1	0.078
21-6, 125	197.05	36.5	−6.9	0.289
23-1, 75	208.25	239.9	17.6	0.017
23-1, 125	208.75	340.9	−68.5	0.026
23-2, 25	209.25	243.6	−67.2	0.019
23-2, 75	209.75	300.7	−37.4	0.007
23-2, 125	210.25	314.6	−2.7	0.760
23-3, 25	210.75	347.1	−18.8	0.042
23-3, 75	211.25	87.7	−25.9	0.036
23-3, 125	211.75	180.3	−20.4	0.008
23-4, 25	212.25	230.9	14.6	0.210
23-4, 75	212.75	113.4	−85.8	0.170
23-4, 125	213.25	311.4	−50.7	1.098
23-5, 25	213.75	158.6	−57.7	0.064
23-5, 75	214.25	131.0	−38.4	0.040
23-5, 125	214.75	267.7	−47.0	0.015
23-6, 25	215.25	1.4	−28.0	0.021
23-6, 75	215.75	126.6	18.2	0.049
23-6, 125	216.25	195.8	−4.2	0.940
24-1, 125	218.35	283.6	67.2	0.118
24-2, 25	218.85	200.1	−66.5	0.095
24-2, 75	219.35	272.5	−67.7	0.076
24-2, 125	219.85	157.3	−46.7	0.015
24-3, 25	220.35	173.6	−51.8	0.041
24-3, 75	220.85	123.7	−5.2	0.038
24-3, 125	221.35	287.6	−42.6	0.022
24-4, 25	221.85	132.6	−66.9	0.043
24-4, 75	222.35	234.6	−23.6	0.035
24-4, 125	222.85	170.9	−40.8	0.076
24-5, 25	223.35	244.3	34.1	0.199
24-5, 75	223.85	206.2	−39.3	0.030
24-5, 125	224.35	251.6	57.2	0.016
24-6, 25	224.85	155.4	−29.5	0.119
24-6, 75	225.35	151.7	−10.2	0.033
25-1, 75	227.45	91.8	23.4	0.111

Table 10. (Continued).

Core-Section (interval in cm)	Sub-bottom depth (m)	Declination (°)	Inclination (°)	Intensity (μG)
25-1, 125	227.95	264.9	10.5	0.030
25-2, 25	228.45	253.6	16.2	0.021
25-2, 75	228.95	73.8	13.2	0.020
25-2, 125	229.45	240.9	−18.9	0.078
25-3, 25	229.95	182.3	17.0	0.017
25-3, 75	230.45	272.0	−16.4	0.056
25-3, 125	230.95	98.2	−4.9	0.020
25-4, 25	231.45	343.6	−44.4	0.046
25-4, 75	231.95	168.6	−45.5	0.025
25-4, 125	232.45	201.4	−61.8	0.095
25-5, 25	232.95	207.5	−50.7	0.027
25-5, 75	233.45	178.0	−42.2	0.052
25-5, 125	233.95	178.8	−42.8	0.025
25-6, 25	234.45	153.4	−53.7	0.021
26-1, 75	237.05	177.9	−41.4	0.048
26-1, 125	237.55	227.1	−42.0	0.014
26-2, 25	238.05	238.4	−71.5	0.023
26-2, 75	238.55	263.8	41.0	0.012
26-2, 125	239.05	216.0	−10.8	0.032
26-3, 25	239.55	252.4	−18.7	0.451
26-3, 75	240.05	217.3	−69.1	0.012
26-3, 125	240.55	82.1	−61.2	0.022
26-4, 25	241.05	174.9	−6.1	0.016
26-4, 75	241.55	321.6	−52.1	0.025
26-4, 125	242.05	107.0	−52.7	0.022
26-5, 25	242.55	178.1	−60.5	0.024
26-5, 75	243.05	190.3	5.5	0.016
27-2, 25	247.65	25.4	38.7	0.011
27-2, 75	248.15	239.4	−49.0	0.020
27-2, 125	248.65	199.5	−33.7	0.006
27-3, 25	249.15	169.9	44.1	0.012
27-3, 75	249.65	244.2	−11.3	0.014
27-3, 125	250.15	232.4	60.7	0.040
27-4, 25	250.65	155.5	−32.3	0.025
27-4, 75	251.15	66.1	66.2	0.020
27-4, 125	251.65	211.2	34.6	0.007
27-5, 25	252.15	270.4	−50.3	0.017
27-5, 75	252.65	219.8	−6.3	0.018
27-5, 125	253.15	236.9	−53.8	0.004
28-1, 25	255.75	244.3	−20.3	0.072
28-1, 75	256.25	191.9	−23.7	0.012
28-2, 25	257.25	198.8	80.9	0.011
28-2, 75	257.75	251.8	29.4	0.025
28-2, 125	258.25	308.1	81.5	0.012
28-3, 25	258.75	216.7	16.7	0.010
28-3, 75	259.25	335.3	31.6	0.041
28-3, 125	259.75	172.3	−8.1	0.008
28-4, 25	260.25	124.4	39.5	0.008
28-4, 75	260.75	0.4	38.8	0.025
28-4, 125	261.25	13.5	67.4	0.008
28-5, 25	261.75	271.1	−5.6	0.004
28-5, 75	262.25	266.5	−29.2	0.012
29-1, 75	265.85	187.0	−2.1	0.010
29-1, 125	266.35	220.9	22.4	0.015
29-2, 25	266.85	123.2	−31.0	0.009
29-2, 75	267.35	182.1	−50.5	0.013
29-2, 125	267.85	236.7	−51.2	0.012
29-3, 25	268.35	104.9	−54.1	0.014
29-3, 75	268.85	260.5	−83.2	0.008
29-3, 125	269.35	87.8	−43.0	0.027
29-4, 25	269.85	215.4	27.0	0.006
29-4, 75	270.35	115.4	14.3	0.016
29-4, 125	270.85	274.6	−69.1	0.022
29-5, 25	271.35	148.2	−32.1	0.011
29-5, 75	271.85	185.5	−11.2	0.015
29-5, 125	272.35	87.8	31.1	0.019
29-6, 25	272.85	167.5	−44.3	0.020
29-6, 75	273.35	264.6	−24.1	0.021
29-6, 125	273.85	263.4	−41.4	0.012
30-1, 25	274.95	86.1	−22.5	0.072
30-1, 75	275.45	99.8	−39.1	0.020
30-1, 125	275.95	279.3	−39.6	0.119
30-2, 25	276.45	218.3	−34.7	0.013
30-2, 75	276.95	196.3	−47.4	0.015
30-2, 125	277.45	137.5	43.4	0.026
30-3, 25	277.95	251.6	−81.6	0.008
30-3, 75	278.45	257.8	21.3	0.013

Table 10. (Continued).

Core-Section (interval in cm)	Sub-bottom depth (m)	Declination (°)	Inclination (°)	Intensity (μG)
30-3, 125	278.95	337.7	5.9	0.008
30-4, 25	279.45	195.2	−50.6	0.016
30-4, 75	279.95	240.9	28.1	0.010
30-4, 125	280.45	93.0	82.4	0.011
30-5, 25	280.95	207.3	−9.9	0.011
30-5, 75	281.45	161.8	25.4	0.011
30-5, 125	281.95	118.6	72.6	0.003
30-6, 25	282.45	281.6	−9.5	0.004
31-1, 25	284.55	280.7	−47.4	0.011
31-1, 75	285.05	110.0	−59.0	0.017
31-1, 125	285.55	245.3	−24.3	0.012
31-2, 25	286.05	297.6	−62.4	0.008
31-2, 75	286.55	61.4	−30.0	0.010
31-2, 125	287.05	48.6	−85.4	0.022
31-3, 25	287.55	65.0	−13.8	0.021
31-3, 75	288.05	120.5	−53.8	0.013
31-3, 125	288.55	189.1	−37.6	0.012
31-4, 25	289.05	172.7	−57.1	0.016
31-4, 75	289.55	114.6	18.0	0.012
31-4, 125	290.05	265.3	−50.7	0.006
31-5, 25	290.55	289.1	1.1	0.010
31-5, 75	291.05	198.5	−37.0	0.018
31-5, 125	291.55	127.0	−56.4	0.009
31-6, 25	292.05	346.0	−84.5	0.023
34-1, 25	313.35	26.9	−64.6	0.015
34-1, 75	313.85	294.0	−41.5	0.017
34-1, 125	314.35	227.4	24.5	0.013
34-2, 25	314.85	303.3	59.9	0.025
34-2, 75	315.35	293.2	−72.4	0.010
34-2, 125	315.85	106.0	−59.1	0.009
34-3, 25	316.35	187.4	−61.8	0.013
34-3, 75	316.85	183.8	20.3	0.038
34-3, 125	317.35	357.0	−52.8	0.115
34-4, 25	317.85	89.1	1.1	0.029
34-4, 75	318.35	93.6	−26.4	0.042
34-4, 125	318.85	301.6	−40.2	0.293
34-5, 25	319.35	307.4	73.1	0.013
34-5, 75	319.85	237.8	−61.5	0.012
35-1, 25	322.95	101.0	−2.4	0.060
35-1, 75	323.45	289.5	−39.2	0.013
35-1, 125	323.95	341.6	51.7	0.018
35-2, 25	324.45	167.9	−21.0	0.010
35-2, 75	324.95	244.1	−30.5	0.039
35-2, 125	325.45	54.0	−11.9	0.024
35-3, 25	325.95	142.7	−52.6	0.017
35-3, 75	326.45	271.2	−22.0	0.008
35-3, 125	326.95	328.8	−52.3	0.015
35-4, 25	327.45	280.2	−40.7	0.024
35-4, 75	327.95	59.3	7.1	0.060
35-4, 125	328.45	200.2	−52.1	0.014
35-5, 25	328.95	224.4	−80.6	0.093
35-5, 75	329.45	250.3	−56.3	0.033
35-5, 125	329.95	242.0	67.0	0.055
36-1, 25	332.55	264.0	−31.2	0.027
36-1, 75	333.05	304.6	3.7	0.021
36-1, 125	333.55	310.8	−74.8	0.026
36-2, 25	334.05	225.8	−68.7	0.011
36-2, 75	334.55	309.3	−32.1	0.078
36-2, 125	335.05	203.5	−27.6	0.021
36-3, 25	335.55	250.5	−33.1	0.013
36-3, 75	336.05	278.5	21.4	0.017
36-3, 125	336.55	8.3	4.9	0.020
36-4, 25	337.05	296.3	−18.5	0.041
36-4, 75	337.55	339.5	−27.0	0.014
36-4, 125	338.05	120.2	−15.6	0.160
36-5, 25	338.55	237.9	66.8	0.023
37-1, 75	342.65	25.0	−39.2	0.096
37-1, 125	343.15	240.6	−65.3	0.015
38-1, 27	351.77	37.2	−15.8	0.030
38-1, 75	352.25	243.1	−31.6	0.050
38-1, 125	352.75	72.3	−33.1	0.024
38-2, 25	353.25	340.0	−1.6	0.136
38-2, 75	353.75	134.6	29.2	0.019
38-2, 125	354.25	350.6	−24.0	0.011
38-3, 25	354.75	84.9	23.5	0.448

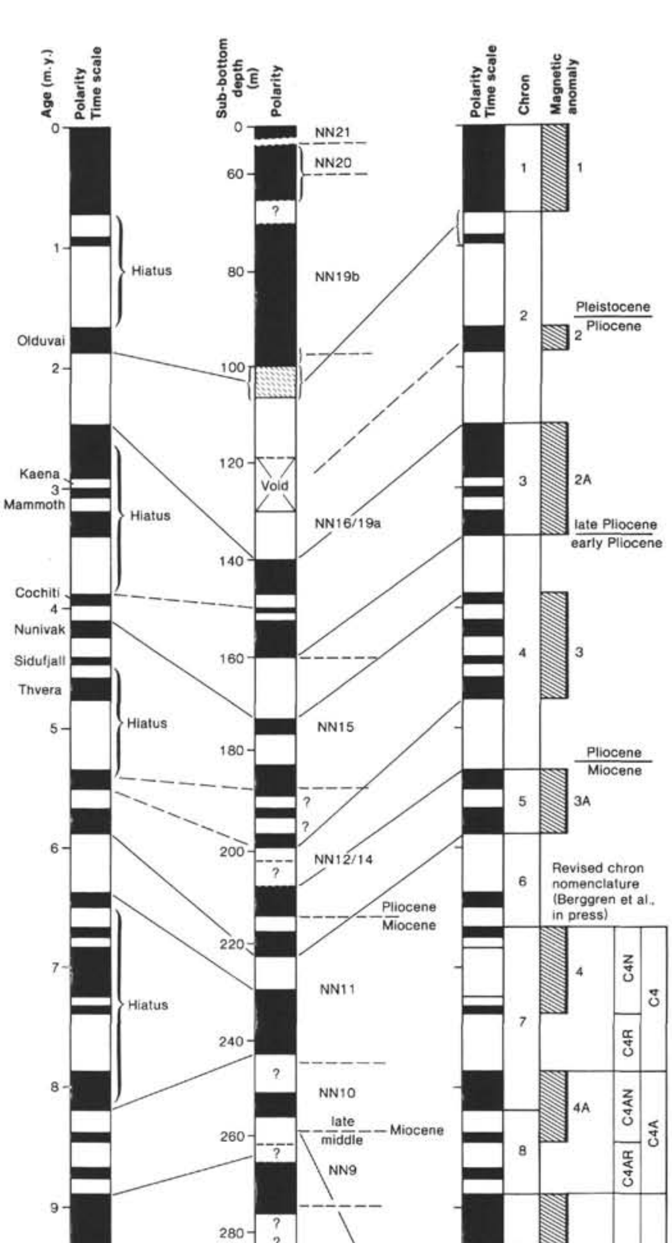

Figure 27. Two interpretations of the paleomagnetic record from Hole 594 (center column). To the left/right is shown the simplest match with the magnetic polarity time scale which is consistent with the diatom-radiolarian/calcareous nannofossil dating schemes, respectively (see text). The diatom-radiolarian scheme incorporates four major hiatuses. The marine magnetic anomaly sequence and the related new magnetic chron nomenclature (Berggren et al., in press) are illustrated on the far right.